UNIVERSIDADE FEDERAL DE PERNAMBUCO
CENTRO DE CIÊNCIAS DA SAÚDE
DEPARTAMENTO DE PRÓTESE E CIRURGIA BUCO FACIAL
PÓS GRADUAÇÃO EM ODONTOLOGIA
DOUTORADO EM ODONTOLOGIA
ÁREA DE CONCENTRAÇÃO EM CLÍNICA INTEGRADA

DANIELA SIQUEIRA LOPES

AVALIAÇÃO DAS ESTRUTURAS DENTÁRIAS HÍGIDAS E CARIADAS POR MEIO DAS TECNOLOGIAS DE ESPECTROSCOPIA TERAHERTZ, TOMOGRAFIA POR COERÊNCIA ÓPTICA E IMAGEAMENTO POR RETROESPALHAMENTO COM LASER ALEATÓRIO EM FIBRA

RECIFE
2020

DANIELA SIQUEIRA LOPES

AVALIAÇÃO DAS ESTRUTURAS DENTÁRIAS HÍGIDAS E CARIADAS POR MEIO DAS TECNOLOGIAS DE ESPECTROSCOPIA TERAHERTZ, TOMOGRAFIA POR COERÊNCIA ÓPTICA E IMAGEAMENTO POR RETROESPALHAMENTO COM LASER ALEATÓRIO EM FIBRA

Tese apresentada ao Programa de Pós-Graduação em Odontologia da Universidade Federal de Pernambuco, como requisito parcial para obtenção do título de Doutora em Odontologia.

Área de Concentração: Clínica Integrada.

Orientador: Prof. Dr. Anderson Stevens Leônidas Gomes

RECIFE

2020

Catalogação na fonte:
Bibliotecária: Elaine Freitas, CRB4:1790

L864a Lopes, Daniela Siqueira

Avaliação das estruturas dentárias hígidas e cariadas por meio das tecnologias de espectroscopia terahertz, tomografia por coerência óptica e imageamento por retroespalhamento com laser aleatório em fibra/ Daniela Siqueira Lopes. – 2020.

117 f. : il.

Orientador: Anderson Stevens Leônidas Gomes.

Tese (doutorado) – Universidade Federal de Pernambuco. Centro de Ciências da Saúde. Programa de pós-graduação em Odontologia. Recife, 2020.

Inclui referências, apêndices e anexos.

1. Espectroscopia terahertz. 2. Tomografia de coerência óptica. 3. Lasers. 4. Nanopartículas metálicas I. Gomes, Anderson Stevens Leônidas. (orientador). II. Título.

617.6 CDD (23.ed.) UFPE (CCS 2020 - 024)

DANIELA SIQUEIRA LOPES

AVALIAÇÃO DAS ESTRUTURAS DENTÁRIAS HÍGIDAS E CARIADAS POR MEIO DAS TECNOLOGIAS DE ESPECTROSCOPIA TERAHERTZ, TOMOGRAFIA POR COERÊNCIA ÓPTICA E IMAGEAMENTO POR RETROESPALHAMENTO COM LASER ALEATÓRIO EM FIBRA

Tese apresentada ao Programa de Pós-Graduação em Odontologia da Universidade Federal de Pernambuco, como requisito parcial para obtenção do título de Doutora em Odontologia.

Aprovada em 28 de janeiro de 2020

BANCA EXAMINADORA

1°_____
Profº Dr. Anderson Stevens Leônidas Gomes (Orientador)
Universidade Federal de Pernambuco

2°_____
Profª. Dra. Andrea dos Anjos Pontual (examinador interno)
Universidade Federal de Pernambuco

3°_____
Profº. Dr. Claudio Heliomar Vicente da Silva (examinador interno)
Universidade Federal de Pernambuco

4°_____
Profª. Dra. Denise Maria Zezell (examinador externo)
Universidade de São Paulo

5°_____
Profª. Dra. Márcia Maria Fonseca da Silveira (examinador externo)

AGRADECIMENTOS

Agradeço a Deus por toda luz e proteção. A minha família, em especial a minha mãe Irenilda, meu pai Juvenal e meu irmão Rafael por não medirem esforços em me apoiar de forma incondicional, pela cumplicidade, força, carinho e amor. Por serem minha base, meu reforço, meu ninho. Por vocês, por sempre, minha eterna gratidão.

Aos verdadeiros amigos que ao longo desta jornada me estimularam, acompanharam e dividiram cada momento de uma maneira única e especial. Àqueles que vivenciaram além de bons momentos, minhas angústias, e que se propuseram a ajudar sempre que necessário. Por toda palavra dita e/ou ouvida, por toda compreensão e por me ensinarem dia após dia o real significado de amizade: Emmanuel Marques, Rafaella Souza, Lia Pontes, Ariela Rizuto, Carol Igrejas, Marcela Valones, João Aroucha, Izabella Lins, Ricardo Alves, Anizabel Ferraz, Flávia Santos, Érica Vanessa e Cássia Borges.

Ao meu orientador Professor Anderson, meu conselheiro, grande exemplo profissional de integridade e um pai da vida acadêmica, toda a minha admiração e reconhecimento. Por todo apoio, dedicação, incentivo, aprendizado, compreensão, paciência com minha ansiedade e os percalços diários do meu caminho, minha gratidão não cabem nesse escopo. Obrigada por entender as individualidades, e respeitá-las. Por passar segurança e resolução.

A minha segunda família Labfoton em especial: Luana, Luciana, Cecilia, Emery, Cláudia, Tereza, Vanda, Evair, Gisele, Melissa, Polly, Audrey, Sandra, Mariana, Bismarck, Manoel, Talita e Jessica, João, Daniel, que conseguiam transformar cada choro em sorriso e cada riso em uma nova esperança.

A professora Denise Zezell, exemplo não apenas de profissional, mas de ser humano, por todos os ensinamentos compartilhados ao longo desses anos, com muita atenção e carinho! À Daísa, pela parceria e tantas outras afinidades que fizeram com que nos tornássemos amigas extra academia e Matheus. Ao professor do Programa de Pós-Graduação em Engenharia Elétrica da UFPE Renato Araújo e Welligton por toda calma em conduzir os experimentos. Todos que em alguma

medida, contribuíram para meu desenvolvimento profissional e amadurecimento como ser humano.

Aos Coordenadores; funcionários da Coordenação de Pós graduação: Oziclere, Tamires, Dona Tânia e Isaac; da Coordenação de Graduação: Michele e Josinaldo; do Departamento de Prótese Buco Facial: Ana; Portarias, Segurança, Bibliotecas e Reitoria.

A Universidade Federal de Pernambuco – UFPE; Coordenação de Aperfeiçoamento de Pessoal de Nível Superior – CAPES, Programa Nacional de Cooperação Acadêmica PROCAD; Instituto Nacional de Ciência e Tecnologia – Instituto de Fotônica - INCT-INFO.

RESUMO

O objetivo do presente trabalho foi avaliar estruturas teciduais dentárias hígidas e cariadas por espectroscopia de Terahertz no domínio de tempo (THz-DT), tomografia por coerência óptica (OCT) e a partir de imageamento por retroespalhamento com Laser aleatório no infravermelho próximo (NIR-RFL). Para isso, foram realizados experimentos laboratoriais com dentes humanos e bovinos recém-extraídos. A configuração do THz-TDS foi desenvolvida no modo de transmissão, com base em um laser infravermelho de femtossegundo (comprimento de onda central a 820 nm, taxa de repetição de 76 MHz e largura de pulso de 150fs) e em antenas fotocondutoras. Como resultado da caracterização, o coeficiente de absorção da dentina úmida de 0,1 a 1,0 THz foi superior ao das amostras de dentina seca. A presença de lesão de cárie no tecido dentário reduz o coeficiente de absorção assim como também os valores do índice de refração. Em sequência, um método de imagem retroespalhamento baseado em laser de fibra aleatória de infravermelho próximo foi construído para fornecer uma imagem óptica de alto contraste entre o tecido hígido e cariado. O contraste obtido foi de 0,70, mais de 8 vezes maior que o contraste obtido na imagem radiográfica. Os estudos com Tomografia por Coerência Óptica empregou o sistema Callisto (Thorlabs Inc, Nova Jersey, EUA), que opera no domínio espectral com 930nm de comprimento de onda central. Sua primeira aplicação foi na análise das superfícies de esmalte irradiadas com laser Er,Cr:YSGG (Biolase Technology Inc., EUA), emitindo 2,78 μm com frequência de 20 Hz em três configurações de potência diferentes, comparados ao grupo controle com condicionamento com ácido fosfórico à 37%. A irradiação com laser promoveu superfícies rugosas em todos os parâmetros utilizados, e a análise OCT revelou maiores alterações ópticas nos grupos irradiados pelo laser quando comparado ao controle. A segunda análise foi a partir de nanopartículas esféricas de ouro (AuNP) e nanobastões de ouro (AuNR) como agentes de contraste óptico (OCAs) comparando com glicerol em imagens de tomografia de coerência óptica (OCT) com lesões de cárie incipientes para melhorar o diagnóstico desta condição. Foi demonstrado que nanopartículas de ouro (AuNP e AuNR) são efetivas como OCAs de lesões incipientes de cárie. Os métodos de espectroscopia e imagem retroespelhada podem ser exploradas na avaliação do tecido dentário. Em adição, a imagem por OCT promove não apenas maiores detalhes sobre rugosidade e alterações ópticas no esmalte, como também proporciona um monitoramento das lesões de cáries incipientes.

Palavras-chave: espectroscopia terahertz. tomografia de coerência óptica. lasers. nanopartículas metálicas.

ABSTRACT

The aim of the present study was to evaluate the sound and carious dental tissue structures by Terahertz Time-Domain Spectroscopy (THz-TDS), Optical Coherence Tomography (OCT) and random fiber laser in backscattering configuration in the near infrared (NIR - RFL). Thereby, laboratory experiments were carried out with freshly extracted human and bovine teeth. A THz-TDS configuration was developed in the transmission mode, based on the femtosecond infrared laser (central wavelength at 820 nm, repetition rate of 76 MHz and pulse width of 150fs) and photoconductive antennas. As a result of characterization, the absorption coefficient of wet dentin from 0.1 to 1.0 THz was higher than that of dry dentin. The presence of tissue damage in the dental tissue reduces the absorption coefficient, as well as the refractive index values. In sequence, a backscattering imaging method based on near infrared with a random fiber laser was created to provide a high contrast optical image between healthy and carious tissue. The contrast was 0.70, more than 8 times greater than the contrast on the radiographic image. Optical Coherence Tomography studies employed Callisto system (Thorlabs Inc, New Jersey, USA), which operate a spectral domain with 930 nm central wavelength. Its first application was analyzed on enamel surfaces irradiated with Er,Cr:YSGG laser (Biolase Technology Inc., USA), emitting 2.78 μm with a frequency of 20 Hz in three different level configurations, compared to the control group with conditioning with 37% phosphoric acid. A laser irradiation promotes rough surfaces in all parameters used, and an OCT analysis showed greater optical changes in the groups irradiated by laser when compared to the control. A second analysis was performed using gold spherical nanoparticles (AuNP) and gold nanorods (AuNR) as optical contrast agents (OCAs) comparing with glycerol in OCT images of incipient caries lesions to improve the diagnosis of this condition. Gold nanoparticles (AuNP and AuNR) have been shown to be effective as OCAs for incipient carious lesions. Spectroscopy and backscattering imaging methods can be explored in the evaluation of dental tissue. In addition, an OCT image promotes not only greater details about roughness and optical changes on enamel, but also provides monitoring of incipient caries lesions.

Keywords: terahertz spectroscopy. optical coherence tomography. lasers. metal nanoparticles.

SUMÁRIO

1 INTRODUÇÃO

A topografia da anatomia dental é complexa e desafiadora. Assim também é a macromorfologia (seu arranjo nas superfícies lisas e irregulares), micromorfologia e composição química de cada estrato: o esmalte eminentemente inorgânico, a dentina em estrutura colagenosa significativa. Frente às condições supracitadas, em adição a fatores como o desequilíbrio ecológico do biofilme, dieta, susceptibilidade, hábitos de higiene oral e o tempo; a cárie dentária constitui a alteração de principal interesse no âmbito de saúde bucal. Caracteriza-se pela perda mineral progressiva do tecido dentário, sendo a cavitação o estágio terminal da doença (GOMEZ, 2015). O contexto crítico do processo de desmineralização é o maior impacto na tomada de decisão, uma vez que a identificação tardia dessas lesões implica na necessidade de intervenção restauradora, consequentemente resultando em uma maior perda tecidual (FEJERSKOV,2004).

Em faces livres, a composição e o fluxo salivar facilitam na lixiviação do biofilme, que poderiam favorecer o desenvolvimento de desmineralizações em superfícies lisas. Contudo, a presença de restaurações, preparos protéticos e bráquetes ortodônticos podem propiciar a desmineralização. Este último, por sua vez, é parte fundamental do tratamento ortodôntico e deve permanecer bem fixado ao dente durante toda a terapia, o que requer uma adesão eficaz. Para isso, o ácido fosfórico representa o condicionador de esmalte padrão na prática ortodôntica, cujo objetivo é criar uma superfície irregular que propicie a ligação adequada dos sistemas adesivos (HORIUCHI *et al*., 2012).

Em superfícies irregulares, tais como as áreas de cicatrículas e fissuras, a detecção de uma lesão cariosa se torna mais difícil em seus estágios iniciais, sendo frequentemente subdiagnosticadas, visto que os prismas de esmaltes apresentam distribuição espacial não homogênea, como exemplo em áreas de cúspide onde há maior densidade, conteúdo mineral e dureza (ITO *et al.*, 2016), desafiando o diagnóstico no exame visual e em imagens bidimensionais por sua sobreposição inerente.

Tradicionalmente, os meios de diagnóstico em Odontologia são conseguidos a partir da inspeção visual, tátil e dos exames por imagem (radiografias

convencionais, digitais e tomografias computadorizadas) (FEJERSKOV,2004; 2015). O exame clínico é soberano e os meios complementares confirmam as hipóteses geradas de forma a orientar a tomada de decisão. Entretanto, por se tratar de uma condição autolimitante, a cárie dentária transita num contínuo estágio de ganhos e perdas minerais. Em adição, as lesões cariosas apresentam características únicas de configuração e propagação de acordo com a variedade de locais anatômicos em que ocorrem. Essa questão suscita problemáticas intrínsecas, tais como: o emprego inadequado de sondas exploradoras no exame tátil e a questionável sensibilidade das radiografias convencionais que emitem radiação ionizante, quando o aspecto visual não identifica a lesão subclínica.

O manejo adequado da estrutura dentária norteará seu plano de tratamento e o prognóstico, aumentando, assim, a probabilidade de sucesso terapêutico. Nesse sentido, o emprego de tecnologias ópticas para uma detecção cada vez mais precisa de forma não destrutiva têm sido analisado por pesquisadores e clínicos, a saber: tomografia de coerência óptica, espectroscopia Raman e Raman próximo, microscopia confocal *in situ*, autofluorescência (SON, 2016), transiluminação (CHUNG *et al*., 2011), e a radiação TeraHertz (AMAECHI, 2009).

Essa preocupação em melhor caracterizar o tecido dentário têm despertado o interesse de pesquisas com a tecnologia TeraHertz (THz = 10^{12} Hz). A radiação TeraHertz, também conhecida como ondas THz, luz THz ou Raios -T, está incluída no intervalo de freqüências entre o infravermelho e microondas, ou seja, encontra-se na transição de duas regiões espectrais envolvendo tecnologias diferentes – óticas e eletrônicas - na faixa entre 0,1 e 10 THz, trazendo desafios tecnológicos para o desenvolvimento de fontes e sensores de radiação (AMAECHI,2009; KAMBUROGLU 2014;2019).

Esta radiação é facilmente transmitida através de muitos meios materiais não metálicos e não polares, portanto são capazes de “enxergar” através de barreiras como: roupas, sapatos, bolsas, malas, etc. Metais refletem completamente esta radiação. Materiais não polares líquidos também apresentam transmissividade nestas freqüências, enquanto líquidos polares como a água são altamente absorvedores. Algumas características são muito adequadas para o uso da banda espectral do THz na Odontologia. Sua energia de fótons é muito baixa e, portanto, não representa perigo de ionização para tecidos biológicos. O nível de energia de 1

THz, por exemplo, é de apenas 4,14 milieletrovolts (meV), inferior à energia emitida pelos raios X (0,12 a 120 kiloeletrovolts (keV), portanto, não representa um risco de ionização (SUN *et al*.,2011).

Esta natureza não ionizante é uma propriedade crucial. Ademais, é muito sensível ao teor de água. Assim, as ondas de THz podem proporcionar um melhor contraste para os tecidos moles, quando comparado aos tradicionais raios-X (SUN *et al*., 2011). A energia vibracional das moléculas que reside na banda espectral do THz exibem diferentes características, que podem ser aplicadas para distinguir diferentes estratos teciduais, como a anatomia dental (BEARD *et al.,* 2002).

Ainda no âmbito das tecnologias ópticas emergentes, especula-se que a aquisição de imagens com base na fonte de luz de infravermelho próximo (NIR) revela como características maior sensibilidade, utilizando radiação não ionizante, de forma não destrutiva e de fácil manuseio, o que o torna adequado como uma ferramenta na Odontologia (YANG *et al*., 2018).

Os lasers aleatórios (Random Laser - RL), são fontes ópticas cujas emissões coerentes são capazes de se propagar em várias direções a partir de uma luz laser convencional. Esta, por sua vez é criada a partir de espelhos de forma unidirecional. Nesse processo, a luz convencional incide sobre um material com propriedades ópticas especiais, ou seja, capaz de absorver, emitir e espalhar a luz de maneira desordenada. Os lasers aleatórios foram demonstrados pela primeira vez de forma preliminar em 1994 (LAWANDY *et al.,* 1994) e, desde então, seu desenvolvimento, características e diversas aplicações têm sido revisados. Uma das características mais interessantes do RL está atribuída a capacidade de atenuar “manchas” (speckles) comumente presentes em meios ópticos convencionais, tais como fontes de luz laser convencional, a partir de pontos luminosos que ofuscam uma imagem obtida.

Assim, ao ser transmitida de forma aleatória, esses pontos são sobrepostos e calculados por uma média a fim de fornecer uma imagem mais nítida (HOKR *et al.,*2016). Do ponto de vista da interação da luz com os tecidos, o esmalte possui alta transmitância e a dentina possui alta refletividade na região NIR. Já a perda mineral causada pela cárie dentária leva a um aumento no espalhamento de fótons em todas as direções, incluindo o refletor, denotando as diferenças identificadas em uma imagem por RL-NIR.

Além disso, os lasers aleatórios possuem como propriedade o alto brilho e a alta densidade espectral, que são úteis para melhorar o desempenho da imagem, superando o desempenho de diodos emissores de luz, lasers em linha estreita e radiografias, além do baixo custo, vantagens desejáveis para detecção de estruturas dentárias e atividade de lesões cariosas (REDDING *et al*.,2012).

Vale salientar que inexiste um método capaz de monitorar o comportamento das lesões cariosas no que tange ao estágio e atividade da doença baseado no estado hígido do dente. Com o aprimoramento de pesquisas que sobrepujassem o obstáculo da interpretação subjetiva em radiografias, a tomografia de coerência óptica (OCT) surgiu nas últimas décadas como um método óptico em outros campos da saúde e hoje traz na literatura científica diversas aplicabilidades, incluindo a detecção precoce de áreas desmineralizadas (FRIED et al., 2002; AMAECHI, 2009; POPESCU et al.,2009; MANDURAH et al.,2013; ITO et al.,2016). É uma técnica não invasiva e não ionizante baseada na interferometria de baixa coerência, que utiliza uma fonte de luz que produz imagens transversais e tridimensionais de tecidos biológicos em profundidades de até 2 mm com uma resolução espacial de 5-15 μm no comprimento de onda da faixa do infravermelho próximo (NIR) (ZAGAYNOVA *et al.*, 2008; ITO *et al*., 2016; BRAZ *et al.,* 2012). O método é baseado em medidas quantitativas da intensidade da luz retroespalhada como uma função da profundidade na região de interesse.

O OCT propicia a análise de faces livres de esmalte, tais como as irradiadas com laser. A irradiação com laser têm atraído cada vez mais atenção desde sua primeira aplicação em 1964 (STERN, SOGNNAES,1964). Entre os lasers de alta potência mais usados para aplicações odontológicas está o laser Er,Cr:YSGG, que emite a 2,78 μm e é fortemente absorvido nos tecidos duros devido à sua interação com a água e íons hidroxila da hidroxiapatita na interface tecidual. Considerando que o tratamento ortodôntico geralmente é de longa duração, outra vantagem promovida pela irradiação com laser Er,Cr:YSGG é o efeito protetor duradouro contra cárie secundária, essencial para a prevenção de lesões da mancha branca que podem ocorrer ao redor dos braquetes durante o procedimento ortodôntico (QUINTO *et al*.,2017). Este fenômeno ocorre pela absorção pela hidroxiapatita e pela água, que altera a estrutura prismática do esmalte, tornando-o ácido resistente.

No entanto, o OCT como técnica óptica de geração de imagens possui como inconveniente a profundidade de escaneamento em tecidos mineralizados devido à natureza altamente dispersante dos tecidos biológicos. Para melhoria da qualidade de imagens da OCT *in situ*, tem sido exploradas pesquisas com agentes de contraste óptico, cujo objetivo base é o de modificar as propriedades de espalhamento da amostra (BRAZ et al., 2012). Tradicionalmente, a água e fluidos como o glicerol, são utilizados para influenciar as imagens no OCT (FRIED 2005; KANG *et al.,* 2016), podendo melhorar significativamente a visibilidade de estruturas como a junção dentina-esmalte e lesões cariosas, pois permitem uma penetração mais profunda da luz. Sendo assim, uma serie de soluções têm sido testadas com o objetivo de aprimorar imagens obtidas pelo OCT, dentre elas as nanopartículas de ouro têm se mostrado eficientes agentes de contraste para imagens ópticas de tecidos biológicos (ZAGAYNOVA *et al.*, 2008).

Assim, também cresce o uso de nanopartículas de ouro na área de bioimagem, pois proporcionam um melhor retroespalhamento da luz devido à sua forte absorção e dispersão derivada de uma intensa ressonância plasmônica de superfície localizadas na região do infravermelho próximo (NIR). Além disso, apresentam uma baixa toxicidade, excelente estabilidade coloidal e são de fácil síntese (JAIN *et al.*, 2006). As características das nanopartículas, como tamanho, forma e propriedades dielétricas vão influenciar as propriedades ópticas permitindo ajustes em tamanho e forma (YEH; CRERAN; ROTELLO, 2012).

Diante do exposto, o objetivo do presente trabalho foi caracterizar estruturas teciduais dentárias por espectroscopia de Terahertz no domínio de tempo (THz-DT) e por imageamento por retroespalhamento com laser aleatório em fibra por infravermelho próximo (NIR-RFL). Em seguida, analisar por meio de tomografia de coerência óptica os efeitos promovidos pelo laser Er,Cr:YSGG na superfície de esmalte, assim como identificar o potencial de nanopartículas de ouro como agentes de contraste óptico em cárie incipiente de dentes posteriores.

2 METODOLOGIA

Para facilitar a compreensão das metodologias empregadas no presente trabalho, os procedimentos experimentais foram organizados na forma de estudos, de acordo com a construção dos artigos científicos, a saber:

2.1 Estudo 1 - Caracterização das estruturas dentárias por Espectroscopia TeraHertz no Domínio de Tempo (THz-DT).

2.1.1 Considerações Éticas

A presente pesquisa foi realizada após a aprovação do projeto de pesquisa pelo Comitê de Ética em Pesquisa com Seres Humanos do CCS/UFPE (CAAE: 95310418.0.3001.5203).

2.1.2 Tipo e Local de estudo

Foi realizado um estudo experimental laboratorial *ex vivo* utilizando dentes permanentes humanos no laboratório de Fotônica e Biofotônica do Departamento de Física da Universidade Federal de Pernambuco (UFPE).

2.1.3 Seleção da amostra

Foram selecionados 15 dentes humanos recém-extraídos, configurando dentes anteriores e posteriores, doados por pacientes submetidos a exodontias em situações que impossibilitavam a manutenção destes na cavidade bucal, obtidos no banco de dentes humanos da Centro Universitário Tabosa de Almeida (ASCES-UNITA). Os dentes foram selecionados de acordo com os critérios abaixo.

Critérios de Inclusão:

Dentes permanentes anteriores e posteriores com superfícies íntegras, podendo apresentar manchas brancas e/ou amarronzadas, com ou sem lesões cariosas cavitadas em superfícies lisas e/ou proximais.

Critérios de Exclusão:

Dentes restaurados e tratados endodonticamente; com facetas de desgaste oclusal; desgaste erosivo, com fraturas coronorradiculares, reabsorções radiculares e demais situações que impossibilitassem inspeção pelo dispositivo TeraHertz.

2.1.4 Preparo da amostra

Todos os tecidos aderentes e sangue foram removidos em água corrente. Os dentes foram debridados com Curetas Periodontais Gracey (HuFriedy®) para a remoção de restos de ligamento periodontal, em seguida polidos com auxílio de escova de Robinson acoplada em micromotor e contraângulo com detergente neutro, lavados com água corrente durante 2 minutos e em seguida, mantidos por 7 dias em solução de Cloramina-T à 0,5%. Após descontaminação, os espécimes foram armazenados em caixa plástica com água deionizada (4ºC) durante 7 dias para manutenção da hidratação dos mesmos de acordo com norma ISO (International Standartization Organization) 11450:2015.

2.1.5 Seccionamento dos espécimes e composição dos grupos

Os dentes foram submetidos à secção coronorradicular no sentido mesiodistal com disco diamantado dupla face (Buehler Ltda., Lake Bluff, IL, EUA) acoplado a uma cortadeira de precisão (Isomet 1000 Speed Saw, Buehler Ltda., Lake Bluff, IL, EUA) e refrigerado a água em baixa rotação (200 rpm). A padronização de espessura (2,0 mm ± 0,2mm) foi controlada com auxílio de um paquímetro digital (Digimatic Caliper, Mitutoyo®, Tokyo, Japan). Ao final, os espécimes foram submetidos a banho em cuba ultrassônica com água deionizada para remoção dos debris e resíduos de godiva (Ultrasonic Cleaner® - Odontobrás, Riberão Preto, SP, Brasil) durante 10 minutos, a uma temperatura de 47ºC, sendo novamente acondicionados em água deionizada à 37°C até o início da caracterização pelo THz (Figura 01).

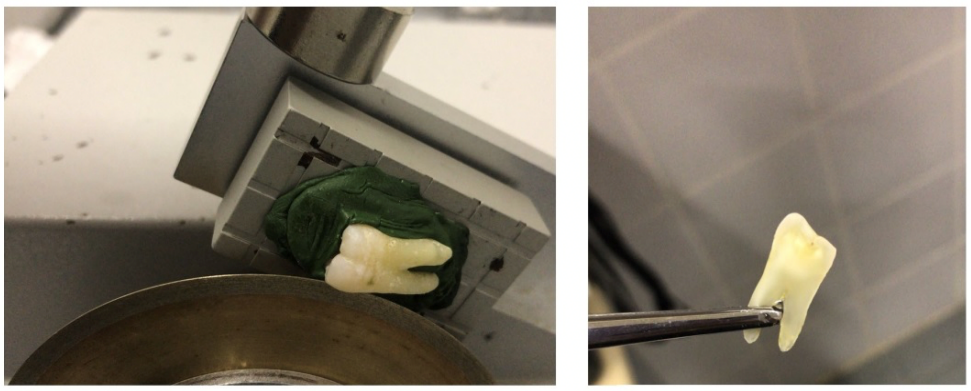

(a) (b)

Figura 1. (a) Sistema para seccionamento dos dentes; (b) Dente seccionado.

Após a análise em estereomicroscópio (Stemi2000; Carl Zeiss, Jena, Alemanha) com aumento de 20X, foram conseguidas 20 fatias dentárias de acordo com os seguintes estratos: esmalte, dentina e cárie em dentina e esmalte de modo a dividir as amostras em grupos (G1, N=10; G2, N=6; G3, N=4).

2.1.6 Espectroscopia THz no Domínio de Tempo (THz-TDS)

O sistema de THz-TDS construído no laboratório de Fotônica é mostrado na Figura 2. A técnica empregada neste trabalho para gerar radiação na faixa do THz foi baseada no uso de antenas fotocondutoras, cuja estrutura básica é composta por metal-semicondutor- metal, juntamente com uma fonte de luz pulsada. No presente trabalho foi utilizado um Laser pulsado (Ti:Safira) com comprimento de onda em torno de 820 nm, taxa de repetição de 76 MHz e com pulsos com largura temporal de 150 fs. As antenas fotocondutoras foram obtidas da *Batop Optoelectronics* (IPCA-21-05-1000-800-h), tendo como substrato o Arseneto de Gálio (GaAs) (Batop Optoelectronics, 2018).

A geração de sinal de THz consiste em direcionar a radiação do laser sobre a antena fotocondutora. O laser de femtossegundo é dividido em dois feixes: um para excitar o substrato presente na antena de emissão, gerando o sinal THz, e outro usado para excitar a antena de deteção. Para que o sinal THz seja detectado, é necessário que o sinal THz chegue ao mesmo tempo que o feixe do laser nesta

antena. Logo, é utilizado um atraso óptico variável no caminho do feixe de excitação. Para criar a linha de atraso entre o pulso de emissão e o pulso de detecção, um conjunto de espelhos planos acoplados a um motor de passos da Thorlabsâ foi utilizado. O sinal medido no detector é proporcional à magnitude e ao sinal do pulso THz em cada instante de tempo. Dessa forma, a variação do atraso temporal (Δt) entre a emissão e a detecção dos pulsos ópticos pode mapear todo o perfil temporal do pulso THz, como mostra a Figura 3.

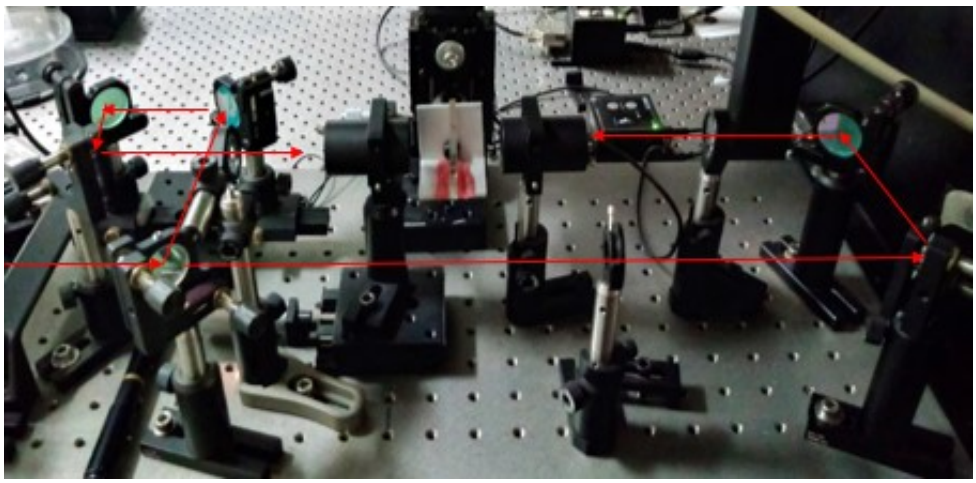

Figura 2. Amostra dental posicionada entre as antenas fotocondutivas em dispositivo THz construído no laboratório de fotônica e biofotônica UFPE.

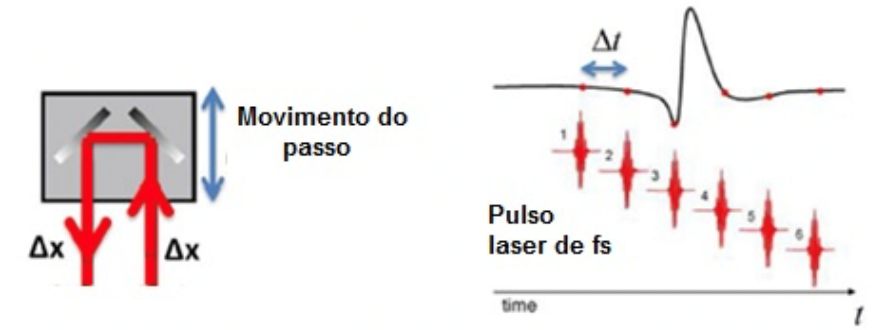

Figura 3. Atraso temporal. Fonte adaptada do estudo de DADRASNIA, 2015

No emissor THz, uma tensão de polarização é aplicada (tensão de pico de 15V, 1KHz), direcionando os portadores (elétrons e buracos) para os eletrodos da antena. A corrente transitória na antena fotocondutora impulsiona a geração de radiação de pulso THz. No detector terahertz, sem tensão de polarização, também é aplicado um pulso óptico para gerar portadores de carga no substrato da antena. A radiação THz incidente promove um deslocamento de carga na antena e, portanto, uma fotocorrente de saída é gerada com magnitude proporcional à amplitude do

campo terahertz do incidente. O sistema THz-TDS foi definido com dois caminhos ópticos: os braços de geração e detecção de pulso, como mostrado na figura 4. Uma potência de laser média de 62,5 mW foi aplicada em cada antena. Após a geração do pulso THz, uma lente de colimação de silício e uma lente de polimetilpenteno (f = 30 mm) foram usadas para focalizar a radiação THz na estrutura dentária. A onda THz foi focada em uma área de 5 mm de diâmetro da amostra. Um par de lentes semelhante foi usado para coletar a radiação THz transmitida. A figura 2 ilustra também a amostra colocada entre as lentes THz. Para medir a radiação THz transmitida, um amplificador lock-in foi explorado (SR810, ThinkSRS, Zurich Instruments, Alemanha). Durante a caracterização, as fatias foram posicionadas entre duas placas de alumínio de 5cm X 5 cm cuja porção central é perfurada em formato circular com diâmetro de 6mm.

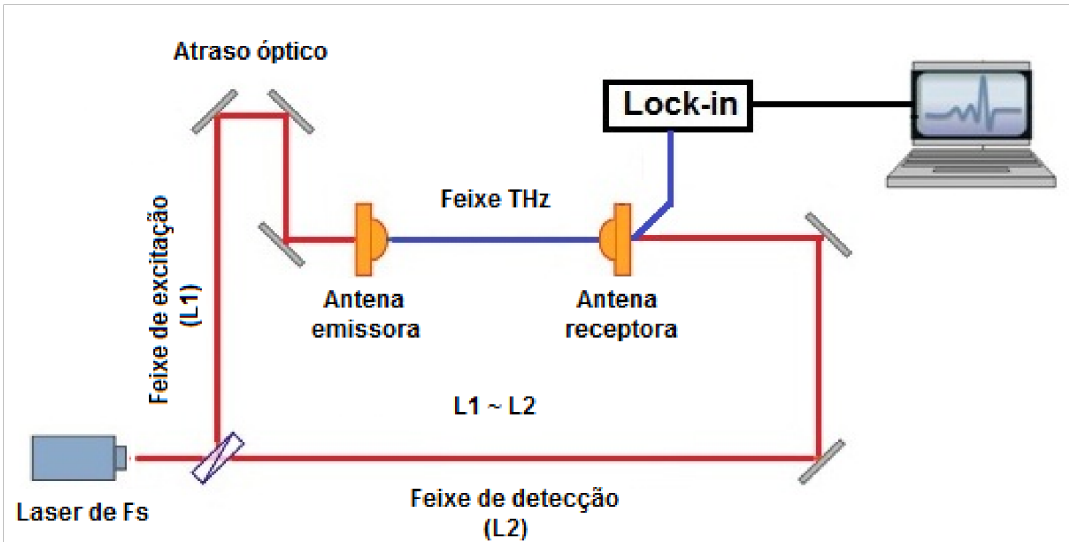

Figura 4 - Esquema do sistema desenvolvido para geração e detecção do sinal THz.

2.1.6.1 Coeficiente de Absorção

Quando a radiação eletromagnética atravessa uma amostra, determinadas frequências podem ser absorvidas, promovendo os átomos, íons ou moléculas que a compõe do seu estado fundamental para um ou mais estados energéticos excitados. De acordo com a teoria quântica, para que a absorção da radiação ocorra, a energia do fóton de excitação deve ser idêntica à diferença de energia entre o estado

fundamental e um dos estados excitados da espécie absorvente. Já que estas diferenças são características de cada espécie, uma análise das frequências da radiação absorvidas constitui uma forma de caracterização dos componentes de uma amostra (LEE,2009).

A análise da amplitude da onda THz transmitida pela amostra é utilizada para determinar o coeficiente de absorção. Quando se determina a potência do sinal em função da frequência THz, a região avaliada apresenta um pico de absorção específico. Para determinar a absorbância do estrato tecidual em função da frequência THz utilizar-se-á a seguinte relação:

$$\alpha(f) = \frac{1}{d}.\ln\left(\frac{A_{amostra}}{A_{referência}}\right)$$

Neste caso α é coeficiente de absorção, f é a frequência THz, $A_{amostra}$ corresponde a amplitude do sinal da amostra, $A_{referência}$; corresponde a amplitude do sinal de referência e ln o logaritmo natural.

2.1.6.2 Índice de Refração

Fisicamente, o índice de refração (η) é determinado pela razão entre a velocidade da luz no vácuo (ou no ar) e a velocidade da luz no meio, e é sempre maior que 1. É proporcional à densidade das células e da estrutura da célula. Assim, o índice de refração é o resultado da razão entre o aumento no comprimento do caminho óptico induzido pela amostra e sua real espessura, devido à variação da velocidade da luz no meio (MENG et al., 2009).

Ao propagar pela amostra, o pulso do sinal THz sofre um deslocamento temporal na ordem de picossegundos (ps) em relação ao pulso de referência (pulso não propagado na amostra) . Este deslocamento está diretamente relacionado com o índice de refração do material. Assim, o índice de refração dos estratos teciduais do presente estudo, a saber: esmalte, dentina, lesão cariosa; foi determinado pela seguinte expressão:

$$n(f) = 1 + \frac{(\phi_s - \phi_{air})c}{2\pi f d}$$

Onde c é a velocidade da luz no vácuo, ϕ_s e ϕ_{ar}são as fases do feixe THz

após a propagação pela amostra e pelo ar, d é a espessura do material e f a frequência THz. Desta forma, a fase do sinal é o indicativo primordial para o cálculo desta propriedade.

2.1.7 – Análise das amostras

Inicialmente, logo após o processo de fatiamento, as amostras foram armazenadas em água deionizada e medidas no estado úmido para tomada dos primeiros espectros. Em seguida, foram levadas para secagem em uma estufa biológica modelo 515 B (Fanem/Guarulhos-SP-Brasil) por um período de 24 horas a uma temperatura de 37º C com 100% de umidade relativa para tomada de novos espectros agora em estado seco. É possível constatar que, de acordo com a hidratação da amostra, existe uma absorção de THz específica, possibilitando a quantificação desta propriedade de uma maneira não-invasiva (KAMBUROGLU et al., 2014).

Os dados foram analisados descritivamente através de medidas: média e desvio padrão (média ± DP) para as variáveis numéricas. A margem de erro utilizada nas decisões foi de 5% e os intervalos foram obtidos com 95% de confiança.

2.1.8 Hipóteses

2.1.8.1 Hipótese Nula (H0)

Não será possível observar diferenças estruturais entre as bandas do espectro TeraHertz entre os grupos analisados.

2.1.8.2 Hipótese Alternativa (H1)

O dispositivo TeraHertz medirá um coeficiente de absorção e um índice de refração específico para cada estrato dentário, possibilitando a quantificação desta propriedade de uma maneira não-invasiva.

2.2 Estudo 2 - Imagem dental de alto contraste por retroespalhamento usando um laser aleatório em fibra a partir de radiação por infravermelho próximo

2.2.1 Considerações Éticas

A presente pesquisa foi realizada após a aprovação do projeto de pesquisa pelo Comitê de Ética em Pesquisa com Seres Humanos do CCS/UFPE (CAAE: 95310418.0.3001.5203).

2.2.2 Tipo e Local do Estudo

Foi realizado um estudo experimental laboratorial *ex vivo* utilizando 5 dentes permanentes humanos. A construção do dispositivo e coleta das imagens foram desenvolvidas no Centro de Pesquisa em Fibra Óptica, pelo Laboratório de Detecção e Comunicação de Fibra Óptica, da Universidade de Ciência e Tecnologia Eletrônica da China (Chengdu, China), onde foram realizadas as imagens retroespalhadas a partir do laser aleatório em fibra por infravermelho próximo. O preparo dos espécimes, bem como a análise das imagens obtidas foram realizados no laboratório de Fotônica e Biofotônica do Departamento de Física da Universidade Federal de Pernambuco (UFPE, Recife-Brasil).

2.2.3 Seleção e preparo das amostras

O preparo amostral partiu do mesmo protocolo estabelecido no estudo 3.1. Os dentes foram identificados com uma área hígida ou de lesão cariosa no esmalte e / ou dentina. O exame total de 5 fatias da superfície dos dentes revelou uma distribuição de áreas cariosas e saudáveis dos dentes da amostra estudada.

2.2.4 Configuração Experimental – Laser Aleatório em Fibra de Infravermelho Próximo (NIR-RFL)

A configuração experimental que consiste na fonte de luz e a parte da imagem, é ilustrado na Figura 5. O RFL é gerado através de uma estrutura semi-aberta composta por um espelho de loop de fibra (isto é, formado a partir de um acoplador 3dB) e uma fibra de modo único (SMF) de 25 km de comprimento. Uma fonte de excitação Raman com comprimento de onda central de 1455 nm é injetada

na SMF através de um multiplexador de divisão de comprimento de onda de 1455/1550 nm (WDM 1). Outro WDM, WDM2, é usado no final do SMF para separar a luz residual da excitação e garantir que apenas a luz gerada pelo RFL seja injetada na parte da imagem. Um isolador (ISO) é usado para eliminar a reflexão da luz, garantindo que o laser seja gerado apenas através da dispersão de Rayleigh distribuída aleatoriamente. Para ajustar a luz de saída na potência apropriada para geração de imagens, é usado um atenuador óptico variável (VOA). Para comparação, uma fonte de luz com emissão espontânea amplificada (ASE) baseada em fibra dopada com érbio e um laser de largura de linha estreita (NLL) de 1550 nm também são usados separadamente para substituir o RFL para geração de imagens.

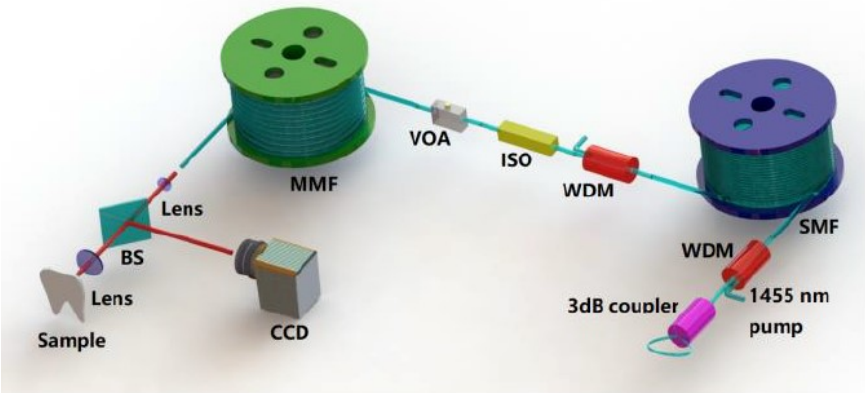

Fig 5. Esquema da configuração experimental. WDM, multiplexador de divisão de comprimento de onda. SMF, fibra monomodo. ISO, isolador. VOA, atenuador óptico variável. MMF, fibra multimodo. BS, separador de feixe. Imagem do dispositivo construído no Laboratório de Detecção e Comunicação de Fibra Óptica, da Universidade de Ciência e Tecnologia Eletrônica da China (Chengdu, China)

Para criação das imagens, empregou-se uma configuração de retroespalhamento. Uma fibra multimodo (MMF) é emendada após o VOA e antes do sistema de imagem para reduzir a coerência espacial da fonte de luz. A luz da MMF foi colimada pela lente 1 (com distância focal de 6,2 mm) e direcionada por um divisor de feixe para a amostra. A luz refletida da amostra é colimada pela lente 2 (distância focal de 120 mm) e direcionada pelo divisor de feixe para o CCD (Xenics, Bobcat-640GigE).

2.2.5 Hipóteses

2.2.5.1 Hipótese Nula (H0)

Não será possível observar diferenças estruturais entre as áreas hígidas e cariadas do esmalte e dentina a partir do RFL-NIR.

2.2.5.2 Hipótese Alternativa (H1)

A imagem por RFL promoverá um maior contraste entre estruturas hígidas e cariadas, quando comparada a outras fontes, traçando o perfil de uma nova ferramenta de diagnóstico na Odontologia.

2.3 Estudo 3 - Avaliação da superfície do esmalte condicionado por laser Er,Cr:YSGG para fins ortodônticos através de Tomografia de Coerência Óptica

3.3.1 Considerações Éticas

A presente pesquisa foi realizada após a aprovação do projeto de pesquisa pelo Comitê de Ética em Experimentação Animal do CEUA/UFPE (CAAE: 230760158692015/65).

3.3.2 Tipo e Local de estudo

Foi realizado um estudo experimental laboratorial *ex vivo* utilizando 40 dentes bovinos desenvolvido no Instituto de Pesquisas Energéticas e Nucleares da Universidade de São Paulo (IPEN/USP), onde foram realizados: irradiação com laser Er,Cr:YSGG e análise com Microscópio Eletrônico de varredura (MEV). O preparo das amostras e o escaneamento pela Tomografia de Coerência Óptica foram realizadas no laboratório de Fotônica e Biofotônica do Departamento de Física da Universidade Federal de Pernambuco (UFPE). O ensaio mecânico cisalhamento foi realizado no laboratório de engenharia mecânica pela UFPE.

3.3.3 Seleção da amostra

Os procedimentos para a preparação da amostra estavam de acordo com as especificações da ISO / TS 11405: 201511. Logo, 45 incisivos bovinos recémextraídos foram selecionados e armazenados em solução de cloramina-T a 0,5% durante 48 horas para desinfecção. A porção radicular de todos os dentes foi removida e as coroas tiveram sua superfície bucal polida manualmente com lixa P600 (3M Unitek, EUA) para reduzir os sulcos apresentados no esmalte bovino. As amostras foram incluídas em um suporte cilíndrico e embebidas em resina acrílica, mantendo a superfície bucal paralela à base do molde. As amostras foram armazenadas em água destilada (4ºC) até os procedimentos de colagem. Eles foram distribuídos aleatoriamente em quatro grupos experimentais (n = 10), conforme Tabela 1.

Tabela 1. Desenho experimental considerando como principais fatores: sistema adesivo, substrato e condições de condicionamento da superfície

Condições de condicionamento da superfície	Substrato	Sistema Adesivo
Grupo I: Condicionamento com ácido fosfórico 37%	Esmalte	Primer + sistema adesivo Transbond XT
Grupo II: irradiação com laser Er,Cr:YSGG (1,1W)	Esmalte	Primer + sistema adesivo Transbond XT
Grupo III: irradiação com laser Er,Cr:YSGG (1,7W)	Esmalte	Primer + sistema adesivo Transbond XT
Grupo IV: irradiação com laser Er,Cr:YSGG (2,41W)	Esmalte	Primer + sistema adesivo Transbond XT

Para o grupo controle, o condicionamento foi realizado com um gel de ácido fosfórico a 37% (FGM Produtos Odontológicos, Brasil) por 15 segundos, seguido de 15 segundos de enxágue com água. As amostras foram secas ao ar até obter uma aparência esbranquiçada. A resina Transbond XT foi escolhida devido ao seu alto índice de resistência ao cisalhamento obtido em diversos estudos (REYNOLDS,1975; TANAKA *et al*., 2013; TADINADA *et al*., 2016).

2.3.4 Laser de Er,Cr:YSGG

A irradiação foi realizada com um laser de Er,Cr:YSGG (Biolase Technology Inc., EUA), emitindo um comprimento de onda de 2,78 μm com frequência de 20 Hz e a largura do pulso de aproximadamente 140 μs por 15 segundos, em três configurações de potência diferentes (Figura 6 e Tabela 2). Uma ponta de safira MZ6 de 600 μm de diâmetro e 6 mm de comprimento foi utilizada com 55% de ar e 45% de líquido de refrigeração. Durante a irradiação, as amostras foram posicionadas em um tradutor motorizado de alta precisão (Newport, EUA), a 1 mm da ponta do laser, ajustado a uma velocidade de 3,8 mm / s, padronizando a condição de irradiação.

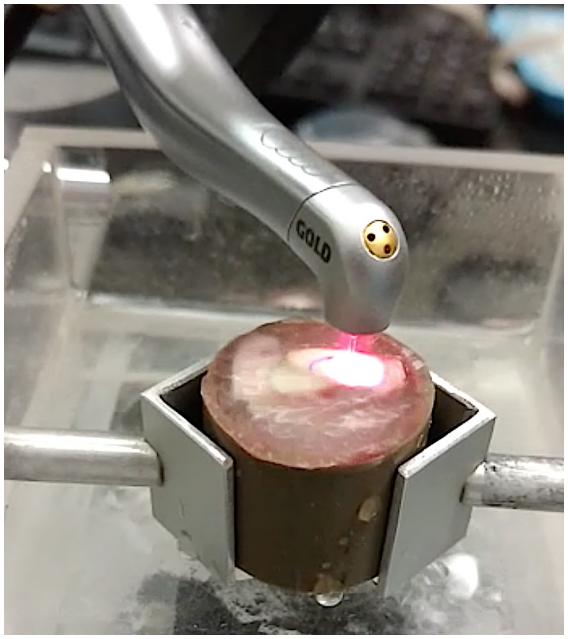

Figura 6. Irradiação das Amostras. Laboratório IPEN/USP.

Table 2. Parâmetros utilizados pela irradiação a laser

Grupo	Potência (W)	Energia por pulso (mJ)	Densidade de Energia (J/cm^2)
II	1,1	54,1	19,1
III	1,7	83	29,3
IV	2,4	120	42,4

Foram utilizados braquetes para os incisivos superiores com área base de 15,3 mm2 (Dental Morelli, Brasil). Os braquetes foram colados de acordo com as instruções do fabricante (Tabela 3) e posicionados no centro da superfície bucal para simular o procedimento clínico. O excesso de cimento ortodôntico foi cuidadosamente removido antes da fotopolimerização. A fotoativação foi realizada usando uma unidade de cura por LED emitindo 1.200 mW / cm2 (Bayswater, Austrália) por 10 segundos em cada lado proximal do suporte (mesial e distal).

2.3.5 Armazenamento e termociclagem

Após a colagem dos brackets, as amostras foram armazenadas submersas em água na estufa a 37ºC ± 1ºC por 24 horas. Em seguida, todas as amostras foram termocicladas (Ética Equipamentos Científicos S / A, Brasil). Foram realizados 500 ciclos de banhos alternativos (5-55 ± 2 ° C), 30 segundos em cada banho e 2 segundos de tempo de transferência. (Figura 7)

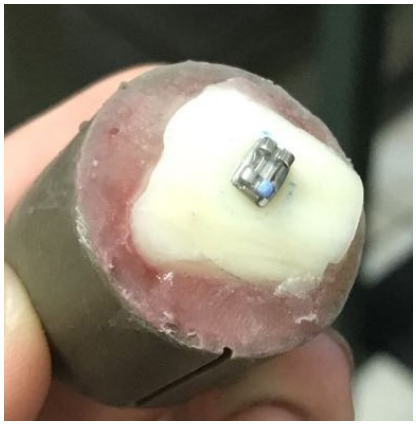

Figura 7. Amostras após colagem dos bráquetes

2.3.6 Ensaio de cisalhamento

As amostras foram preparadas para o teste de resistência ao cisalhamento (SBS), em uma máquina universal de testes (Emic Equipamentos Industriais Ltda, Brasil) (figura 8), com um cinzel à velocidade de 0,5 mm / min e célula de carga de 200 kgf. Para avaliar o SBS, o tamanho da base do suporte tem uma importância significativa, pois a força de sustentação aumenta em função da dimensão da área base. Portanto, os valores foram medidos considerando a resistência à ruptura e o tamanho da base do braquete. A força de cisalhamento (F) foi obtida em Newtons (N) e a força em megaPascal (MPa).

Após a descolagem, os dentes foram examinados sob um estereomicroscópio com ampliação de 20x (Zeiss, Alemanha) e classificados de acordo com o Índice de Remanescente Adesivo (ARI) 13:

- Pontuação 0 - nenhum resíduo adesivo deixado no dente;
- Escore 1 - menos de 50% de adesivo remanescente deixado no dente;
- Escore 2 - mais de 50% de adesivo remanescente no dente;
- Pontuação 3 - restante adesivo 100% deixado no dente.

Figura 8. Máquina de ensaio universal. Laboratório de engenharia mecânica, UFPE

2.3.7 Análise das amostras

2.3.7.1 Tomografia de Coerência Óptica

Todas as amostras foram submetidas à microscopia eletrônica de varredura (Hitachi, Japão) e tomografia de coerência óptica (OCT) antes e após o condicionamento com ácido ou laser. O sistema OCT (Thorlabs Inc, EUA) opera a 930 nm de comprimento de onda central, largura de banda espectral de 100 nm, potência máxima de saída de 5 mW, resolução axial de 7 / 5,3 µm (ar / água), resolução lateral de 8 µm, resolução máxima de imagem profundidade de 1,6 mm e taxa de varredura axial de 1,2 kHz, capturando dois quadros por segundo com 105 dB de sensibilidade. Imagens bidimensionais (2D) da OCT foram capturadas com 2000 colunas x 512 linhas e varredura transversal de 6 mm, enquanto imagens tridimensionais (3D) foram capturadas com colunas 400x400x400 em cada eixo XZ, YZ, XY. Essas duas técnicas se complementam na análise morfológica, devido às suas resoluções espaciais muito diferentes.

2.3.8 Análise estatística

Estatística descritiva, média e desvio padrão foram calculados para cada grupo. A análise estatística foi realizada usando o GraphPad Prism 6 (GraphPad Software, EUA). Múltiplas comparações foram realizadas para os valores de SBS entre os grupos usando ANOVA one-way e teste post hoc de Tukey. Para a avaliação do IRA, foi utilizado o teste do qui-quadrado. Foi adotado um nível de significância de 5%.

2.3.9 Hipóteses

2.3.9.1 Hipótese Nula (H0)

Não será possível observar diferenças estruturais entre os grupos analisados.

2.3.9.2 Hipótese Alternativa (H1)

A ação do laser Er:Cr;YSGG é capaz de condicionar a superfície do esmalte criando força adesiva suficiente e comparável ao já estabelecido método de condicionamento com ácido fosfórico.

2.4 Estudo 4 - Utilização de Nanoestruturas de Ouro como Agentes de Contraste Óptico para Análise de Cárie Incipiente em Tomografia por Coerência Óptica

2.4.1 Tipo e Local do Estudo

Um estudo laboratorial experimental *ex vivo* utilizando dentes humanos para avaliar cáries incipientes na Tomografia por Coerência Óptica com as nanopartículas e nanobastões de ouro como agente de contraste óptico.

A pesquisa foi realizada no Laboratório de Fotônica e Biofotônica do Departamento de Física da Universidade Federal de Pernambuco, que disponibilizou o aparelho de Tomografia por Coerência Óptica, o Microscópio Óptico com Luz Polarizada, assim como a confecção das nanopartículas de ouro.

2.4.2 Seleção da Amostra

Foram utilizados dentes molares permanentes com presença de manchas brancas e amarronzadas nas fossas e fissuras que se enquadram no critério 1 e 2 do Internacional Caries Detection and Assessment System (ICDAS). Foram excluídos os dentes que apresentavam cavidades de cárie ao exame visual, restaurações, abertura coronária ou tratamento endodôntico.

2.4.3 Preparo da Amostra

Molares permanentes com coroa íntegra (n=10) extraídos nos últimos 6 meses foram obtidos através do Banco de Dentes do Centro Universitário Tabosa de Almeida (ASCES-UNITA). Todas amostras foram descontaminadas com Cloramina T 0,5% e higienizados com escova de Robinson acoplada ao contra ângulo (GNATUS, São Paulo, SP, BR) e detergente neutro, sendo armazenadas em soro fisiológico para hidratação.

Utilizando uma matriz de metal previamente confeccionada e padronizada, os dentes tiveram suas raízes incluídas em blocos de resina acrílica transparente (Jet Clássico, São Paulo, SP, BR) sempre deixando livre a junção amelocementária. Isso permitiu o posicionamento em uma base de PVC específica para o escaneamento no OCT.

2.4.4 Nanopartículas esféricas e Nanobastões de Ouro

As nanopartículas esféricas de ouro (AuNP) foram produzidas e caracterizadas no Departamento de Física e Química da Universidade Federal de Pernambuco através do tratamento de tetracloroaurato de hidrogênio (HAuCl4) com polivinilpirrolidona (PVP -M_W @ 55.000) em água fervente, onde a PVP atua como agente estabilizante. As nanopartículas de ouro coloidal resultantes são esféricas e têm um tamanho de 2,0 ± 1,0 nm disperso em solução aquosa, e o pico de ressonância plasmônica é em 550 nm (BRITO-SILVA *et al.*, 2013). Os nanobastões de ouro (AuNR) foram adquiridos da Nanopartz™, com diâmetros de 50 nm e comprimento de 160 nm também dispersos em solução aquosa, com dois picos de ressonância plasmônica em 520 nm e 825 nm.

Com o objetivo avaliar se glicerol juntamente com as AuNP e AuNR aumentariam o coeficiente de atenuação, as soluções aquosas de nanopartículas e nanobastões foram diluídas em glicerol. Uma balança de precisão foi utilizada para a diluição na proporção de 50% do peso da solução contendo a AuNP com 50% de glicerol, a mesma proporção será utilizada para as AuNR.

2.4.5 Análise das Amostras

2.4.5.1 Tomografia por Coerência Óptica

O sistema de OCT selecionado para este estudo é um modelo comercial, o Callisto (Thorlabs Inc, Nova Jersey, EUA), operando no domínio espectral (SD-OCT). A fonte de luz utilizada é um diodo superluminescente com comprimento de onda central de 930 nm e largura de banda de 100 nm e potência máxima de saída de 3 mW. Este sistema possui um espectrômetro de alta velocidade de captura de dados, permitindo a geração de imagens transversais bi e tridimensionais, com resolução axial de 7/5,3 μm (ar/água) e resolução lateral de 8 μm e 1,6 mm de profundidade de penetração da luz no interior da amostra. As imagens foram capturadas na forma de matriz com 2000 colunas x 512 linhas e 400 colunas x 400 linhas, respectivamente. A frequência de varredura axial deste sistema é 1,2 kHz, o que permite a captura de duas imagens por segundo com 105 dB de sensibilidade (MOTA, 2014).

As amostras foram analisadas de forma padronizada, através do posicionamento em uma plataforma de PVC com uma marcação linear coincidindo com a marcação da plataforma da mesa do OCT (Figura 9). Esse posicionamento foi averiguado e registrado e serviu de controle para saber se foi reposicionado corretamente.

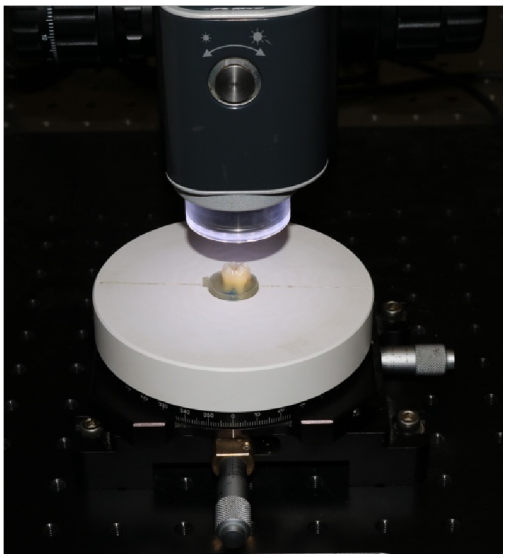

Figura 9. Base de PVC para posicionamento no OCT

Cada amostra foi analisada num total de 6 vezes, além do controle negativo (1) com cinco diferentes agentes de contraste óptico (ACO). Um dos ACO foi o glicerol puro como controle positivo (2). Os outros ACOs foram: (3) nanopartículas esféricas de ouro (AuNP) dispersa em água (HAuCl4 · 3H2O); (4) AuNP dispersas em água e diluída em 50% de peso de glicerol; (5) nanobastões (AuNR) disperso em água (HAuCl4 · 3H2O); (6) (AuNR) disperso em água e diluído em 50% de peso de glicerol (Tabela 3).

Tabela 3: Distribuição dos grupos

GRUPO	AGENTE DE CONTRASTE
G1	Controle negativo
G2	Glicerol
G3	AuNP + água
G4	AuNP + água + glicerol
G5	AuNR + água
G6	AuNR + água + glicerol

Após a aplicação do agente de contraste óptico, toda a superfície dental foi escaneada obtendo a captura das imagens da varredura do elemento a cada 250 µm de deslocamento da plataforma. Terminada a varredura a amostra era removida da plataforma, lavada com água corrente e realizada a profilaxia com detergente neutro e escova de Robinson acoplada a contra ângulo e micromotor, seguido de banho na cuba ultrassônica com água deionizada. Em seguida, a amostra era novamente colocada na base e feita a confirmação do posicionamento correto para iniciar uma nova varredura com um agente de contraste seguinte.

2.4.5.2 Mensuração do coeficiente de atenuação

Após a aquisição, as imagens foram analisadas em software criado para mensuração do coeficiente de atenuação óptica (CAO) (Figura 10). CAO é um valor quantitativo que caracteriza o decaimento do sinal da OCT quando a luz se propaga através do tecido analisado. Assim, através do CAO, é possível usar o sinal OCT para discriminar quantitativamente entre diferentes tipos de tecidos e seu estado de saúde.

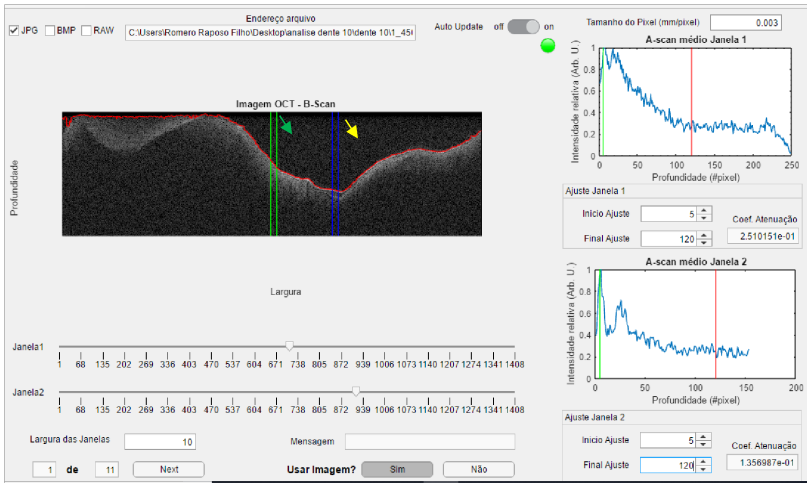

Figura 10. Software para mensuração do coeficiente de atenuação, janela 1 (seta verde) selecionando uma área hígida e janela 2 (seta amarela) na região de fossa e fissura.

O operador de software importou as imagens de cada grupo estudado. Em cada imagem, o operador selecionou a largura e a posição da janela de duas regiões de interesse (ROI). Para padronização, a largura da janela foi mantida constante (10 A-scan) durante todas as análises. Como cada amostra biológica apresenta características morfológicas distintas, a posição das janelas foi ajustada para cada

imagem, sempre posicionando uma janela em uma região de tecido saudável e a outra em uma região de tecido anormal.

Com a imagem B-scan, o software identifica a superfície do tecido (interface ar-tecido ou OCA-tecido) e usa-o como referência para realizar uma média do A-scan normalizado dentro de cada janela de ROI, iniciando a leitura a partir deste ponto. O A-scan foi normalizado pelo valor máximo para evitar valores errados devido à possível reflexão na primeira superfície.

A média A-scan de cada janela de ROI foi usada para ajustar um decaimento exponencial, baseado na lei de Beer-Lambert (MAIA *et al.*, 2016; POPESCU DP, SOWA MG, HEWKO MD, 2009), onde I (z) é a intensidade em função da profundidade z e μ é o coeficiente de atenuação óptica. O valor obtido foi registrado para posterior análise. Este procedimento foi repetido para cada imagem até que todas fossem analisadas.

$$I(z) = I_0 \exp(-2 \mu z)$$

2.4.5.3 Microscopia Óptica de transmissão por polarização cruzada

Para a confirmação das lesões da cárie incipiente em cicatrículas e fissuras foi realizada a Microscopia Óptica de transmissão por polarização cruzada como método comparativo a análise em OCT.

Para tal, os espécimes foram seccionados em fatias com aproximadamente 800 μm de espessura no sentido mesiodistal com disco diamantado dupla face (Buehler Ltda., Lake Bluff, IL, EUA) acoplado a uma cortadeira de precisão (Isomet 1000 Speed Saw, Buehler Ltda., Lake Bluff, IL, EUA). Em seguida as fatias foram lixadas manualmente na sequência das lixas de carbono números 600, 800, 1000, 1200 e 2000 até obter 80 μm de espessura. A planificação e padronização de espessura foi controlada com auxílio de um paquímetro digital.

Em seguida as fatias foram analisadas no microscópio óptico Olympus BX31 (Olympus Optical Co. Ltd., Tokyo, Japan) para análise com luz transmitida e uso de polarizadores. O meio de imersão utilizado foi água e as imagens foram

capturadas com uma câmera acoplada ao microscópio, com aumento de magnitude de 50x.

2.4.6 Análise Estatística

A análise estatística foi realizada utilizando o software GraphPad Prism 7 (GraphPad Software, Inc.). Foram calculadas a média e o desvio-padrão de cada grupo. A distribuição normal foi determinada pelo teste de Kolmogorov-Smirnov. Para verificar a possibilidade de diferença entre os grupos, foi usado o teste "repeated measures analysis of variance" RM-ANOVA". A significância estatística de todos os testes deve ser considerada como $p<0,05$.

2.4.7 Hipóteses

2.4.7.1 Hipótese Nula (H0)

Não foi possível observar diferenças entre o esmalte dentário sadio e cariado em regiões de cicatrículas e fissuras em cáries incipientes analisadas com nanobastões de ouro como agentes de contraste, quando comparadas aos demais agentes.

2.4.7.2 Hipótese alternativa (H1)

Os nanobastões de ouro promoveram um aumento da intensidade de luz nas áreas desmineralizadas, melhorando a distinção entre o esmalte dentário sadio e cariado nas regiões de cicatrículas e fissuras em cáries incipientes.

3 RESULTADOS E DISCUSSÃO

Os resultados e discussão destes estudos encontram-se apresentados por meio de 4 artigos científicos, os quais estão dispostos nos Apêndices a seguir:

Apêndice A, intitulado “Terahertz Time-Domain Spectroscopy of Healthy and Carious Dental Tissue” referente ao estudo 1, caracterizou estruturas teciduais dentárias hígidas e cariadas por espectroscopia de Terahertz no domínio de tempo (THz-DT) de forma a analisar as propriedades espectrais dos diferentes estratos dos tecidos duros dentais , entre elas, o índice de refração e o coeficiente de absorção. Este estudo será submetido a revista *Caries Research*.

O segundo artigo presente no Apêndice B, intitulado “High contrast dental imaging using a random fiber laser in backscattering configuration” buscou investigar o método de imagem retroespalhada dos dentes com base no laser aleatório em fibra de infravermelho próximo (NIR-RFL) como fonte óptica, foi aceito revista *Applied Optics*.

O terceiro estudo resultou no artigo “Surface evaluation of enamel etched by Er,Cr:YSGG laser for orthodontics purpose” , que para comparar o efeito do laser (Er,Cr:YSGG) em diferentes parâmetros de irradiação e condicionamento ácido na resistência de união ao cisalhamento (SBS) dos braquetes ortodônticos ao esmalte, foi aceito pela revista *The Journal of Contemporary Dental Practice*, presente no Apêndice C

O artigo “Gold nanostructures for imaging enhancement of incipient occlusal caries using Optical Coherence Tomography” fruto do estudo 4, objetou comparar o uso de agentes de contraste óptico a base de nanopartículas de ouro para o escaneamento de dentes por OCT com a finalidade de facilitar o diagnóstico de cáries oclusais incipientes através desta ferramenta óptica. Este estudo foi submetido à revista *Nanotechnology* e encontra-se no Apêndice D.

4 CONCLUSÕES

Foi possível concluir que:

- A espectroscopia THz pode ser explorada na avaliação do tecido dental. Os tecidos saudáveis e cariados mostraram diferenças significativas no que se refere aos coeficientes de absorção e o índice de refração na frequência THz. Além disso, a capacidade de geração de imagens e a resolução mais alta deste dispositivo serão analisadas em pesquisas futuras.

- A irradiação com laser Er,Cr;YSGG promoveu maior rugosidade e alterações ópticas no esmalte quando avaliada pela técnica de tomografia de coerência óptica. Dessa forma, a OCT é uma ferramenta promissora para avaliação clínica dos efeitos do laser na superfície do esmalte.

- O monitoramento das lesões de cárie incipiente, com base na atenuação do sinal da OCT ao longo do tempo, demonstrou ser uma abordagem promissora para o seu diagnóstico precoce. As nanopartículas de ouro são adequadas para aplicações in vivo e a segurança da técnica com agentes de contraste deve ser aprofundada, principalmente na odontologia. O método deve ser estendido para uma gama maior de lesões com várias formas, estruturas e profundidades em novos estudos de forma prévia aos procedimentos clínicos.

- O método de imagem retroespalhada dos dentes com base no NIR-RFL indica que, devido à sua baixa coerência, alta densidade espectral e natureza livre de manchas, têm o melhor desempenho abrangente como fonte óptica na busca de detalhes dentários como áreas desmineralizadas e de rachaduras, separando o esmalte do dentina, bem como identificar a concentração mineral, em comparação com outras fontes de luz NIR, como NLL e ASE. Ele também supera outros métodos de medição de imagem, como radiografia e microscopia óptica, com maior contraste de imagem. Recomenda-se que tecnologicamente seja possível projetar uma RFL compacta ou uma técnica de imagem com retroespalhamento aleatório baseado em laser semicondutor, que possa potencialmente ser usada em ambiente clínico.

Além destes artigos, paralelamente foram publicados e/ou submetidos, bem como apresentados em congressos os seguintes trabalhos:

LOPES, DANIELA; MOTA, CLAUDIA; PEREIRA, DAISA ; ZEZELL, DENISE M. ; GOMES, ANDERSON S. . A Comparative Study Between Acid-etching and Er,Cr:YSGG Laser Irradiation on Enamel Surface Evaluated by OCT and SEM. In: Clinical and Translational Biophotonics, 2018, Hollywood. Biophotonics Congress: Biomedical Optics Congress 2018 (Microscopy/Translational/Brain/OTS), 2018. p. JTh3A.15.

DS LOPES; LOPES, M. S. ; PEREIRA, D. L. ; MOTA, C. C. B. O. ; ZEZELL, D. M. ; GOMES, A. S. L. . CARACTERIZAÇÃO ÓPTICA DO ESMALTE E RESISTÊNCIA AO CISALHAMENTO DE BRAQUETES LINGUAIS APÓS MÉTODOS ASSOCIADOS DE CONDICIONAMENTO. In: 35ª reunião - Sociedade Brasileira de Pesquisa Odontológica (Brazilian Division of the IADR), 2018, campinas. Brazilian Oral Research 35th SBPqO Annual Meeting, 2018. v. 32. p. 453-543.

LOPES, D. S.; PEREIRA, D. L. ; ZEZELL, D. M. ; MOTA, C. C. B. O. ; MELO, L. S. A. ; GOMES, A. S. L. . Influência da irradiação com laser Er,Cr:YSGG sobre a resistência de união de braquetes ortodônticos. In: 34º SBPqO, 2017, Campinas - SP, BRASIL. Brazilian Oral Research. são paulo: caboverde, 2017. v. 31. p. 395-395.

LOPES, D. S.; PEREIRA, D. L. ; ZEZELL, D. M. ; MOTA, C. C. B. O. ; GOMES, A. S. L. ; MELO, L. S. A. . Optical Coherence Tomography and shear bond strength of brackets on enamel surface submitted to acid-etching or Er,Cr:YSGG laser irradiation. In: world federation for laser dentistry, 2017, Thessaloniki. bringing laser to sunlight, 2017.

LOPES, D. S.; SOUZA W.S; ARAÚJO R.E; GOMES ASL**.** Terahertz Time-Domain Spectroscopy of healthy and carious dental tissue. CLEO/Europe-EQEC 2019, 23 - 27 June 2019, Munich, Germany.

REFERÊNCIAS

Abogazalah, N., Eckert, J. G. & Ando, M. *In vitro* performance of near infrared light transillumination at 780-nm and digital radiography for detection of non cavitated approximal caries. *J Dent.* 63, 44–50 (2017).

Amaechi BT. Emerging technologies for diagnosis of dental caries: The road so far. J. of Appl. Physics 2009; 105: 102047-102049.

Ana PA, Velloso WF Jr, Zezell DM. Three-dimensional finite element thermal analysis of dental tissues irradiated with Er,Cr:YSGG laser. Rev Sci Instrum. 2008 Sep;79(9):093910.

Artun J, Bergland S. Clinical trials with crystal growth conditioning as an alternative to acidetch enamel pretreatment. Am J Orthod. 1984; 85(4):333-40.

Atam P. Dhawan ; Brian D'Alessandro ; Xiaolei Fu, Optical Imaging Modalities for Biomedical Applications, IEEE Reviews in Biomedical Engineering 3, 69-92 (2010)

Basaran, G.; Ozer, T.; Berk N.; Hamamci, O. Etching enamel for orthodontics with an Erbium, Chromium:Yttrium-Scandium-Gallium-garnet laser system. Angle Orthod. 2007; 77:117-23.

Batop Optoelectronics, Instruction manual and data sheet iPCA-21-05-1000-800-h, disponível em: https://www.batop.de/products/terahertz/photoconductive-antenna/photoconductiveantenna-800nm.html, acesso em: 20 de julho 2018.

Beard M, Turner G, and Schmuttenmaer C. Terahertz Spectroscopy. J. Phys. Chem 2002; 106: 7146–7159.

Benetti C, Ana PA, Bachmann L, Zezell DM. Mid-Infrared Spectroscopy Analysis of the Effects of Erbium, Chromium:Yattrium-Scandium-Gallium-Garnet (Er,Cr:YSGG) Laser irradiation on Bone Mineral and Organic Components. Appl Spectrosc. 2015; 69(12):1496-504.

Bishara SE, VonWald L, Lafoon JF, Warren JJ. Effect of a self-etch primer/adhesive on the shear bond strength of orthodontic brackets. Am J Orthod Dentofacial Orthop. 2010; 119:6214.

Botta SB, Ana PA, Zezell DM, Powers JM, Matos AB. Adhesion after erbium, chromium:yttrium-scandium-gallium-garnet laser application at three different irradiation conditions. Lasers Med Sci. 2009; 24(1):67-73.

Braz AKS, Araujo RE De, Ohulchanskyy TY, Shukla S, Bergey EJ, Gomes ASL, et al. In situ gold nanoparticles formation: contrast agent for dental optical coherence tomography for dental optical coherence tomography. J Biomed Opt. 2012;17(6):1–5.

Brito-Silva AM, Sobral-Filho RG, Barbosa-Silva R, de Araújo CB, Galembeck A, Brolo AG. Improved synthesis of gold and silver nanoshells. Langmuir. 2013; 29(13): 4366–72.

Bykov A, Hautala T, Kinnunen M, Popov A, Karhula S, Saarakkala S, Nieminen MT, Tuchin VV and Meglinski I. Imaging of subchondral bone by optical coherence tomography upon optical clearing of articular cartilage, J. Biophotonics 2016; 9 (3): 270–275.

Carmen Todea. Non-invasive diagnostic methods in dentistry, Proceedings Volume 9670, Sixth International Conference on Lasers in Medicine; 967002 (2016).

Carneiro VSM, Mota CCBO, Souza AF, Silva EJ, Silva AF, Evair J, et al. Silver nanoparticles as optical clearing agent enhancers to improve caries diagnostic by optical coherence tomography. Proc SPIE 2018; 10507: 1050719.

Carvalho MT et al, “Random laser illumination: an ideal source for biomedical polarization imaging? ” Multimodal Biomedical Imaging XI, San Francisco, CA, 2016, pp. 9701.

Chan KH, D. Fried, “Multispectral cross-polarization reflectance measurements suggest high contrast of demineralization on tooth surfaces at wavelengths

beyond 1300 nm due to reduced light scattering in sound enamel," Journal of Biomedical Optics, vol. 23, no. 6, pp. 060501, Jun. 2018.

Chan KH, Tom H, Darling CL, Fried D. A method for monitoring enamel erosion using laser irradiated surfaces and optical coherence tomography. Lasers Surg Med. 2014 Nov;46(9):6728.

Chen Q, Zhu H, Xu Y, Lin B, Chen H. Discrimination of Dental Caries Using Colorimetric Characteristics of Fluorescence Spectrum. Caries Res. 2015;49(4):401-7.

Christiano J. S. de Matos, Leonardo de S. Menezes, Antônio M. Brito-Silva, M. A. Martinez Gámez, Anderson S. L. Gomes and Cid B. de Araújo, Random Fiber Laser, Phys. Rev. Lett. 99, 153903-1/4 (2007).

Chung S, D. Fried, M. Staninec, C.L. Darling, "Multispectral near-IR reflectance and transillumination imaging of teeth," Biomed. Opt. Express, vol. 2, no. 10, pp. 2804–2814, Oct. 2011.

Churchley D, Lynch Rj, Lippert F, Eder JS, Alton J, Cabezas CG. Terahertz pulsed imaging study to assess remineralization of artificial caries lesions. J Biomed Opt 2011; 16: 026001-8.

Churkin DV, S. Sugavanam, I. D. Vatnik, Z. Wang, E. V. Podivilov, S. A. Babin, Y. Rao, and S. K. Turitsyn, "Recent advances in fundamentals and of random fiber lasers", Adv. Opt. Photonics, vol. 7, no. 3, pp. 516-569, Sep. 2015.

Crawley DA, Longbottom C, Cole BE, Ciesla CM, Arnone D, Wallace VP, et al. Terahertz pulse imaging: a pilot study of potential applications in dentistry. Caries Res 2003; 37: 352–9.

Auston DH, K. P. Cheung and P. R. Smith, Picosecond photoonudting Hertzian dipoles, Appl. Phys. Lett. 45, 284 (1984).

Dadrasnia E. Terahertz Time-Domain Spectroscopy to Characterize Graphene

Nanostructures for New Optoelectronic Applications, Universidade de Madri, 2015.

Fejerskov O. Changing Paradigms in Concepts on Dental Caries : Consequences for Oral Health Care. Caries Res. 2004;38:182–91. free imaging," Opt. Lett., vol. 40, no. 20, pp. 4607– 4610, Oct. 2015.

Frencken JE, Sharma P, Stenhouse L, Green D, Laverty D, Dietrich T. Global epidemiology of dental caries and severe periodontitis – a comprehensive review. J Clin Periodontol 2017; 44 (Suppl. 18): S94–S105.

Fried D, Xie J, Shafi S, Featherstone JDB, Breunig TM, Le C. Imaging caries lesions and lesion progression with polarization sensitive optical coherence tomography. J Biomed Opt. 2002;7(4):618.

Fried WA, D. Fried, K. H. Chan, C.L. Darling, "High contrast reflectance imaging of simulated lesions on tooth occlusal surfaces at near-IR wavelengths," Lasers Surg. Med., vol. 45, no.8, pp.533–541, 2013.

Fujimoto, J.; Swanson. E. The Development, Commercialization, and Impact of Optical Coherence Tomography. Investigative Ophthalmology & Visual Science, v. 57, n.9, pp. 1-13, 2016.

Geibel MA, S. Carstens, U. Braisch, A. Rahman, M. Herz, A. Jablonski-Gomez J. "Detection and diagnosis of the early caries lesion," BMC Oral Health, vol. 15, no. 1, pp. S3, 2015.

He Y, Liu K, Au C, Sun Q, Parrott EPJ, Macpherson EP. Determination of terahertz permittivity of dehydrated biological samples Phys Med Biol. 2017; 62:8882-8893.

Hokr BH et al, "A narrow-band speckle-free light source via random Raman lasing," Journal of Modern Optics, vol. 63, no. 1, pp. 46-49, 2016.

Hokr BH et al, “Lighting up microscopy with random Raman lasing,” Real-time Measurements, Rogue Events, and Emerging Applications, San Francisco, CA, 2016, pp. 9732.

Horiuchi S, Kuroda S, Hiasa M, Suge T, Saku S, Hamada K, Matsuo T, Asaoka K, Tanaka E. Reinforcement of bond strength of self-etching orthodontic adhesive. Angle Orthod. 2012;82(1):30-5.

Hoshing UA,Patil S,Medha A, Bandekar SD.Comparison of shear bond strength of composite resin to enamel surface with laser etching versus acid etching: an in vitro evaluation. J Conserv Dent. 2014;17(4):320-4.

Hu J, Abujetas DR, Tsoutsi D, Leggio L, Rivero F, Rodríguez EM, Torres RA, Sánchez-Gil JA, Ramírez HL, Gallego D, Rivera HL, Gil PR, Alfonso F, Solé JG and Jaque D. Experimental evaluation of gold nanoparticles as infrared scatterers for advanced cardiovascular optical imaging. APL Photonics 2018; 3, 080803.

International Standardization Organization. Dental materials – Testing of adhesion to tooth structure. ISO/TS 11405, 1-17, 2014.

Ito S, Shimada Y, Sadr A, Nakajima Y, Miyashin M, Tagami J. Assessment of occlusal fissure depth and sealant penetration using optical coherence tomography. Dent Mater J. 2016;35(3):432–9.

Jacques SL. Optical properties of biological tissues: a review , Phys. Med. Biol. 2013; 58, R37– R61 .

Jones RS, Fried D. The effect of high index liquids on PS-OCT imaging of dental caries. Lasers Dent XI. 2005; 5687(2): 34–41.

Kamburoğlu K, Karagöz, B.; Altan, H.; Özen, D. An ex vivo comparative study of occlusal and proximal caries using terahertz and X-ray imaging. Dentomaxillofac. Radiol. 2019, 48, 20180250.

Kamburoğlu K, Yetimoğlu NÖ, And Altan H. Characterization of primary and permanent teeth using terahertz spectroscopy. Dentomaxillofacial Radiol 2014;43:1-6.

Kang H, Darling CL, Fried D. Enhancing the detection of hidden occlusal caries lesions with OCT using high index liquids. Proc SPIE--the Int Soc Opt Eng. 2014;8929:89290.

Kang H, Darling CL, Fried D. Use of an optical clearing agent to enhance the visibility of subsurface structures and lesions from tooth occlusal surfaces. J Biomed Opt. 2016; 21(8).

Karlsson L, Ana M. A. Maia, Bernardo B. C. Kyotoku, Sofia Tranæus, Anderson S. L. Gomes and Walter Margulis, Near-infrared transillumination of teeth: measurement of a system performance, Journal of Biomedical Optics 15, 036001 2010.

Kim JH, Kwon OW, Kim H, Kwon YH. Acid resistance of Erbium-doped Yttrium Aluminum Garnet laser-treated and phosphoric acid-etched enamels. Angle Orthodontist 2006; 76(6):1052-6.

Kirillin M, Shirmanova M, Sirotkina M, Bugrova M and Khlebtsov B. Contrasting properties of gold nanoshells and titanium dioxide nanoparticles for optical coherence tomography imaging of skin: Monte Carlo simulations and in vivo study. Journal of Biomedical Optics, 2009; 142, 021017.

Kohns P, Zhou P, Störmann R. Effective laser ablation of enamel and dentine without thermal side effects. J Laser Appl. 1997;9(3):171-4.

Larin KV, Ghosn MG, Bashkatov AN, Genina EA, Trunina NA and Tuchin VV. Optical Clearing for OCT Image Enhancement and In-Depth Monitoring of Molecular Diffusion, IEEE journal of selected topics in quantum electronics, 2012; 18, 1244.

Lawandy NM, R. M. Balachandran, A. S. L. Gomes, and E. Sauvain, “Laser action in strongly scattering media,” Nature, vol. 369, no.6478, pp. 340-340, 1994.

Leão Filho JC, Braz AK, de Souza TR, de Araujo RE, Pithon MM, Tanaka OM. Optical coherence tomography for debonding evaluation: an in-vitro qualitative study. Am J Orthod Dentofacial Orthop. 2013; 143(1):61-8.

Lee BS, Hsieh TT, Lee YI, Lan WH, Hsu YJ, Wen PH,et al. Bond strengths of orthodontic bracket after acid-etched Er:YAG laser irradiated and combined treatment on enamel surface. Angle Orthod. 2003;73(5):565-70.

Liang Y, Yuan W, Mavadia-Shukla J, Li X. Optical clearing for luminal organ imaging with ultrahigh-resolution optical coherence tomography. J Biomed Opt. 2016; 21(8), 081211.

Liu Yu, Liu Hao, Tang Meiqiong, Huang Jiaoqi, Liu Wei, Dong Jinying, Chen Xueping, Fu Weiling and Zhang Yang, The medical application of terahertz technology in non-invasive detection of cells and tissues: opportunities and challenges, RSC Adv., 2019, 9, 9354

Luan F, Bobo Gu, Anderson S. L. Gomes, Ken-Tye Yong, Shuangchun Wen and Paras N. Prasad, Lasing in Nanocomposite Random Media, Review Paper, Nano Today 10, 168-192 (2015).

M. J. Cozin, R. C. Lee, D. Fried, “Near-IR transillumination and reflectance imaging at 1300nm and 1500-1700-nm for in vivo caries detection,” Lasers Surg. Med., vol. 48, no. 6, pp. 828– 836, 2016.

Ma R, J. Q. Li, J. Y. Guo, H. Wu, H. H. Zhang, B. Hu, Y. J. Rao, W. L. Zhang, “High-power low spatial coherence random fiber laser,” Optics Express, Vol.27, no. 6, pp. 8738-8744, 2019.

Ma R, W. L. Zhang, J. Y. Guo, Y. J. Rao, “Decoherence of fiber supercontinuum light source for speckle-free imaging,” Optics Express, Vol.26, no. 20, pp. 26758-26765, 2018.

Ma R, Y. J. Rao, W. L. Zhang, B. Hu, “Multimode Random Fiber Laser for Speckle-Free Imaging,” IEEE Journal of Selected Topics in Quantum Electronics, Vol.25, no. 1, pp. 0900106, 2019.

Machoy M, Seeliger J, Szyszka-Sommerfeld L, Koprowski R, Gedrange T, and Woźniak K, (Review Article) The Use of Optical Coherence Tomography in

Dental Diagnostics: A Stateof-the-Art Review, Journal of Healthcare Engineering 2017, Article ID 7560645, 31 pages.

Mahdian M, Salehi HS, Lurie AG, Yadav S, Tadinada A. Tissue characterization using optical coherence tomography and cone beam computed tomography: a comparative pilot study.Oral Surg Oral Med Oral Pathol Oral Radiol. 2016;122(1):98-103.

Maia AMA, de Freitas AZ, de L. Campello S, Gomes ASL, Karlsson L. Evaluation of dental enamel caries assessment using Quantitative Light Induced Fluorescence and Optical Coherence Tomography. J Biophotonics. 2016; 9(6):596–602.

Maia AMA, L. Karlsson, W. Margulis; A. S. L. Gomes Evaluation of two imaging techniques: near-infrared transillumination and dental radiographs for the detection of early proximal enamel caries, Dento-Maxillo-Facial Radiology, v. 40, p. 429-433, 2011.

Mandurah MM, Sadr A, Shimada Y, Kitasako Y, Nakashima S, Bakhsh TA, et al. Monitoring remineralization of enamel subsurface lesions by optical coherence tomography. J Biomed Opt. 2013;18(4):046006.

Melo M, Pascual A, Camps I, del Campo Á, Ata-Ali J. Caries diagnosis using light fluorescence devices in comparison with traditional visual and tactile evaluation: a prospective study in 152 patients. Odontology. 2016;105(3):283–90.

Meng Z, Yao XS, Yao H, Liang Y, Liu T, Li Y, et al. Measurement of the refractive index of human teeth by optical coherence tomography. J Biomed Opt 2009;14:034010.

Mitchell JK, A. R. Furness, R. J. Sword, S. W. Looney, W. W. Brackett, M. G. Brackett, “Diagnosis of Pit-and-fissure Caries Using Three-dimensional Scanned Images,” Operative Dentistry, vol. 43, no. 3, pp. E152-E157, 2018.

Momeni, “Radiographic diagnosis of proximal caries-influence of experience and gender of the dental staff,” Clinical Oral Investigations, vol. 21, no. 9, pp. 2761-2770, 2017.

Oldenburg AL, Hansen MN, Ralston TS, Wei A and Boppart SA. Imaging gold nanorods in excised human breast carcinoma by spectroscopic optical coherence tomography. J. Mater. Chem., 2009, 19, 6407–6411.

Pashley DH. The effects of acid etching on the pulpodentin complex. Operative Dent. 1992;17:229-34.

Perschbacher S. Interpretation of panoramic radiographs. *Aust Dent J* 2012; 57(Suppl 1): 40–5.

Petersen PE. Global policy for improvement of oral health in the 21st century – implications to oral health research of World Health Assembly 2007, World Health Organization. Community Dent Oral Epidemiol 2009; 37: 1–8.

Pickwell E, Wallace VP, Cole BE, Ali S, Longbottom C, Lynch RJ, et al. A comparison of terahertz pulsed imaging with transmission microradiography for depth measurement of enamel demineralisation in vitro. *Caries Res* 2007; 41: 49–55.

Popescu DP, Sowa MG, Hewko MD C-SL. Assessment of early demineralization in teeth using the signal attenuation in optical coherence tomography images. J Biomed Opt. 2009; 13(5):1– 17.

Quinto Jr J, Amaral MM, Francci CE, Ana PA, Moritz A, Zezell DM. Evaluation of Intra Root
Canal Er,Cr:YSGG Laser Irradiation on Prosthetic Post Adherence. Journal of Prosthodontics. 2017; 0:1-5.

R. A. Katkar, S. A. Tadinada, B. T. Amaechi and D. Fried, Optical Coherence Tomography, Dent. Clin. North Am., 2018, 62, 421–434

Rajagopal R, Padmanabhan S, Gnanamani J. A comparison of shear bond strength and debonding characteristics of conventional, moisture-insensitive, and self-etching primers in vitro. Angle Orthod. 2004; 74(2):264-8.

Ratheesh KM, Prabhathan P, Seah LK and Murukeshan VM. Gold nanorods with higher aspect ratio as potential contrast agent in optical coherence tomography and for photothermal applications around 1300nm imaging window. Biomed. Phys. Eng. Express, 2016; 2: 055005.

Redding B, M. A. Choma, and H. Cao, “Speckle-free laser imaging using random laser illumination,” Nature Photon., vol. 6, no.6, pp. 355–360, Jun. 2012.

Redding B, P. Ahmadi, V. Mokan, M. Seifert, M. A. Choma, and H. Cao, “Low-spatialcoherence high-radiance broadband fiber source for speckle free imaging,” Opt. Lett., vol. 40, no. 20, pp. 4607–4610, 2015.

Reynolds IR. A review of direct orthodontic bonding. Br J Orthod. 1975;2:171-80.

Schwendicke F, Tzschoppe M, Paris S., J Dent. Radiographic caries detection: A systematic review and meta-analysis; 2015 Aug;43(8):924-33.

Shi Y, Fan S, Li L, Li Q, Chai X, Ren Q and Zhou C. PEGylated Aucore–Agshell Nanorods as Optical Coherence Tomography Signal Nanoamplifiers. Plasmonics, 2015; 10(6): 1381-1389.

Si P, Yuan E, Liba O, Winetraub Y, Yousefi S, SoRelle ED, Yecies DW, Dutta R and Zerda A. Gold Nanoprisms as Optical Coherence Tomography Contrast Agents in the Second Near-Infrared Window for Enhanced Angiography in Live Animals. ACS Nano 2018; 12, 11986-11994.

SIM YC, Maeng I, and SON JH. Frequency-dependent characteristics of terahertz radiation on the enamel and dentin of human tooth. Curr. Appl. Phys 2009; 9: 946–949.

Simon JC, S. A. Lucas, M. Staninec, H. Tom, K. H. Chan, C. L. Darling, M. J. Cozin, R. C. Lee, D. Fried, “Near-IR transillumination and reflectance imaging at 1300nm and 1500-1700-nm for in vivo caries detection,” Lasers Surg. Med., vol. 48, no. 6, pp. 828– 836, 2016.

Son SA, K. H. Jung, C.C. Ko, Y. H. Kwon, “Spectral characteristics of caries-related autofluorescence spectra and their use for diagnosis of caries stage,” J. Biomed. Opt., vol. 21, no. 1, pp. 015001, 2016.

Stern RH, Sognnaes RF. Laser beam effect on dental hard tissues. J Dent Res1964; 43:87373.

Sudheendran N, Mohamed M, Ghosn MG, Tuchin VV And Larin KV. Assessment of tissue optical clearing as a function of glucose concentration using optical coherence tomography. J Innov Opt Health Sci., 2010; 3(3): 169–176.

Sun YW, SY MY, Wang YXJ, Ahuja AT, Zhang YT *et al*. A promising diagnostic method: Terahertz pulsed imaging and spectroscopy. World J Radiol 2011; 3: 55–65.

Swanson EA and Fujimoto JG. The ecosystem that powered the translation of OCT from fundamental research to clinical and commercial impact [Invited] Biomedical optics express 2017; 8, 1638.

Wen X, Jacques SL, Tuchin VV and Zhua D. Enhanced optical clearing of skin in vivo and optical coherence tomography in-depth imaging, Journal of Biomedical Optics, 2012; 17(6), 066022.

Xia Q, Li H, Liu Y, Zhang S, Feng Q, Xiao K. The effect of particle size on the genotoxicity of gold nanoparticles. J Biomed Mater Res. 2016; 00A(00):1–10.

Xu J, Ma Y, Yu T and Zhu D. Quantitative assessment of optical clearing methods in various intact mouse organs, J. Biophotonics. 2019;12:e201800134.

Yang VB, Curtis DA, Fried D. Use of Optical Clearing Agents for Imaging Root Surfaces With Optical Coherence Tomography. IEEE J Sel Top Quantum Electron [Internet]. 2019;25(1):1–7.

Yang VB, D. A. Curtis, D. Fried, “Cross-polarization reflectance imaging of root caries and dental calculus on extracted teeth at wavelengths from 400 to 2350 nm,” Journal of Biomedical Optics, vol. 11, no.11, pp. 10.1002, 2018.

Yang X et al., Biomedical applications of terahertz spectroscopy and imaging. Trends Biotechnol 2016; 34: 810–824.

Yeh YC; Creran B.; Rotello VM. Gold nanoparticles: preparation, properties, and applications in bionanotechnology. *Nanoscale*, v. 4, n. 6, p. 1871–1880, 2012.

Zagaynova EV, Shirmanova MV, Kirillin MY, Khlebtsov BN, Orlova1 AG, Balalaeva IV, Sirotkina MA, Bugrova ML, Agrba PD and Kamensky VA. Contrasting properties of gold nanoparticles for optical coherence tomography: phantom, in vivo studies and Monte Carlo simulation, Phys. Med. Biol. 2008; 53: 4995–5009.

Zamataro CB, Ana PA, Benetti C, Zezell DM. Influence of Er,Cr:YSGG laser on CaF_2-like products formation because of professional acidulated fluoride or to domestic dentifrice application. Microsc Res Tech. 2013;76(7):704-13.

Zezell DM, Adriana da Costa Ribeiro, Luciano Bachmann, Anderson Stevens Leonidas Gomes, Christel Rousseau, John Girkin, Characterization of natural carious lesions by fluorescence spectroscopy at 405 nm excitation wavelength, J. Biomedical Optics 12, 0640131/5 (2007).

Zhou J, Ralston J, Sedev R, Beattie DA. Functionalized gold nanoparticles: Synthesis, structure and colloid stability. J Colloid Interface Sci . 2009;331(2):251–62.

Zhu D, Larin KV, Luo Q, Tuchin VV. Recent progress in tissue optical clearing. Laser Photonics Rev. 2013;757(5):732–57.

APÊNDICE A - ARTIGO "TERAHERTZ TIME-DOMAIN SPECTROSCOPY OF HEALTHY AND CARIOUS DENTAL TISSUE"

Original Paper

Caries Research

TITLE PAGE

Terahertz Time-Domain Spectroscopy of Healthy and Carious Dental Tissue

Daniela S. Lopes[1], Wellington S. Souza[2,3], Renato E. de Araujo[3], Anderson S. L. Gomes[1,4]

1. Graduate Program in Dentistry, Federal University of Pernambuco, Recife, PE, Brazil
2. Federal Institute of Education, Science and Technology of Sertão Pernambucano, Salgueiro, PE, Brazil
3. Laboratory of Biomedical Optics and Imaging, Federal University of Pernambuco, Recife, PE, Brazil
4. Department of Physics, Federal University of Pernambuco, Recife, PE, Brazil

Corresponding author:

Anderson S. L. Gomes e-mail: anderson@df.ufpe.br or gomesanderson@hotmail.com phone:

55-81-21267636

Laboratory of Photonics and Biophotonics, Department of Physics, University of Pernambuco

Av. Prof. Luis de Barros Freire , Cidade Universitária, Recife

50670-901 – PE – Brazil.
Lopes DS, Souza WS, Araujo RE, Gomes ASL

Keywords: THz spectroscopy, dentistry, dental enamel, dentin, dental diagnosis

ABSTRACT

We report a study on healthy and carious teeth, in dry and wet environment, using a Terahertz Time-Domain Spectroscopy (THz-TDS) system in transmission mode. Extracted permanent teeth were sectioned mesiodistally with mean thicknesses of d ≈ 2.0 mm ± 0.2. The studied samples were 20 slices of healthy dentin, enamel and carious lesions in dentin, considering wet and dry samples. The THz-TDS setup was developed based on a femtosecond IR laser (center wavelength at 820 nm, repetition rate of 76 MHz and pulse width of 150fs) and on photoconductive antennas. As a result of the characterization, the absorption coefficient of wet dentin from 0.1 to 1.0 THz was higher than that of dry dentin samples. The presence of carious lesion on the tooth tissue reduces the absorption coefficient and refractive index values of the tissue, as also inferred from our measurements.

Introduction

The diagnosis in dentistry, particularly for teeth diseases, is traditionally made by visual and tactile clinical examination, associated with radiographic images (Schwendicke et al.,2015; Amaechi,2009). According to the World Health Organization, the two most prevalent oral diseases, caries and periodontal disease, have been of concern for many years (Petersen, 2007). This lead researchers and clinicians to search for new noninvasive diagnostic methods, especially using non-ionizing radiation, including: in situ confocal microscopy (Todea, 2016; Atam et al., 2010), optical coherence tomography OCT (Fujimoto 2016; Katkar et al., 2018), optical spectroscopy (Todea 2016; Atam et al., 2010; Chen et al., 2015). Some methods are well established and getting close to the clinic, such as optical coherence tomography (Fujimoto et al., 2016; Katkar et al., 2018), while other methods are still in the laboratory or pre-clinical stages, such as Terahertz spectroscopy (Beard et al., 2002; Sun et al., 2016; Yang et al., 2016; Liu et al., 2019).

Among the promising methods, one of the most recent is the exploitation of Terahertz (THz) radiation in spectroscopy and bioimaging (Beard et al., 2002; Sun et al., 2016; Yang et al., 2016; Liu et al., 2019). THz radiation falls in the 0.1-10THz range, between the microwaves and infrared spectral region. Among the exploited THz advantages for diagnostic in life sciences, we highlight the low photon energies, which make them safe; extreme water absorption, therefore avoiding deep penetration in the human body; the longer wavelength (compared to visible and infrared) implies that Mie scattering is less important; many molecules strongly absorb in the THz regime, and can therefore be fingerprinted.

THz technology has already been applied to dentistry (Kamburoglu et al., 2014; Churchley et al., 2011; Sim et al., 2009; Pickwell et al., 2007; Crawley et al., 2003). Although the penetration depth of THz waves into biological tissues is limited because of the high attenuation of water in THz frequencies, three dimensional investigation of biological structures such as teeth are possible by using reflection-based THz imaging systems (Kamburoglu et al., 2014). Moreover, small refractive index variations which occur as a result of these structural changes can also be monitored and changes in mineral density of the media can be accurately detected (Kamburoglu et al., 2014, Pickwell et al., 2007). Recent findings regarding THz characterization of extracted teeth samples revealed that healthy teeth and carious lesions can be identified by THz spectroscopy and by THz pulsed imaging (Kamburoglu et al., 2014). The dental caries is a consequence of mineral loss in enamel and dentine, thus frequency-dependent THz spectra offer the possibility of investigating mineralization level in this tissue. In addition, it has been showed

that THz could be used to measure the remineralization of artificial caries lesions under simulated clinical conditions in human (Churchley et al., 2011) and bovine teeth (Pickwell et al., 2007). Sim et al., 2009 revealed different dental (dentin and enamel) THz attenuation for dry and wet sample.

Although few studies described the THz properties of dental tissue, the discriminate of sound and carious dental structures (enamel and dentin) under different hydration (wet and dried) states still need to be reveled. The objective of the present study is to characterize dental tissue structures by Terahertz time-domain spectroscopy (THz-TDS), in order to quantitatively and qualitatively analyze health and carious teeth in dry and wet environment.

Materials and Methods

Sample preparation

Ethical approval for this research was obtained from the ethical committee of the Federal University of Pernambuco, Pernambuco, Brazil 95310418.0.3001.5203. Fifteen newly extracted human permanent teeth for orthodontics purpose were cleaned and stored in deionized water. Each tooth was sectioned mesiodistally in parallel with the long axis of the crown using a double-sided diamond disco (Buehler Ltda., Lake Bluff, IL, USA) coupled to a precision cutter (Isomet 1000 Speed Saw, Buehler Ltda., Lake Bluff, IL, USA). A mean thickness of $d \approx 2.0$ mm $\pm$ 0.1 was obtained. Afterwards, both sides of each section were examined under a stereomicroscope at 20x magnification (Stemi 2000; Carl Zeiss, Jena, Germany). Teeth were identified as either sound or as having a caries lesion, which was defined as a demineralized white or yellowish-brown discoloured area in the enamel and/or dentine. Examination of the 20 slices of teeth surfaces revealed a distribution of the studied sample teeth as follows: sound enamel (10 slices), sound dentin (6 slices) and dentin and enamel carious lesion (4 slices), considering wet and dry samples.

Characterization of the terahertz time-domain spectroscopy system

The homemade THz-TDS system is schematically shown in Figure 1a and a picture of the real system on the right figure. It explores an ultrashort Ti:sapphire pulsed femtosecond laser with a wavelength around 820 nm operating at 76 MHz and two commercial photocondutive antennas (IPCA -21-05-1000-800-h), with Gallium Arsenide (GaAs) as substrate. The laser pump is incident on the photoconductive antenna emitter, generating electron-holes pairs in the

GaAs antenna substrate. At the THz emitter, a bias voltage is applied (15V peak voltage, 1KHz) inducing drift of the carriers (electron and holes) to the antenna electrodes. The transient current on the photoconductive antenna drives the generation of THz pulse radiation. On the THz detector, with no bias voltage, an optical pulse is also applied to generate charge carriers on the antenna substrate. The incident THz radiation induces carriers' drift to the antenna contacts, and therefore, an output photocurrent is generated with magnitude proportional to the incident terahertz field amplitude. As shown in Figure 1a, the THz-TDS system was defined with two optical paths: the THz pulse generation and detection arms. A 62.5 mW average laser power were incident on each antenna. After generation of THz pulse, a silicon collimating lens and a polymethylpentene lens (f=30mm) were used to focus the THz radiation on the sample. THz wave was focused on a 5-mm diameter area of the sample. Similar pair of lens were used to collect the transmitted THz radiation. Figure 1b shows the sample placed between the THz lens. To measure the transmitted THz radiation, a lock-in amplifier was explored (SR810, ThinkSRS, Zurich instruments, Germany)

(a) (b)

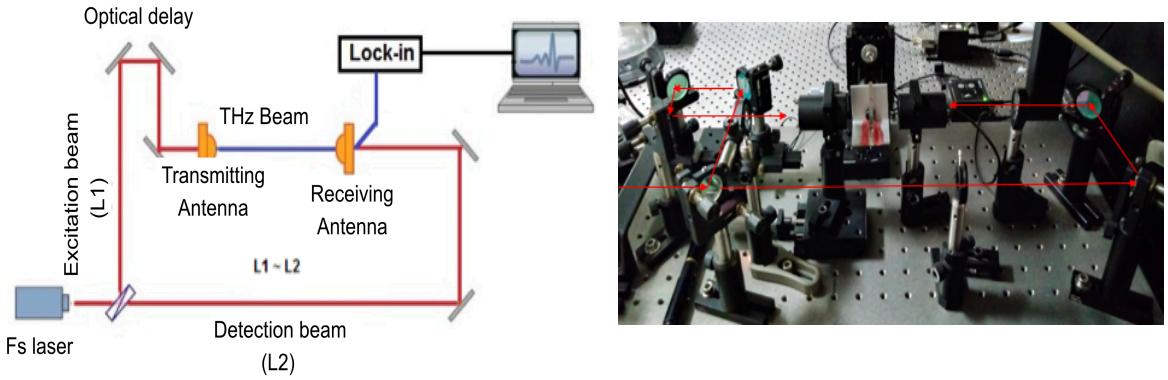

Fig. 1 – TDS-THz experimental setup (a) and photo of the real system (b).

The measured THz radiated electric field in the time and the frequency-domain is presented in figure 2a and 2b, respectively. Figure 2a indicates that the pulse width of the generated THz signal was approximately 3 ps. The THz frequency spectrum, in Figure 2b, was obtained by using a Fast Fourier Transform algorithm (FFT) on the time-domain signal. The radiated THz power was detected up to 1.25 THz, after which the noise of the system limited the detection.

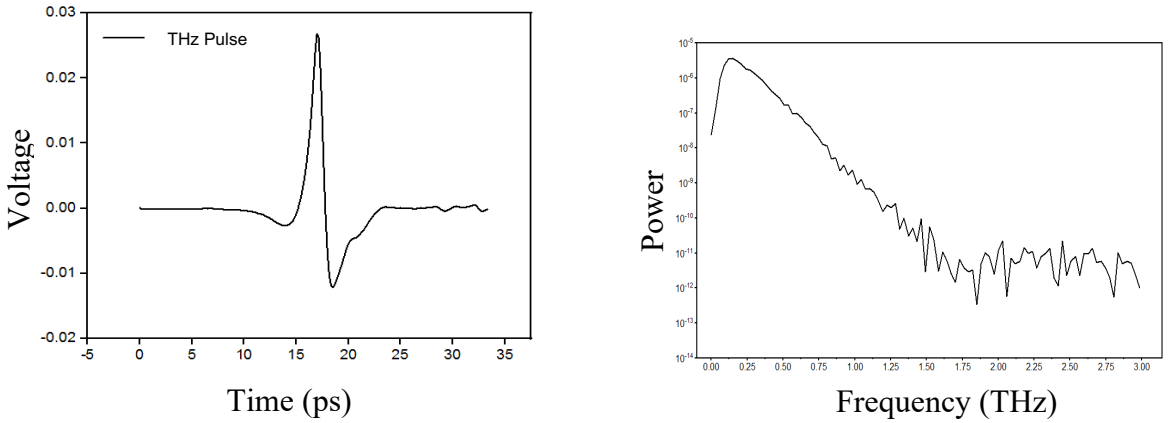

Figure 2: (a) The radiated THz field in the time domain and (b) the radiated THz power in the frequency domain.

Results

From the measured transmitted pulses, two basic information were acquired: refractive index and absorption coefficient, for dry and wet samples, from 0.1 and 1.0 THz range. The time-dependent data were converted to the frequency domain using fast Fourier transform (FFT) algorithm. Therefore, the amplitude *(A)* and phase (ϕ) of the THz beam in the frequency domain are obtained. Here, changes in refractive index can be interpreted as a resulting from changes in density of the medium. The amplitude of the transmitted THz signal is considered to be a combination of both scattering and resonant effects if any. From the THz signal, obtained with and without the sample, the refractive index and extinction (absorption and scattering) coefficient properties of the teeth sections were analysed using the following equation:

$$n_s = 1 + \frac{(\phi_s - \phi_{air})c}{2\pi f d} \quad (1) \qquad \text{and} \qquad \alpha = \frac{1}{d}.\ln\left(\frac{A_s}{A_{air}T^2}\right) \quad (2)$$

where n_s is the sample refractive index, c is speed of light, ϕ_s and ϕ_{ar} are the THz phase of the beam after propagation through the sample and through air, respectively. Moreover, d is the sample thickness and f is the THz frequency. On the analyses of the absorption coefficient α , A_s and A_{air} corresponds to the signal amplitude of the THz beam after propagating through the sample and through the air (without sample). In equation 2, T is the sample transmittance defined by:

$$T = \frac{4n_s}{(1+n_s)^2} \quad (3).$$

Figure 3(a) and 3(b) show the average spectra of the samples refractive index and extinction coefficient, respectively. The THz spectra are limited from 0.1 to 1 THz, avoiding the high absorption at higher frequencies. Figure 3a shows that refractive index is higher for enamel than for dentin. It was also observed that the refractive index of enamel is not affect by the sample hydration. Moreover, wet dentin present high values of n than dry dentin. Figure 3b shows that the samples extinction cross-section increases as the radiation frequency increases. On average, the α values of wet dentin are slightly higher than dry samples. Although water has high absorption coefficient values at THZ, the presence of water in the dentin structure can reduce the tissue scattering and therefore decreasing the extinction cross-section values.

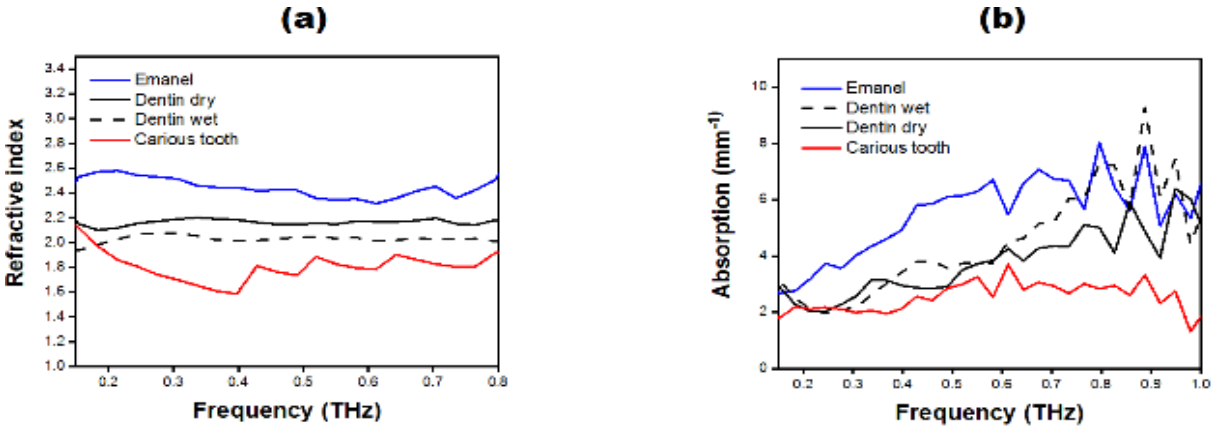

Fig 3 – Refractive index (a) and extinction coefficient measurements conducted for carious and healthy teeth as a function of frequency between 0.1 and 1.0 THz.

Figure 3(a) indicates that the material refractive index is weak dependent on frequency, therefore an average value of n could be determined for the whole THz spectral, raging from 0.1 to 1.0 THz. Figure 4 depicted the n and α average values of samples.

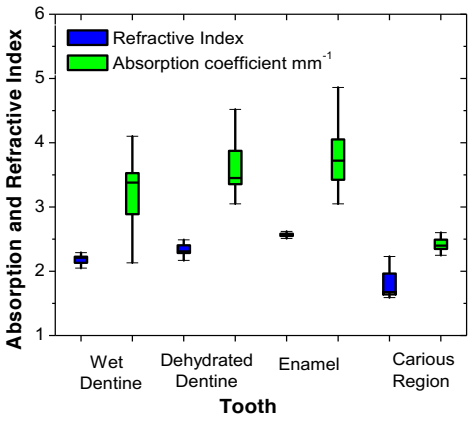

Fig 4 - Refractive index and extinction coefficient comparisons according to dental structures

It is straightforward to observe that carious dentin tooth samples were found to have lower extinction coefficient than those of healthy teeth. The absorption coefficient of the healthy enamel was higher than those of healthy dentin. Median absorption coefficient values for dry and wet healthy dentin was found to be 3.47 and 3.77, respectively. Median refractive index values for healthy wet and dry dentin were similar (2.02 and 2,16 respectively) and enamel was 2.46. The carious teeth were found a refractive index value of 1.80. The α and n measured average values are presented on Table 1.

Table 1. Extinction coefficient and refractive index values obtained with the THz-TDS system.

Dental structure	Average absorption coefficient (mm^{-1})	Average refractive index
Healthy Dentin wet	3.77	2.02
Healthy Dentin dry	3.47	2.16
Healthy Enamel	5.55	2.46
Carious tooth (Enamel and Dentin wet)	2.42	1.80

Discussion/ Conclusion

Table 1 revealed high extinction coefficient values for healthy teeth when compared with carious teeth, in contrast to that observed in studies of KAMBUROĞLU et al., in 2014. This

might be owing to the fact that the structure of enamel and dentin has peculiarities of the morphological structure and chemical composition at various clinical conditions of hard teeth tissues. This peculiarity can be associated with a decrease of enamel density, that is associated with a decrease in the number of prisms in the non-carious teeth pathology and an increase of the gaps between them can be due to enhanced scattering in carious tissues, influenced by air on cavitated carious lesions and which can be brought on by sclerotic dentine formation (Sun et al., 2016). It has been noted in another study that the changes in porosity of the dental tissue, which result from caries, have a similar scale to THz wavelengths (Yang et al., 2016; Yu et al., 2019). This may suggest that the carious tissue is not absorbing but rather scattering the THz radiation. This phenomenon has also been observed in other non-invasive technologies, such as Laser induced fluorescence (QLF, DIAGNOdent), Fiber Optic Transillumination (FOTI), Digital Imaging Fiber Optic Transillumination (DIFOTI) (Amaechi, 2009; Todea, 2016) and Optical Coherence Tomography (OCT) (Fujimoto et al., 2016).

Measurement of refractive index has important clinical implications, too; decrease of this one depends on the extent of demineralization, and, conversely, its may serve as an indicator for caries diagnosis and monitoring (Kamburoglu et al., 2014). Although the large probing area gave an effective spectrum of the tooth medium.

CRAWLEY et al., 2003 and KAMBUROĞLU et al., in 2014 found the mean refractive index for dentine to be 2.6 and 2.53, respectively. Authors of the mentioned studies also suggested that caries appeared as a region of higher absorption relative to healthy structures. This finding is in line with our results.

In this study, a special care has been taken on the analyses of wet and dry tissues. Our findings showed a higher extinction coefficient in hydrated dentin slices than in the same dry samples. In carious lesions, because of the porous structure, there might be a higher liquid concentration than in healthy teeth.THz spectroscopy can be explored on the evaluation of dental tissue. Healthy and carious tissue showed significant differences of refractive index and extinciton values at THz frequency. The sensitivity of THz signals to hydration, which is often a key indicator, is very high, and competing techniques such as high resolution magnetic resonance imaging are less convenient and more expensive. The same high extinction coefficient that limits tissue penetration also promotes extreme contrast between substances with lower or higher water content, which may help to show different contrast between wet and dry samples.

Acknowledgements

This study was financed by The Federal University of Pernambuco through a PhD program.

Conflicts of interest

The authors declare no conflicts of interest.

References

Amaechi BT. Emerging technologies for diagnosis of dental caries: The road so far. J. of Appl. Physics 2009; 105: 102047-102049.

Atam P. Dhawan ; Brian D'Alessandro ; Xiaolei Fu, Optical Imaging Modalities for Biomedical Applications, IEEE Reviews in Biomedical Engineering 3, 69-92 (2010)

Auston DH, K. P. Cheung and P. R. Smith, Picosecond photoonudting Hertzian dipoles, Appl. Phys. Lett. 45, 284 (1984).

Beard M, Turner G, and Schmuttenmaer C. Terahertz Spectroscopy. J. Phys. Chem 2002; 106: 7146–7159.

Chen Q, Zhu H, Xu Y, Lin B, Chen H. Discrimination of Dental Caries Using Colorimetric Characteristics of Fluorescence Spectrum. Caries Res. 2015;49(4):401-7.

Churchley D, Lynch RJ, Lippert F, Eder JS, Alton J, Cabezas CG. Terahertz pulsed imaging study to assess remineralization of artificial caries lesions. J Biomed Opt 2011; 16: 026001-8.

Crawley DA, Longbottom C, Cole BE, Ciesla CM, Arnone D, Wallace VP, et al. Terahertz pulse imaging: a pilot study of potential applications in dentistry. Caries Res 2003; 37: 352–9.

Fujimoto, J.; Swanson. E. The Development, Commercialization, and Impact of Optical Coherence Tomography. Investigative Ophthalmology & Visual Science, v. 57, n.9, pp. 1-13, 2016

He Y, Liu K, Au C, Sun Q, Parrott EPJ, Macpherson EP. Determination of terahertz permittivity of dehydrated biological samples Phys Med Biol. 2017; 62:8882-8893.

Kamburoğlu K, Karagöz, B.; Altan, H.; Özen, D. An ex vivo comparative study of occlusal and proximal caries using terahertz and X-ray imaging. Dentomaxillofac. Radiol. 2019, 48, 20180250.

Kamburoğlu K, Yetimoĝlu NÖ, and Altan H. Characterization of primary and permanent teeth using terahertz spectroscopy. Dentomaxillofacial Radiol 2014;43:1-6.

Katkar RA, Tadinada SA, Amaechi BT and Fried D, Optical Coherence Tomography, Dent. Clin. North Am., 2018, 62, 421–434

Liu Yu, Liu Hao, Tang Meiqiong, Huang Jiaoqi, Liu Wei, Dong Jinying, Chen Xueping, Fu Weiling and Zhang Yang, The medical application of terahertz technology in non-invasive detection of cells and tissues: opportunities and challenges, RSC Adv., 2019, 9, 9354.

Petersen PE. Global policy for improvement of oral health in the 21st century – implications to oral health research of World Health Assembly 2007, World Health Organization. Community Dent Oral Epidemiol 2009; 37: 1–8.

Pickwell E, Wallace VP, Cole BE, Ali S, Longbottom C, Lynch RJ, et al. A comparison of terahertz pulsed imaging with transmission microradiography for depth measurement of enamel demineralisation in vitro. Caries Res 2007; 41: 49–55.

Schwendicke F, Tzschoppe M, Paris S., J Dent. Radiographic caries detection: A systematic review and meta-analysis; 2015 Aug;43(8):924-33.

Sim YC, Maeng I, and Son JH. Frequency-dependent characteristics of terahertz radiation on the enamel and dentin of human tooth. Curr. Appl. Phys 2009; 9: 946–949.

Sun YW, Sy MY, Wang YXJ, Ahuja AT, Zhang YT et al. A promising diagnostic method: Terahertz pulsed imaging and spectroscopy. World J Radiol 2011; 3: 55–65.

Todea C. Non-invasive diagnostic methods in dentistry, Proceedings Volume 9670, Sixth International Conference on Lasers in Medicine; 967002 (2016).

Yang X et al., Biomedical applications of terahertz spectroscopy and imaging. Trends Biotechnol 2016; 34: 810–824.

Figure legends

Figure 1

TDS-THz experimental setup (a) and photo of the real system (b).

Figure 2

The radiated THz field in the time domain and (b) Radiated THz power in the frequency domain.

Figure 3

Refractive index (a) and absorption coefficient measurements conducted for carious and healthy teeth as a function of frequency between 0.1- and 1.0 THz.

Figure 4

Refractive index and absorption coefficient comparisons according to dental structures

APÊNDICE B – ARTIGO "HIGH CONTRAST DENTAL IMAGING USING A RANDOM FIBER LASER IN BACKSCATTERING CONFIGURATION"

Original Paper

Applied Optics

High contrast dental imaging using a random fiber laser in backscattering configuration

Jia Yu Guo[1], Wei Li Zhang[1], Yun Jiang Rao[1], Hua Hui Zhang[1], Rui Ma[1], Daniela S. Lopes[2] Izabella C. X. Lins[2], and Anderson S. L. Gomes[2,3]

[1]Fiber Optics Research Centre, Key Laboratory of Optical Fiber Sensing and Communications, Education

Ministry of China, University of Electronic Science and Technology of China, Chengdu 611731, China

[2]Graduate Program in Dentistry, Universidade Federal of Pernambuco, Recife, PE 50670-901, Brazil

[3]Physics Department, Universidade Federal of Pernambuco, Recife, PE 50670-901, Brazil

Abstract—In this work, a backscattering imaging method based on near infrared random fiber laser is shown to provide a high contrast optical image between carious and sound enamel. The obtained contrast is 0.70, which is more than 8 times higher than the contrast obtained from radiographic imaging. Caries and cracks in enamel could clearly be identified against healthy enamel using the optical system. The near infrared wavelength, high spectral density and low coherence of random fiber laser contribute to its deep penetration, high brightness and low speckle contrast, making it a suitable light source for caries diagnosis. Using the method in a backscattering configuration opens potential clinical use.

Index Terms—caries detection, near infrared, random fiber laser

I. INTRODUCTION

Examination of oral cavity diseases rely on visual, tactile and technology based methods. Besides visual and tactile, the most commonly employed imaging examination method in dental practice for the detection and evaluation of caries lesions is radiography [1], which has evolved from analogic to digital, and can be used for a dental regions [2] or for panoramically view [3]. Three-dimensional radiographic imaging has also been exploited [4]. However, the size or depth of such lesions can be underestimated or even overlooked when the caries is at its early stage or in proximal regions, and can be dependent on dental staff [5].

Recent investigations have been made to find more accurate optically based diagnostic approaches for early dental caries detection, which includes auto-fluorescence [6,7], transillumination [8-10], and reflection [11,12]. Compared with radiography, imaging based on near infrared (NIR) light source has much higher sensitive, uses non-ionizing radiation, handling and operation is simple, which makes it suitable for tooth caries detection. For example, the dental enamel has high transmittance and the dentin has high reflectivity in the NIR region. The mineral loss caused by dental caries leads to an increase in scattering coefficient, thus leading to higher photon scattering (in all directions, including back reflected) than sound enamel and behave differently when imaged (i.e., high imaging contrast). The contrast between sound and demineralized enamel regions was investigated at different wavelengths, and the results showed that wavelengths beyond 1400nm have better performance for caries detection since the photons in sound enamel are absorbed by water [13,14]. Thus, a NIR light source with low cost, high brightness, deep penetration and low spatial coherence is highly desirable for caries detection systems at those wavelengths, and the so-called random laser is very suitable for this purpose, outperforming light-emitting diodes, narrow line lasers and radiography. In brief, random lasers (RLs), are optical sources whose coherent emission arise due to multiple scattering feedbacks within a disordered gain medium, instead of having a cavity formed by two mirrors. They were first unambiguously demonstrated in 1994 [15], and their development, characteristics and several applications have been reviewed in [16]. One of their most interesting characteristics of RL is that speckle patterns caused by independent optical modes are superimposed and averaged out to provide a speckle-free radiation which is favorable for imaging [17,18]. Besides, RLs have the property of high brightness and high spectral density, which are useful to improve the performance of speckle-free imaging [19]. Carvalho et al [20] used a RL as the light source in an epi-illumination configuration and demonstrated that it has potential for biological imaging applications due to its image quality and spectral density.

A more compact and flexible light source can be directly generated in an optical fiber, and a fiber-based amplified spontaneous emission (ASE) sources is an example [21]. Random fiber lasers (RFL) have also been demonstrated in 2007 [22], and a review on this subject can be found in [23]. Among the advantages already mentioned for bulk RL, RFL have the additional advantage of directional emission, and can be made very compact. It has been recently demonstrated, that RFL has better imaging capability than ASE for deeper penetration due to its high spectral density [24-26].

In this manuscript, we demonstrate a tooth imaging system based on the backscattered radiation from a NIR-RFL, which is based on the RFL developed in ref. 24. In there, the proof of concept for using the RFL was introduced. Here, we perform bio-imaging application in extracted human teeth. Our hypothesis is that, since the scattering coefficients of the carious tissue compared to healthy tissue in enamel and dentin are different, the number of photons collected by the detector changes, which can be translated into an image and the basic component of teeth can be analyzed. Our experimental results show that using the RFL as a source has much better imaging quality due to its speckle-free property than narrow line lasers (NLL) and has higher

imaging contrast of caries and enamel than ASE or light-emitting diode. Our results are also compared with radiography and optical microscope imaging, and it indicates that the RFL imaging can better detect caries thanks to its wavelength-related merits.

II. METHODS

II.1 – Experimental Setup

The experimental setup consists of light source and imaging part, as shown in Fig.1. The RFL is generated through a half-opened structure composed of a fiber loop mirror (i.e., formed from a 3dB couple) and 25 km-length single mode fiber (SMF). A Raman pump with central wavelength of 1455 nm is injected into the SMF through a 1455/1550 nm wavelength division multiplexer (WDM 1). Another WDM, WDM2, is used at the end of the SMF in order to split out the residual pump light and make sure only the generated RFL injects into the imaging part. An isolator (ISO) is used to eliminate light reflection, making sure that the laser is generated only through randomly distributed Rayleigh scattering. To adjust the output light in appropriate power for imaging, a variable optical attenuator (VOA) is used. For comparison, an ASE light source based on Erbium doped fiber and a 1550 nm narrow line width laser (NLL) are also used separately to replace the RFL for imaging.

The imaging part employs a backscattering configuration. A 30 m extra-large mode area stepindex MMF (core and cladding diameter are 105 and 125 μm respectively, NA is 0.22, YOFC) is spliced after the VOA and before the imaging system to reduce the spatial coherence of light source(s). The illumination light from the MMF is collimated by lens1 (focal length of 6.2 mm) and directed by a beam splitter to the sample. The reflected light from the sample is collimated by lens2 (focal length of 120 mm) and directed by the beam splitter to the CCD (Xenics, Bobcat640-GigE).

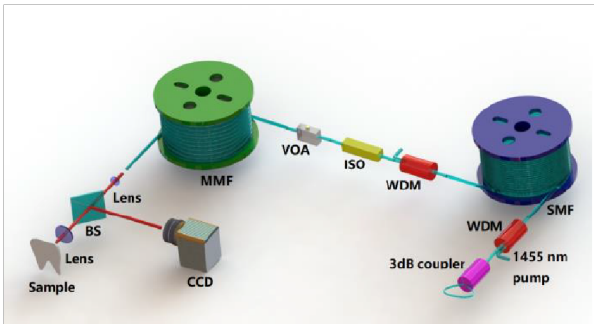

Fig. 1. Schematic of experimental setup. WDM, wavelength division multiplexer. SMF, single mode fiber. ISO, isolator. VOA, variable optical attenuator. MMF, multimode fiber. BS, beam splitter

II.2 – Sample preparation

Ethical approval was obtained from the ethical committee of the Federal University of Pernambuco, Pernambuco, Brazil. Newly extracted human permanent molar teeth were cleaned and stored in deionized water. Each tooth was sectioned mesiodistally in parallel with the long axis of the crown using a double-sided diamond disco (Buehler Ltda., Lake Bluff, IL, USA) coupled to a precision cutter (Isomet 1000 Speed Saw, Buehler Ltda., Lake Bluff, IL, USA). Samples with a mean thickness of d ≈ 1.00 ± 0.1mm were obtained. Afterwards, both sides of each section were examined under a stereomicroscope at 20x magnification (Stemi 2000; Carl Zeiss, Jena, Germany). Teeth were identified with a sound or carious lesion area in the enamel and/or dentine. Examination of the 5 slices of teeth surfaces revealed a distribution carious and healthy areas of the studied sample teeth. Figure 2 shows a representative tooth slice and the cutting procedure.

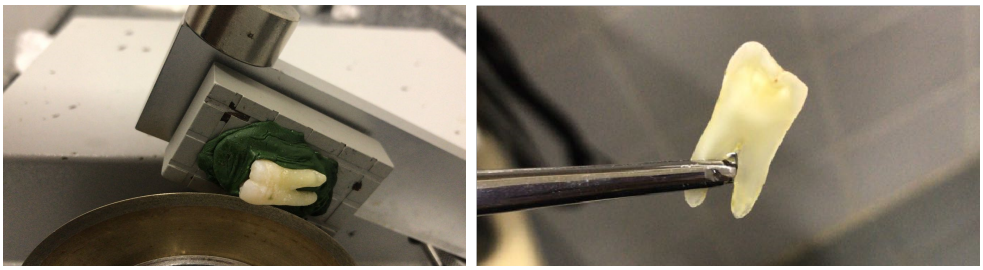

Figure 2 – (left) tooth sample being cut; (right) representative tooth sample slice.

III. RESULTS AND DISCUSSION

We initially show the optical spectra of the three light sources used in this experiment (RFL, ASE, and NLL) are shown in Fig. 3(a). The full width at half maxima (FWHM) of the RFL is ~1.5 nm, which is obtained at the pump power of 33.4 dBm. The FWHM of ASE is 5 times broader than the RFL, which is about 7nm and the NLL has the narrowest FWHM of less than 0.01 nm. The coherence length, D_c, is calculated as $D_c = \lambda^2/D\lambda$, where λ and $D\lambda$ are the center wavelength and spectral bandwidth respectively. RFL, thus, has much shorter coherent length than NLL. Our previous work has demonstrated that after the decoherence of a 30m extra-large mode area step index MMF, the RFL, and ASE can reach a speckle contrast of ~0.049 and 0.039, which is near the threshold of human perception and is lower enough for speckle-free imaging [24-26]. The power reaching the teeth specimens from each of the sources was controlled to be at most 4dBm. Care was taken to avoid saturation of the CCD detector.

The backscattering imaging result of RFL, ASE, and NLL are shown in Fig. 3 (b)-(d), respectively. The enamel has high transmittance, most of the light penetrates the enamel and only a small percentage is scattered back to the detector. Therefore, the enamel part appears as dark region, while the dentin has high reflection and appears as a bright region. Moreover, the mineral loss of the carious region would cause more than two orders of magnitude increase in scattering coefficient and thus also appear as bright region in backscattering image [28]. This difference in scattering coefficient makes enamel and caries high contrast and easy to be identified. For RFL and ASE, the enamel, dentin and demineralized enamel regions of tooth specimen can be clearly identified, while for NLL, strong speckle patterns occur

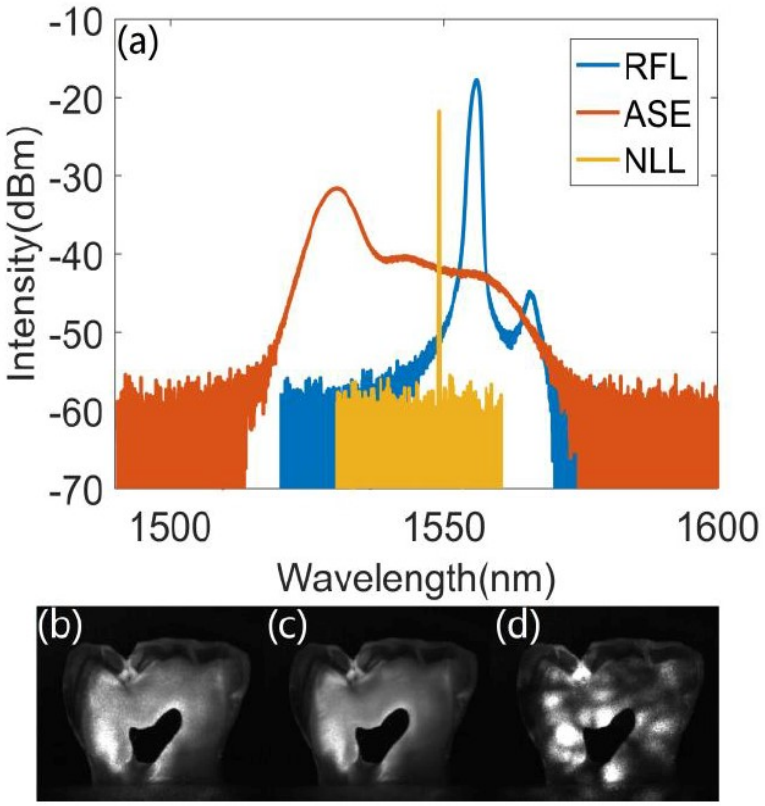

Fig. 3. Imaging from different sources. (a) spectrum of RFL, ASE, and NLL (b)-(d)imaging result of RFL, ASE and NLL, respectively.

and blur the image. It is because RFL and ASE have relatively broad spectrum and short coherence length, which lead to low speckle contrast after decoherence of the MMF. For NLL, its long coherence length causes strong modal interference and obvious speckle patterns that makes the image too obscure to distinguish between the demineralized from healthy areas. Images of the sample for different powers from the RFL and the ASE are shown in Fig. 4 for comparison.

It can be seen that the RFL images are a bit brighter than ASE images at the same radiation power, because the former has higher spectral density and lower absorption. For a quantitative comparison, the intensity integration of each figure of Fig. 4(a)- (f) is calculated, and is given in Fig. 4(g), as a function of the output power. It is observed that, the RFL image is brighter than the ASE image for all the output power, and has comparable speckle contrast to guarantee image quality. Although the bandwidth of RFL is narrower than ASE, its coherence after the MMF is low enough for speckle-free imaging, and the high spectral density and low absorption make the RFL image brighter. Furthermore, it has been shown that even though RL or RFL have narrow bandwidth, they are highly multimode and speckle free [18].

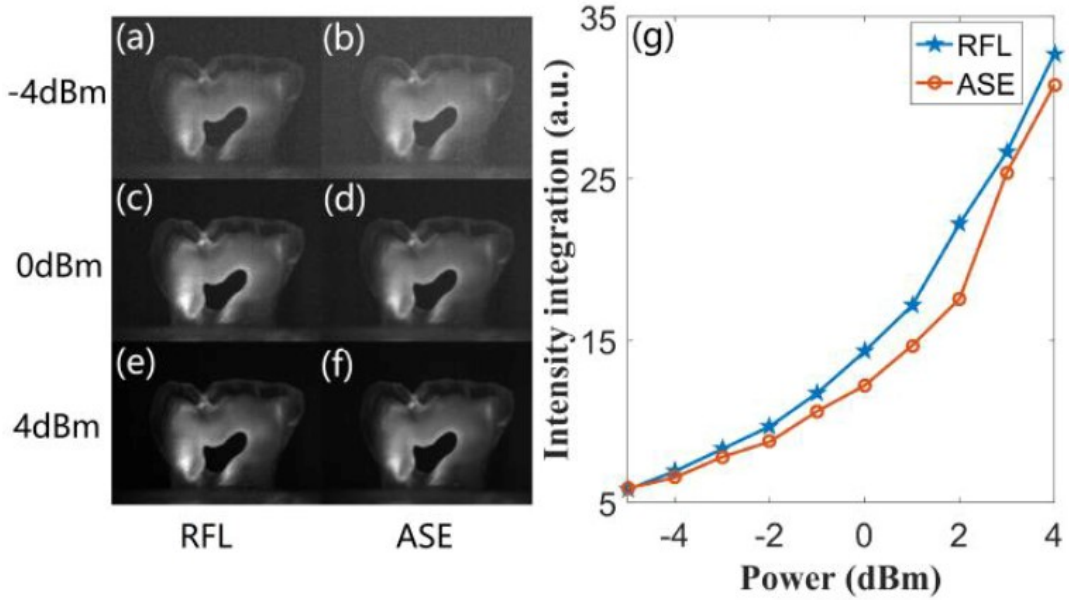

Fig. 4. Imaging at different pump power. (a)-(f) image of different power for RFL and ASE, (g) the integral intensity of RFL and ASE.

As mentioned before, the cavities and fissures could open the way to mineral loss, which lead to two orders of magnitude increase in scattering coefficient at NIR region. Caries and cracks thus appear as bright regions on the image because more light is scattered back to the CCD. Fig.5(a-d) compares the results from RFL and ASE illumination at power of 4 dBm. Figs. 5 (a,b) shows the images formed, while Fig. 5(c) gives intensity fluctuation among enamel and crack (along the red dashed curve), and Fig.5(d) depicts the intensity fluctuation along the red solid curve. The peak in Fig. 5(c) represents the crack region, and other part of the curve represents the enamel region. It can be seen that the RFL image has higher contrast between the crack and health region of the enamel, than the ASE image, this is in agreement with the conclusion of Fig. 4. We also calculate the contrast ratio between crack and sound enamel for RFL and ASE imaging. The contrast I defined as in Eq. (1)

$$C = (I_{crack} - I_{enamel}) / (I_{crack} + I_{enamel}) \quad (1)$$

where I_{crack} and I_{enamel} are the average intensities of the crack and the sound enamel. The contrast is 0.32 and 0.25 for RFL and ASE respectively, indicating that the RFL image can better identify the crack region. Fig.4(d) compares the intensity between enamel and dentin. Note that the two light sources, RFL and ASE, have enough low speckle contrast to fulfill speck-free imaging, thus the fluctuation in intensity arises from different concentrations of dentin. The standard deviation of intensity is calculated to be 0.18 and 0.14 for RFL and ASE, respectively, which means RFL has a better performance for dentin concentration detection.

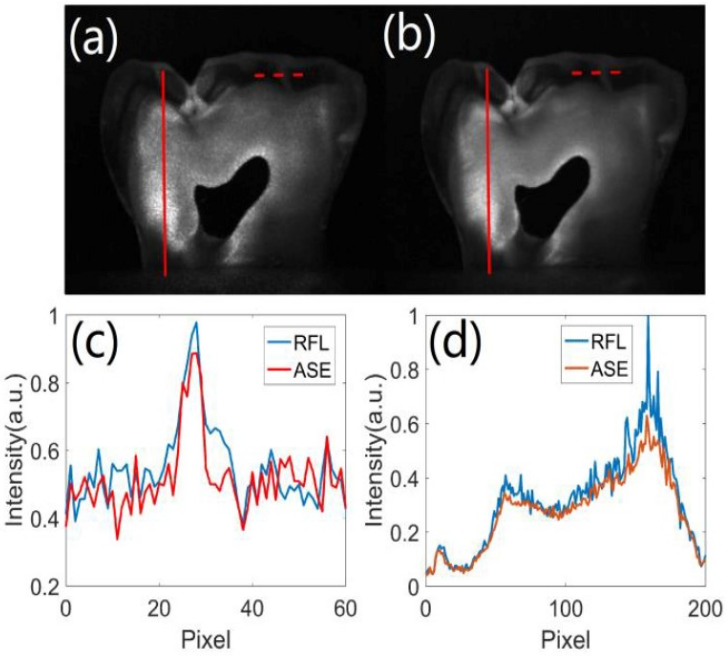

Fig. 5. Imaging comparison between RFL and ASE. (a) RFL image, (b) ASE image, (c) Intensity along the red dotted curve, (d) Intensity along red solid curve.

Furthermore, we compare the RFL imaging with other two different imaging methods, i.e., radiography and microscope. In Fig. 6(b), the radiography could only identify enamel and dentin, while not capable to detect all details in enamel and dentin. For example, the crack observed in Fig.6(a) is not detected by radiography. In Fig. 6(c), the optical microscope can show crack in enamel but the dentin region appears uniform. By contrast, in Fig. 6(a), the RFL based backscattering image method could further distinguish the mineral concentration showing different brightness in the dentin region thanks to the penetration ability of its NIR wavelength, as well as its high spectral density.

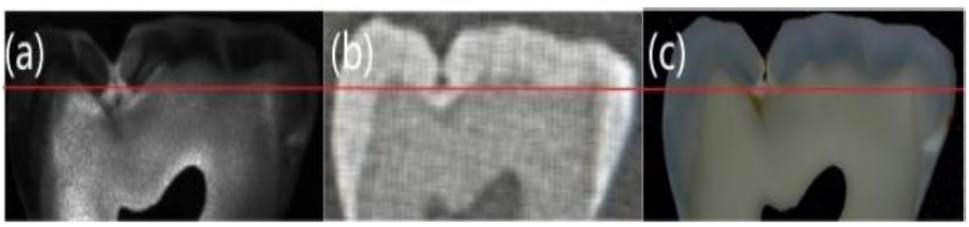

Fig. 6. Imaging from different methods. (a) RFL, (b)Radiography, (c)Microscope.

For quantitative comparison, Fig. 7 depicts the intensity profile of the backscattered photons along the red curve marked in each images of Fig. 6. Note that the RFL (blue curve)

and microscope (red curve) detect the backscattered light while radiography (yellow curve) detect the transmitted light, and that leads to different patterns for intensities as seen in fig. 7.

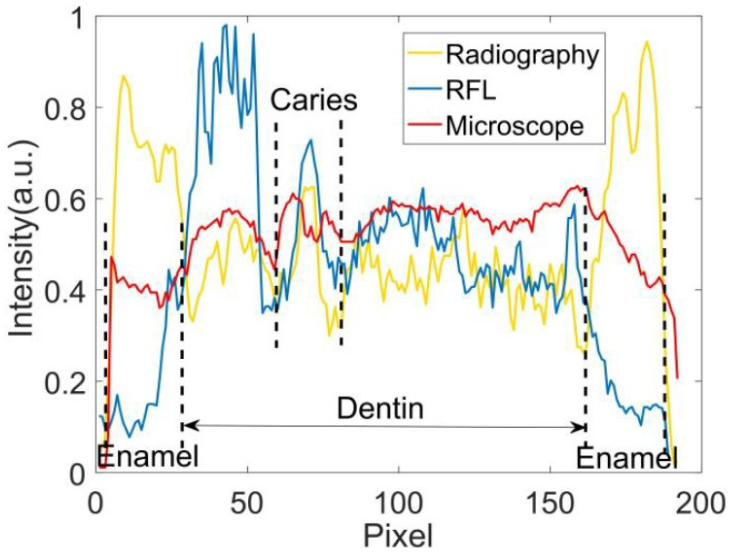

Fig. 7. Intensity of cross section of tooth specimen.

From fig 7, we first calculated the contrast between enamel and dentin from Eq. 2, where $I_{dentine}$ and I_{enamel} are average intensities of the dentin and enamel, respectively. The values of C_{de} are given in Table 1.

$$Cde = (Identine - Ienamel) / (Identine + Ienamel) \quad (2)$$

TABLE I
THE CONTRAST OF RFL, RADIOGRAPHY, AND MICROSCOPE

Contrast	RFL	Radiography	Microscope
C_{de}	0.44	0.22	0.15
C_{ce}	0.70	0.08	0.18

The RFL has the highest value of C_{de}, which verifies that the RFL is the best light source to distinguish enamel and dentin.

Secondly, we also consider the contrast between the caries and the sound enamel. The caries regions appear as the brighter region in the reflective image (Fig. 5 (a) and (c)) and as a darker region in the transmitted image. The quantitative value of contrast is defined as in Eq. 3, which is 0.70, 0.08 and 0.18 for the RFL image, radiography and microscope

$$Cee = (Icaries - Ienamel) / (Icaries + Ienamel) \quad (3)$$

respectively, as given in Table 1. It is obvious that the RFL imaging has the best performance in distinguishing enamel from both dentin and caries.

IV. Conclusion

In conclusion, backscattering tooth imaging method based on NIR-RFL as the optical source has been investigated. The experimental results indicate that, owing to its low coherence, high spectral density and speckle-free nature, the RFL (and random lasers) have the best comprehensive performance as an optical source in finding dental details like demineralized and crack areas, separating enamel from dentin as well as identifying mineral concentration, compared to other NIR light sources such as NLL and ASE. It also outperforms other imaging measuring methods like radiography and optical microscopy, with a higher imaging contrast, as shown in table I. Therefore, the RFL is an ideal light source for dental caries lesions diagnosis. Whitin the limitations of this study, we anticipate that technologically it is feasible to design a compact RFL or a semiconductor random laser based backscattering imaging technique, which can potentially be used in clinical environment as of subjective analysis.

Acknowledgments

This work was supported in part by the National Natural Science Foundation of China under Grants 61575040, 61635005, and 61811530062. The work of ASLG in China was partially supported by the Ministry of Science, Technology and Innovation, under grant number 400011/2016-6, program Brazil-China Center for Research and Innovation in Nanotechnology. ASGL, ICXL and DSL also acknowledge the financial support from the Brazilian agencies CNPq, CAPES, FACEPE, and the INCT of Photonics program.

REFERENCES

[1] J. Gomez, “Detection and diagnosis of the early caries lesion,” BMC Oral Health, vol. 15, no. 1, pp. S3, Sep. 2015.

[2] Abogazalah, N., Eckert, J. G. & Ando, M. *In vitro* performance of near infrared light transillumination at 780-nm and digital radiography for detection of non cavitated approximal caries. *J Dent.* **63**, 44–50 (2017).

[3] Perschbacher S. Interpretation of panoramic radiographs. *Aust Dent J* 2012; 57(Suppl 1): 40–5.

[4] J. K. Mitchell, A. R. Furness, R. J. Sword, S. W. Looney, W. W. Brackett, M. G. Brackett, “Diagnosis of Pit-and-fissure Caries Using Three-dimensional Scanned Images,” Operative Dentistry, vol. 43, no. 3, pp. E152-E157, May-Jun. 2018.

[5] M. A. Geibel, S. Carstens, U. Braisch, A. Rahman, M. Herz, A. Jablonski-Momeni, “Radiographic diagnosis of proximal caries-influence of experience and gender of the dental staff,” Clinical Oral Investigations, vol. 21, no. 9, pp. 2761-2770, Dec. 2017.

[6] S. A. Son, K. H. Jung, C.C. Ko, Y. H. Kwon, "Spectral characteristics of caries-related autofluorescence spectra and their use for diagnosis of caries stage," J. Biomed. Opt., vol. 21, no. 1, pp. 015001, Jan. 2016.

[7] Denise Maria Zezell, Adriana da Costa Ribeiro, Luciano Bachmann, Anderson Stevens Leonidas Gomes, Christel Rousseau, John Girkin, Characterization of natural carious lesions by fluorescence spectroscopy at 405 nm excitation wavelength, J. Biomedical Optics 12, 064013-1/5 (2007).

[8] S. Chung, D. Fried, M. Staninec, C.L. Darling, "Multispectral near-IR reflectance and transillumination imaging of teeth," Biomed. Opt. Express, vol. 2, no. 10, pp. 2804–2814, Oct. 2011.

[9] Lena Karlsson, Ana M. A. Maia, Bernardo B. C. Kyotoku, Sofia Tranæus, Anderson S. L. Gomes and Walter Margulis, Near-infrared transillumination of teeth: measurement of a system performance, Journal of Biomedical Optics 15, 036001 (May/June 2010).

[10] A. M. A. Maia, L. KARLSSON, W. Margulis; A. S. L. Gomes Evaluation of two imaging techniques: near-infrared transillumination and dental radiographs for the detection of early proximal enamel caries, Dento-Maxillo-Facial Radiology, v. 40, p. 429-433, 2011.

[11] W. A. Fried, D. Fried, K. H. Chan, C.L. Darling, "High contrast reflectance imaging of simulated lesions on tooth occlusal surfaces at near-IR wavelengths," Lasers Surg. Med., vol. 45, no.8, pp.533–541, Oct. 2013.

[12] J. C. Simon, S. A. Lucas, M. Staninec, H. Tom, K. H. Chan, C. L. Darling, M. J. Cozin, R. C. Lee, D. Fried, "Near-IR transillumination and reflectance imaging at 1300nm and 1500-1700-nm for in vivo caries detection," Lasers Surg. Med., vol. 48, no. 6, pp. 828–836, Nov. 2016.

[13] K. H. Chan, D. Fried, "Multispectral cross-polarization reflectance measurements suggest high contrast of demineralization on tooth surfaces at wavelengths beyond 1300 nm due to reduced light scattering in sound enamel," Journal of Biomedical Optics, vol. 23, no. 6, pp. 060501, Jun. 2018.

[14] V. B. Yang, D. A. Curtis, D. Fried, "Cross-polarization reflectance imaging of root caries and dental calculus on extracted teeth at wavelengths from 400 to 2350 nm," Journal of Biomedical Optics, vol. 11, no.11, pp. 10.1002 Nov. 2018.

[15] N. M. Lawandy, R. M. Balachandran, A. S. L. Gomes, and E. Sauvain, "Laser action in strongly scattering media," Nature, vol. 369, no.6478, pp. 340-340, May. 1994.

[16] Feng Luan, Bobo Gu, Anderson S. L. Gomes, Ken-Tye Yong, Shuangchun Wen and Paras N. Prasad, Lasing in Nanocomposite Random Media, Review Paper, Nano Today 10, 168-192 (2015).

[17] B. Redding, M. A. Choma, and H. Cao, "Speckle-free laser imaging using random laser illumination," Nature Photon., vol. 6, no.6, pp. 355–360, Jun. 2012.

[18] B. H. Hokr et al, "A narrow-band speckle-free light source via random Raman lasing," Journal of Modern Optics, vol. 63, no. 1, pp. 46-49, 2016.

[19] B. H. Hokr et al, “Lighting up microscopy with random Raman lasing,” Real-time Measurements, Rogue Events, and Emerging Applications, San Francisco, CA, 2016, pp. 9732.

[20] Mariana T. Carvalho et al, “Random laser illumination: an ideal source for biomedical polarization imaging? ” Multimodal Biomedical Imaging XI, San Francisco, CA, 2016, pp. 9701.

[21] B. Redding, P. Ahmadi, V. Mokan, M. Seifert, M. A. Choma, and H. Cao, “Low-spatialcoherence high-radiance broadband fiber source for speckle free imaging,” Opt. Lett., vol. 40, no. 20, pp. 4607–4610, Oct. 2015.

[22] Christiano J. S. de Matos, Leonardo de S. Menezes, Antônio M. Brito-Silva, M. A. Martinez Gámez, Anderson S. L. Gomes and Cid B. de Araújo, Random Fiber Laser, Phys. Rev. Lett. 99, 153903-1/4 (2007).

[23] D. V. Churkin, S. Sugavanam, I. D. Vatnik, Z. Wang, E. V. Podivilov, S. A. Babin, Y. Rao, and S. K. Turitsyn, “Recent advances in fundamentals and of random fiber lasers”, Adv. Opt. Photonics, vol. 7, no. 3, pp. 516-569, Sep. 2015.

[24] R. Ma, Y. J. Rao, W. L. Zhang, B. Hu, “Multimode Random Fiber Laser for Speckle-Free Imaging,” IEEE Journal of Selected Topics in Quantum Electronics, Vol.25, no. 1, pp. 0900106, Jan.-Feb., 2019.

[25] R. Ma, W. L. Zhang, J. Y. Guo, Y. J. Rao, “Decoherence of fiber supercontinuum light source for speckle-free imaging,” Optics Express, Vol.26, no. 20, pp. 26758-26765, Oct. 2018.

[26] R. Ma, J. Q. Li, J. Y. Guo, H. Wu, H. H. Zhang, B. Hu, Y. J. Rao, W. L. Zhang, “Highpower low spatial coherence random fiber laser,” Optics Express, Vol.27, no. 6, pp. 8738-8744, Mar. 2019.

APÊNDICE C – ARTIGO "SURFACE EVALUATION OF ENAMEL ETCHED BY Er,Cr:YSGG LASER FOR ORTHODONTICS PURPOSE"

Original Paper

The Journal of Contemporary Dental Practice

Surface evaluation of enamel etched by Er,Cr:YSGG laser for orthodontics purpose

Er,Cr:YSGG laser for orthodontics purpose

Daniela S. Lopes[a], Daisa L. Pereira[b], Claudia C. B. O. Mota[c], Luciana S. A. Melo[d], Patricia Aparecida Ana[e], Denise M. Zezell[f], Anderson S. L. Gomes[g]

[a] School of Dentistry, Federal University of Pernambuco (UFPE), Recife-PE, Brazil

[b]University of Sao Paulo and Center for Lasers and Applications, Nuclear and Energy Research Institute (IPEN – CNEN/SP), Sao Paulo-SP, Brazil

[c] School of Dentistry, Caruaruense Association of Technical and Higher Education (ASCES), Caruaru-PE, Brazil

[d] Physics Department, Federal University of Pernambuco (UFPE), Recife-PE, Brazil

[e] Biomedical Engineering Department, Federal University of ABC (UFABC), Sao Bernardo do Campo-SP, Brazil

[f] Center for Lasers and Applications, Nuclear and Energy Research Institute (IPEN – CNEN/SP), Sao Paulo-SP, Brazil

[g] Physics Department and School of Dentistry, Federal University of Pernambuco (UFPE), Recife-PE, Brazil

Corresponding author:

Anderson S. L. Gomes

e-mail: anderson@df.ufpe.br or gomesanderson@hotmail.com phone:

55-81-21267636

Laboratory of Optoelectronics and Photonics, Department of Physics, University of Pernambuco

Av. Prof. Luis de Barros Freire , Cidade Universitária, Recife 50670-901

– PE – Brazil.

Abstract

Aim: To compare the effect of Erbium, chromium: yttrium-scandium-gallium-garnet (Er,Cr:YSGG) laser at different irradiation parameters and acid etching on the shear bond strength (SBS) of orthodontic brackets to enamel.

Materials & Methods: Forty bovine incisors were randomly distributed into groups (n=10): G1: 37% phosphoric acid etching; G2: Er,Cr:YSGG laser etching 19.1 J/cm2; G3 :Er,Cr:YSGG, 29.3J/cm2; and G4: Er,Cr:YSGG, 42.4 J/cm2. After treatments, metallic brackets were bonded using Transbond XT adhesive system. After light curing, the samples were subjected to 500 thermal cycles, debonded with a universal testing machine, and the SBS values were recorded. After debonding, surface morphology was evaluated using scanning electron microscopy and optical coherence tomography. The values of SBS testing were analyzed by one-way ANOVA analysis of variance and Tukey post hoc test, at 5% significance level.

Results: The mean SBS values of G1, G2, G3 and G4 groups were 6.2±1.7 MPa, 4.6±2.5 MPa, 7.0±2.2 MPa and 8.0±3.6 MPa, respectively. Laser irradiation promoted rough surfaces in all parameters used, and OCT analysis revealed higher optical changes on lased groups when compared to phosphoric acid.

Conclusion: Er,Cr:YSGG laser irradiation operated at 42.4 J/cm2 and 29.3 J/cm2 is a better alternative for etching enamel prior the orthodontics treatment than the phosphoric acid.

Clinical Significance: Er,Cr:YSGG laser irradiation is better than the phosphoric acid for etching enamel prior the orthodontics treatment because laser irradiation promotes similar shear bond strengths and preventing demineralization around orthodontic brackets.

Keywords: enamel conditioning, Er,Cr:YSGG laser, laboratory research, orthodontics brackets

Introduction

Brackets are a fundamental part in orthodontic treatment and they must remain well fixed to the teeth throughout the therapy[1], which requires adequate conditioning, without secondary effects. The phosphoric acid represents the standard enamel conditioner in orthodontic practice, whose aim is to prepare and to create an irregular surface that propitiate the adequate bonding of etch-and-rinse adhesive systems[2]. The main advantage of phosphoric acid etching is the high level of shear bond strength achieved[3].

Alternative methods to prepare dental surfaces, such as laser irradiation, have attracted increasing attention since the first laser application reported in 1964[4]. Among the high-power lasers most used for dental applications is the Er,Cr:YSGG laser, which emits at 2.78 μm and is strongly absorbed in hard tissues due to its interaction with both water and OH^- from hydroxyapatite at the tissue interface[5]. Due to the ablation process, the tissue becomes more resistant to demineralization; also, laser irradiation promotes bacterial removal and reduces secondary caries lesion susceptibility increasing the success of the procedure.

It can be emploed without creating a smear layer[6] and can offer a similar bonding effect when compared to conventional acid-etching and roughening the surface can markedly increase the bonding area between the substrate and resin[6-8].

Considering that orthodontic treatment is often of long duration, another advantage promoted by Er,Cr:YSGG laser irradiation is the long-lasting protective effect against

secondary caries[9], essential for the prevention of the white spot lesions that may occur around the brackets during the orthodontic treatment.

Many factors are known to influence the effects of Er,Cr:YSGG laser treatment on dental hard tissues, such as the output power, energy density, the repetition rate and cooling water/air ratio[10].

Concerning the laser parameters used for enamel etching prior bonding of brackets, the literature is controversial and it was not identified studies that relate the use of Er,Cr:YSGG for this purpose, which motivated the accomplishment of the present study.

In this way, the objective of this study was to evaluate the effects promoted by Er,Cr:YSGG laser, when operated at different laser parameters aiming enamel etching for orthodontics purposes, through the following factors: the shear bond strength, the adhesive remnant index and the surface morphology of the enamel.

Materials and methods

This study was approved by the Ethical Committee on Animal Experiments. The procedures for sample preparation were in accordance with the specifications of ISO/TS

11405:2015[11]. Forty freshly extracted bovine incisors were selected and stored in 0.5% Chloramine-T solution during 48 hours for disinfection. The root portion of all teeth was removed and the crowns had their buccal surface manually polished with sandpaper P600 (3M Unitek, USA) to reduce the grooves presented in bovine enamel. The specimens were included in a cylindrical support and embedded in acrylic resin, keeping the buccal surface parallel to the mold base. Specimens were stored in

distilled water (4ºC) until bonding procedures. They were randomly distributed into four experimental groups (n=10), according to Table 1.

For the control group, etching was performed with a 37% phosphoric acid gel (FGM Produtos Odontológicos, Brazil) for 15 seconds followed by a 15 seconds water rinse. Specimens were air dried until a frosty white appearance was achieved.

Laser irradiation was performed with an Er,Cr:YSGG laser (Biolase Technology Inc., USA), emitting at 2.78 μm with 20 Hz repetition rate and the pulse width was approximately 140 μs for 15 seconds, at three different power settings (Table 2). A sapphire MZ6 tip of 600 μm diameter and 6 mm length was used with 55% air and 45% water coolant[12].

During the irradiation, the samples were positioned in a high-precision motorized translator (Newport, USA) 1 mm away from the laser tip adjusted to a speed of 3.8mm/s, thus standardizing the irradiation condition.

Brackets for upper incisors with a 15.3 mm^2 base area were used (Dental Morelli, Brazil). Brackets were bonded according to the manufacturer's instructions (Table 3) and were positioned at the center of the buccal surface to simulate the clinical procedure. The excess of orthodontic cement was carefully removed before light curing. Photoactivation was performed using a LED curing unit emitting 1,200 mW/cm^2 (Bayswater, Australia) for 10 seconds in each proximal side of the bracket (mesial and distal).

After 24h storage in distilled water at 37±1ºC, all specimens were thermocycled (Ética Equipamentos Científicos S/A, Brazil). 500 cycles of alternate baths (5-55± 2ºC), 30 seconds in each bath and 2 seconds transfer time were performed.

Specimens were prepared for the shear bond strength (SBS) test, under a universal testing machine (Emic Equipamentos Industriais Ltda, Brazil) with a chisel at 0.5 mm/min speed and 200 kgf load cell.

To evaluate the SBS, the size of the bracket base has a meaningful importance, since the sustaining force increases as a function of the base area dimension. Therefore, the values were measured considering the rupture strength and the size of the bracket base[8]. The debonding force (F) was obtained in Newtons (N) and the strength in megaPascal (MPa).

After debonding, teeth were examined under a stereomicroscope at 20x magnification (Zeiss, Germany) and classified according to the Adhesive Remnant Index (ARI)[13]:

- Score 0 - no adhesive remnant left on the tooth;
- Score 1 - less than 50% adhesive remnant left on the tooth; • Score 2 - more than 50% adhesive remnant left on the tooth;
- Score 3 - 100% adhesive remnant left on the tooth.

All specimens were submitted to scanning electron microscopy (TM 3000, Hitachi, Japan) and optical coherence tomography (OCT) analysis before and after the acid or laser etching. The OCT system (Callisto SD-OCT, Thorlabs Inc, USA) Thorlabs Inc, USA) operates at 930 nm central wavelength, spectral bandwidth of 100 nm, maximum output power of 5 mW, axial resolution of 7/5.3 μm (air/water), lateral resolution of 8 μm, maximum imaging depth at 1.6 mm, and axial scan rate 1.2 kHz, capturing two frames per second with 105 dB of sensitivity. Two-dimensional (2D) OCT images were captured with 2000 columnsx512 rows and 6 mm transversal scanning, whilst three-dimensional (3D) images were captured with 400x400x400

columns in each of XZ, YZ, XY axis. These two techniques complements each other in morphological analysis, due to their very different spatial resolutions.

Descriptive statistics, means and standard deviation were calculated for each group. Statistical analysis was performed using GraphPad Prism 6 (GraphPad Software, USA). Multiple comparisons were performed for SBS values between groups using one-way ANOVA and Tukey *post hoc* test. For the ARI evaluation, Chi-square test was used. A 5% significance level was adopted.

Results

Descriptive statistics for comparison of shear bond strength scores are given in Table 4. Group 4 yielded the highest mean shear bond strength (8.0±3.6 MPa), whilst the phosphoric acid had mean shear bond strength of 6.2±1.7 MPa. ANOVA analysis did not reveal statistically significant differences among the groups (P=0.1310).

ARI scores are listed in Table 5 and Chi-square test showed no statistically significant differences among the four groups (P=0.5508).

Figure 1 shows the SEM images of enamel surface after the acid etching and the laser irradiation under different protocols. The treatment with 37% phosphoric acid produced qualitatively rough surfaces in a pattern way, due to the dissolution of prisms and boundary regions. The laser-ablated surfaces of all experimental groups of this study presented depressions with fissures and conical craters and sharp enamel projections, without evidence of melting or carbonization. All laser-treated surfaces were accompanied by the appearance of slight dehydration cracks that can aid the penetration of resin. After debonding, it was possible to observe the presence of fragments of the adhesive system in all images. Also, all samples presented

qualitatively rough surfaces, and laser-ablated ones presented higher projections, depressions and cracks when compared to the surface conditioned with the phosphoric acid.

The optical characteristics of enamel after conditioning and after debonding by representative OCT images are shown in Figure 2. In sample conditioned with phosphoric acid, it is observed an intense backscattered signal at the enamel surface, represented by a bright zone, and darkened regions below the surface, which correspond to the loss of signal with increasing depth into the sample. After laser irradiation, the OCT images showed irregularities on the surface, which were more intense with the increase of laser energy density. The subsurface regions presented bright areas interspersed with dark areas, and these regions appeared in greater quantity in the samples irradiated with higher energy density. These irregularities in the backscattered signal from the subsurface of lased samples decreased after debonding, in which it is observed a decrease on bright areas when compared to samples after irradiation.

Discussion

In this study, the effect of phosphoric acid etching or laser irradiation on surface characteristics, SBS values of brackets, and ARI scores were evaluated.

The etching of enamel with Er,Cr:YSGG laser for orthodontic purposes has several advantages, mainly considering the temperature rises promoted by laser irradiation on enamel surface[14]. The heating promoted by laser irradiation is enough to change the crystallinity and composition of enamel (such as the elimination of carbonate, the increase the hydroxyapatite crystals and the formation of new

crystalline phases), and these changes can be responsible to increase the resistance of laser etched enamel to the development of early caries lesions[15].

The removal of material using erbium lasers occurs by thermal ablation. In this process, the absorption of laser irradiation by bounded water molecules in the hard tissue leads to a temperature increase that promotes their microexplosions. To achieve ablation in any material, the laser energy density must be adjusted so that it is above the ablation threshold[15].

The present study determined the shear bond strength of brackets to enamel and the surface characteristics of enamel etched, comparing with different output power of Er,Cr:YSGG laser, using the Transbond XT bonding system, considered as the “gold standard” for this clinical application[6].

We found the highest bond strength value in the 2.41W laser-etched group (G4) (8.0 MPa ± 3.6 MPa). This result is in accordance with the findings of Basaran *et al.* 2007[6], which worked with power output between 0.5 W, 1W and 2 W. In the case of this study it was obtained (4.34 ± 3.16) MPa, (9.88 ± 4.43) MPa, and (11.14 ± 4.75) MPa, respectively and with brackets bonded with Transbond XT.

Reynolds reported that adequate bond forces in orthodontics range from 6 to 8 MPa[16]. This *ex vivo* study demonstrated that mean bond strength values of G3 and G4 groups remained within this range.

When the morphological effects of Er,Cr:YSGG lasers on dental tissues were examined, this research showed that all laser parameters used (G2, G3 and G4) were able to promote higher morphological changes on enamel than the acid etching (G1). SEM images revealed that the morphological changes have a positive relation with

the energy density used. The acid-etched sample had regular and slight grooves visible, whereas the laser groups created uneven and heterogeneous surface characteristics with microcracks in SEM analysis, as observed in Figure 1.

OCT analysis supported the findings of SEM evaluation. The ability to reveal the enamel morphology without sectioning or dehydrating the samples is a significant advantage of OCT. Due to this fact, the feasibility of OCT to evaluate the effects of laser irradiation on optical characteristics of enamel when used for etching was also evaluated. In this study, the SEM and OCT images were acquired to allow the visual evaluation of the groups and characterization of enamel structure after debonding (Figure 2). The SEM explored dental surface analysis. OCT provides cross-sectional tomographic imaging of tissue microstructures, carrying structural information of the biological sample by the reflected and backscattered light from the tissue within a penetration depth of ~1mm in enamel[17-19].

By analyzing the OCT images after enamel etching, it is possible to observe the loss of the backscattered signal in the subsurface of enamel after phosphoric acid application, which can be due to chemical effects of phosphoric acid. After debonding, however, the subsurface is uniform and does not present the loss of backscattered signal. This fact occurred most probably due to the primer application, which penetrates the micropores of enamel after surface conditioning and changed its optical properties[20].

However, in the laser-treated groups, the subsurface of the tissue appears brighter in OCT images obtained immediately after laser irradiation. This aspect can be due to the thermal effects of laser irradiation, as well as the qualitatively roughness promoted, which increase

with the augment of energy density and scattering, confirmed by the literature data[1,2,4,5], which also presented a positive relation with energy density in this study. The OCT images also show that the roughness promoted by laser irradiation, at any energy density, is higher than that promoted by phosphoric acid, which agrees with the findings observed by SEM analysis. These aspects were more indicative of microexplosion than of melting, some microcracking may occur as a result of local thermal stresses induced during the irradiation process. If the appropriated parameters for the laser radiation are properly used, there is no expected or reported side effects, particularly due to de fact that the laser beam used is a non-ionizing radiation.

After debonding, the brighter aspect of subsurface of laser etched samples is almost fully missed; however, the surface remains rough. This finding can be also due to the primer penetration in the subsurface, which promoted chemical changes on enamel and, in this way, changed its optical aspect in the same way that occurred in samples that were conditioned with phosphoric acid. Therefore, OCT analysis allowed the observation that the primer adsorption is similar on phosphoric acid or laser treated enamel. The primer penetration has a positive effect on adhesion of brackets, and this fact is supported by the SBS values obtained in the present study. The ARI most prevalent score was 0, demonstrating that shear occurred mainly between the dental surface and the adhesive system. The laser treated groups, particularly groups II and IV, presented the largest number of specimens classified as score 0 when compared to the other groups. The evaluation of the ARI scores did not show statistically significant difference in the sites of link failure among the groups.

This result, which agrees with earlier studies, leads to the conclusion that the adhesive failure between the enamel and the bonding system is advantageous[15]

because there will be less adhesive remnant and, consequently, less time will be spent to remove it, besides a reduced chance of excessive wear. Bichara *et al*. (2010) argue that bond failure within the adhesive or at the bracket-adhesive interface is more desirable than failure at the enameladhesive interface, because it might lead to enamel fracture and risk reduction of cracks while debonding[21]. However, this would lead to longer clinical time, which is not desirable.

The present study is a preliminary step towards incorporating laser in routine dental practice for orthodontics purpose and was carried during 4-6 months. After that, no further measurements were taken. Further in vitro and long term clinical studies at different power settings and studies including variables like microleakage and bond strength in human teeth will provide additional information important for the efficacy of this laser clinically. There are, in principle, no technical limitations or side effects for this use of laser.

In this way, considering the findings observed in the present study, we can consider that laser irradiation is an efficient method for enamel conditioning prior the orthodontics treatment, presenting similar effects on bond strength to brackets when compared to phosphoric acid and presenting the advantage of decontamination of enamel surface and preventing a future demineralization around brackets, which is a serious and common deleterious effect on orthodontic treatments. The cost-benefit of using laser sources is still debatable, but scientifically it is a tool to be considered for clinical purposes.

Conclusion

- Er,Cr:YSGG laser pulse repetition rate and output power are important parameters that might have significant effects on bond strength to irradiated enamel. The mean shear bond strength and enamel surface etching obtained with Er,Cr:YSGG laser operated at 42.4 J/cm^2 (2.41W) and 29.3 J/cm^2 (1.7W) is higher compared to that obtained with acid etching and could be considered clinically acceptable.
- The laser irradiation can be used for enamel etching considering the advantages promoted by laser irradiation when compared to the phosphoric acid, since the adhesive-remnant-index scores was similar between the analyzed groups.
- Laser irradiation promoted higher roughness and optical changes on enamel when evaluated by optical coherence tomography technique. In this way, OCT is a promissing tool for future clinical evaluation of laser effects on enamel surface.

Clinical Significances

Er,Cr:YSGG laser irradiation is better than the phosphoric acid for etching enamel prior the orthodontics treatment because laser irradiation promotes similar shear bond strengths and prevents demineralization around orthodontic brackets.

References

1. Kim JH, Kwon OW, Kim H, Kwon YH. Acid resistance of Erbium-doped Yttrium Aluminum Garnet laser-treated and phosphoric acid-etched enamels. Angle Orthodontist 2006; 76(6):1052-6.

2. Pashley DH. The effects of acid etching on the pulpodentin complex. Operative Dent. 1992;17:229-34.

3. Horiuchi S, Kuroda S, Hiasa M, Suge T, Saku S, Hamada K, Matsuo T, Asaoka K, Tanaka E. Reinforcement of bond strength of self-etching orthodontic adhesive. Angle Orthod. 2012 Jan;82(1):30-5.

4. Stern RH, Sognnaes RF. Laser beam effect on dental hard tissues. J Dent Res1964; 43:873-73.

5. Kohns P, Zhou P, Störmann R. Effective laser ablation of enamel and dentine without thermal side effects. J Laser Appl. 1997 Jun;9(3):171-4.

6. Basaran, G.; Ozer, T.; Berk N.; Hamamci, O. Etching enamel for orthodontics with an Erbium, Chromium:Yttrium-Scandium-Gallium-garnet laser system. Angle Orthod. 2007; 77:117-23.

7. Lee BS, Hsieh TT, Lee YI, Lan WH, Hsu YJ, Wen PH,et al. Bond strengths of orthodontic bracket after acid-etched Er:YAG laser irradiated and combined treatment on enamel surface. Angle Orthod. 2003;73(5):565-70.

8. Botta SB, Ana PA, Zezell DM, Powers JM, Matos AB. Adhesion after erbium, chromium:yttrium-scandium-gallium-garnet laser application at three different irradiation conditions. Lasers Med Sci. 2009; 24(1):67-73.

9. Quinto Jr J, Amaral MM, Francci CE, Ana PA, Moritz A, Zezell DM. Evaluation of Intra Root Canal Er,Cr:YSGG Laser Irradiation on Prosthetic Post Adherence. Journal of Prosthodontics. 2017; 0:1-5.

10. Hoshing UA,Patil S,Medha A, Bandekar SD.Comparison of shear bond strength of composite resin to enamel surface with laser etching versus acid etching: an in vitro evaluation. J Conserv Dent. 2014;17(4):320-4.

11. International Standardization Organization. Dental materials – Testing of adhesion to tooth structure. ISO/TS 11405, 1-17, 2014.

12. Zamataro CB, Ana PA, Benetti C, Zezell DM. Influence of Er,Cr:YSGG laser on CaF_2-like products formation because of professional acidulated fluoride or to domestic dentifrice application. Microsc Res Tech. 2013;76(7):704-13.

13. Artun J, Bergland S. Clinical trials with crystal growth conditioning as an alternative to acidetch enamel pretreatment. Am J Orthod. 1984; 85(4):333-40.

14. Ana PA, Velloso WF Jr, Zezell DM. Three-dimensional finite element thermal analysis of dental tissues irradiated with Er,Cr:YSGG laser. Rev Sci Instrum. 2008 Sep;79(9):093910.

15. Benetti C, Ana PA, Bachmann L, Zezell DM. Mid-Infrared Spectroscopy Analysis of the Effects of Erbium, Chromium:Yattrium-Scandium-Gallium-Garnet (Er,Cr:YSGG) Laser irradiation on Bone Mineral and Organic Components. Appl Spectrosc. 2015; 69(12):1496504.

16. Reynolds IR. A review of direct orthodontic bonding. Br J Orthod. 1975;2:171-80.

17. Leão Filho JC, Braz AK, de Souza TR, de Araujo RE, Pithon MM, Tanaka OM. Optical coherence tomography for debonding evaluation: an in-vitro qualitative study. Am J Orthod Dentofacial Orthop. 2013; 143(1):61-8.

18. Mahdian M, Salehi HS, Lurie AG, Yadav S, Tadinada A. Tissue characterization using optical coherence tomography and cone beam computed tomography: a comparative pilot study.Oral Surg Oral Med Oral Pathol Oral Radiol. 2016;122(1):98-103.

19. Chan KH, Tom H, Darling CL, Fried D. A method for monitoring enamel erosion using laser irradiated surfaces and optical coherence tomography. Lasers Surg Med. 2014 Nov;46(9):672-8.

20. Rajagopal R, Padmanabhan S, Gnanamani J. A comparison of shear bond strength and debonding characteristics of conventional, moisture-insensitive, and self-etching primers in vitro. Angle Orthod. 2004; 74(2):264-8.

21. Bishara SE, VonWald L, Lafoon JF, Warren JJ. Effect of a self-etch primer/adhesive on the shear bond strength of orthodontic brackets. Am J Orthod Dentofacial Orthop. 2010; 119:621-4.

Acknowledgements

The authors are thankful to CAPES, for scholarship of DSL. This study was supported by CAPES/PROCAD 88881.068505/2014-01, FAPESP 17/50332-0, CNPq/INCT 465763/2014-6, CNPq-PQ 309902/2017-7 and CNPq 140619/2015-1.

Figure and Legends

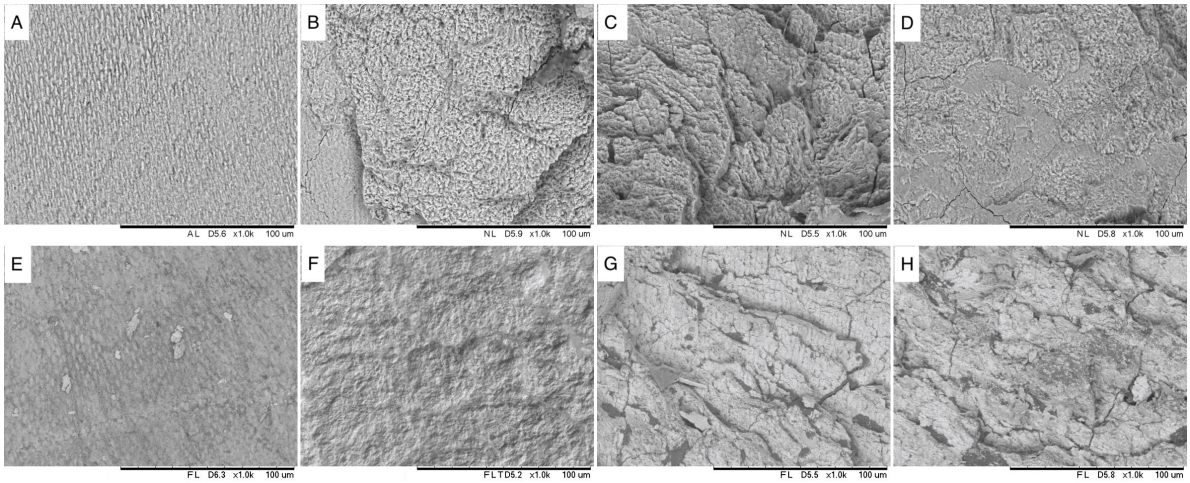

Figure 1: Electron micrographs of enamel after etching (A,B,C,D) and after (E,F,G,H) debonding at 1000x magnification.

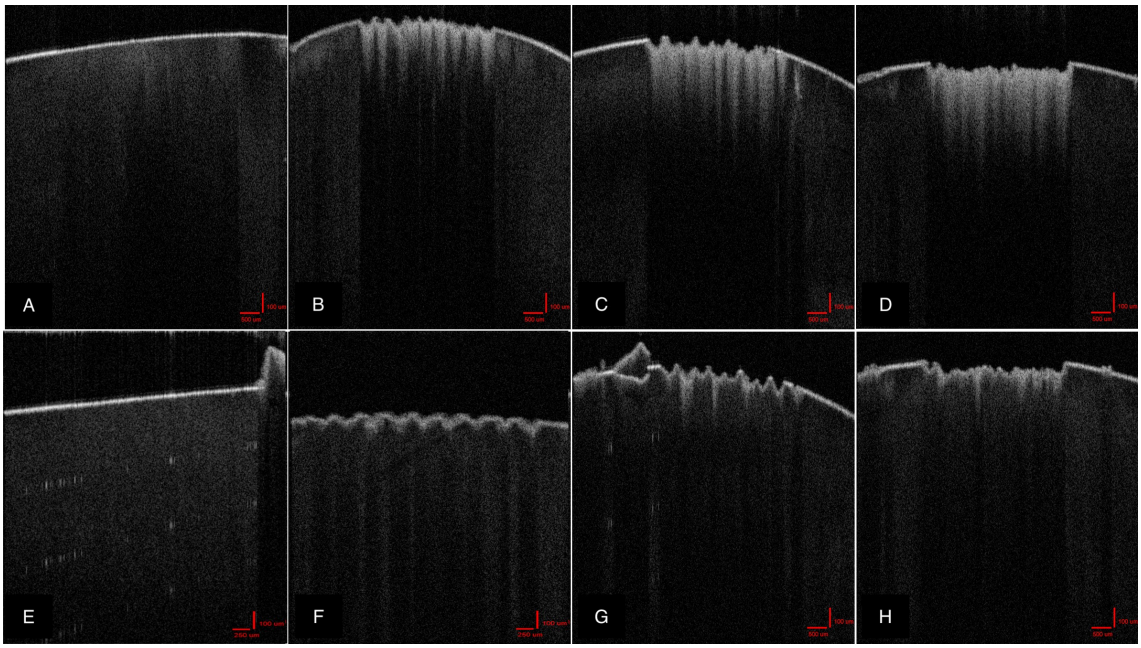

Figure 2: Optical coherence tomography images of enamel after conditioning (A,B,C,D) and after debonding (E,F,G,H).

Tables

Table 1. Experimental design considering as main factors: adhesive system, substrate and surface conditioning conditions

Surface conditioning conditions	Substrate	Adhesive system
Group I: Etching with 37% phosphoric acid	Enamel	Primer + Transbond XT adhesive
Group II: Er,Cr:YSGG laser irradiation (1.1W)	Enamel	Primer + Transbond XT adhesive
Group III: Er,Cr:YSGG laser irradiation (1.7W)	Enamel	Primer + Transbond XT adhesive
Group IV: Er,Cr:YSGG laser irradiation (2.41W)	Enamel	Primer + Transbond XT adhesive

Table 2. Laser irradiation conditions

Group	Power (W)	Energy per pulse (mJ)	Energy Density (J/cm^2)
II	1.1	54.1	19.1
III	1.7	83	29.3
IV	2.4	120	42.4

Table 3. Adhesive System used in this study.

Material	Manufacturer Batch number #	Composition	Aplication Mode
Primer + Transbond XT adhesive	3M Unitek # 503325	Bisphenol A diglycidyl ether dimethacrylate (1020 wt%); Bisphenol A bis (2hydroxyethyl ether) Dimethacrylate (510 wt%); Filler: Silane-treated quartz (70-80 wt%)	The primer was applied with microbrush and then light cured for 20 seconds. Transbond XT adhesive paste should be applied on the bracket, positioned over the tooth surface and photoactivated for 10 seconds in each side of the bracket.

Table 4. Mean of Shear Bond Strengths of 4 groups.

Group	Number of samples	Bond	
		Mean (MPa)	SD
Group I	10	6.2	1.7
Group II	10	4.6	2.5
Group III	10	7.0	2.2
Group IV	10	8.0	3.6

Table 5. Distribution of ARI Scores

Group	ARI Scores			
	0	**1**	**2**	**3**
Group I	9	1	-	-
Group II	10	-	-	-
Group III	9	1	-	-
Group IV	10	-	-	-

Abbreviation: adhesive remnant index

APÊNDICE D – ARTIGO "GOLD NANOSTRUCTURES FOR IMAGING ENHANCEMENT OF INCIPIENT OCCLUSAL CARIES USING OPTICAL COHERENCE TOMOGRAPHY"

Original Paper

Nanotechnology

Gold nanostructures for imaging enhancement of incipient occlusal caries using Optical Coherence Tomography

Gisele Cruz Camboim[a], Daniela Siqueira Lopes[a], Evair Josino da Silva[a], Vanda Sanderana Macêdo Carneiro[b,c], Cláudia Cristina Brainer de Oliveira Mota[b], Marcello Magri Amaral[d], Renato Barbosa Silva[e] e Anderson Stevens Leonidas Gomes*[a,e]

[a] Graduate Program in Dentistry, Universidade Federal de Pernambuco, Recife, 50670-901, Pernambuco, Brazil.

[b] Faculty of Dentistry, Centro Universitário Tabosa de Almeida, Caruaru, 50016-901, Pernambuco, Brazil.

[c] Faculty of Dentistry, Universidade de Pernambuco, Camaragibe, 54756-220, Pernambuco, Brazil

[d] Scientific and Technological Institute, Universidade Brasil, Fernandópolis, 15600-000, São Paulo, Brazil.

[e] Physics Department, Universidade Federal de Pernambuco, Recife, 50670-901, Pernambuco, Brazil.

.

*Corresponding Author: anderson@df.ufpe.br

ABSTRACT

Background: Incipient caries lesions in teeth fissures are difficult to diagnose and are often underestimated in early stages. Optical coherence tomography (OCT) has been shown to be a promising tool for the visualization of these lesions. In order to improve the OCT images, liquid based optical clearing agents and contrast agents based on nanoparticles may allow a better visualization of biological structures. This study evaluated gold spherical nanoparticles (AuNP) and gold nanorods (AuNR) as contrast agents in OCT images of incipient caries lesions to enhance its diagnosis.

Methodology: Ten extracted permanent molars with incipient caries lesions were imaged by OCT. Group (G1) was the control without any agent, whereas other groups were observed using the following components: glycerol (G2), AuNP (G3), AuNP diluted on glycerol (G4), AuNR (G5) and AuNR diluted on glycerol (G6). The groups were investigated for contrast enhancement by the alterations of the light extinction coefficient with OCT.

Results: An increase in the light attenuation occurred in all tested groups when compared to control (0.179). Groups G3 and G6 demonstrated a higher attenuation coefficient (0.224, p=0.341).

Conclusions: The difference of the attenuation coefficient between the affected and non-affected region allowed better/improved localization of demineralized areas due to the contrast enhancement.

Keywords: Optical coherence tomography, optical clearing agents, gold nanoparticles, diagnostic imaging, dental caries

1 Introduction

The complex topography of the occlusal surface of the posterior teeth represents a challenge for diagnosis in dentistry. In this context, incipient caries are difficult to detect in the early stages and are generally underdiagnosed [1,2]. Furthermore, caries remains one of the most prevalent problems in dentistry in public health [3]. Microscopic analysis can show occlusal fissures that appear clinically round and shallow, occasionally harbor deep grooves that are occluded with debris and microorganisms [2].

Occlusal caries lesions are routinely detected using visual, tactile and exploratory methods in combination with radiographic exam [4]. Radiographic methods have low sensitivity for occlusal lesions, and when they are radiolucent, there is already a deep progression in dentin, making inevitable the restorative treatment [5]. Therefore, the early detection of these cavities is important to avoid damage to the dental tissues, thus allowing minimally invasive dentistry.

Optical coherence tomography (OCT) is a non-invasive imaging technique that provides highresolution images of microanatomic structures in living tissues. These systems offer cross-sectional and 3D images with resolution on the order of few microns and a depth of penetration of one to two millimeters [6]. OCT can provide diagnostic information in dentistry regarding dental materials, soft and hard tissues analysis and can effectively be used to identify demineralized tissues such as carious lesions [7]. However, tissue scattering properties may represent a major limiting factor for deeper and higher contrast images from biological samples studied by optical techniques [8].

Optical clearing agents (OCAs) have routinely been used in biological microscopy and have found recent application in clinical imaging, including OCT, as reviewed in [9]. They are used to mitigate scattering issues and provide deeper tissue penetration. There is a vast literature on OCAs associated with OCT applied to skin [10], molecular diffusion in tissue [11], the role of glucose concentration [12] and articular cartilage in subchondral bone [13]. Xu et al. [14] recently reported on quantitative assessment of optical clearing methods in various intact mouse organs.

With similar aiming of enhancing imaging in OCT systems, nanomaterials, particularly gold nanoparticles, nanoprisms and nanorods, besides TiO_2 nanoparticles, have been exploited as contrast agents in cardiovascular OCT imaging [15], angiography [16], breast carcinoma [17], as well as phantoms [18]. Furthermore, gold nanoshells and TiO_2 have been used for in vivo skin studies with Monte Carlo simulations [19]. Gold nanorods have been used for OCT imaging and photothermal applications in the NIR [20], besides their use in PEGylated Aucore–Agshell as OCT signal nanoamplifiers [21].

OCA plays an important role also in Dentistry. When analyzing a tooth surface with the OCT device, the presence of a caries lesions typically promotes a large increase in light scattering due to demineralization, therefore limiting the light penetration and reducing the OCT signal before it even reaches the dentin-enamel junction [22]. In this way, OCA may provide deeper penetration and improve OCT image quality *in situ*, whereas an agent that modifies the diffusion properties of a sample may improve the image contrast. Studies of high index and other liquids as glycerol, transparent vinylpolysiloxane impression material, for OCA with OCT have been reported [23-26].

The use of nanoparticles as contrast agents in dentistry was first report in 2012, when Braz and co-workers described the first use of gold nanoparticles as contrast agent for OCT in dental materials [27]. The gold nanoparticles were synthesized *in situ* in order to enhance the images from dentinal layers and tubules. More recently, silver nanoparticles in aqueous solution and diluted in glycerol have been exploited as optical clearing agent for diagnostic of occlusal incipient caries lesions through OCT imaging, based on the changes on enamel birefringence and highlighting demineralized areas [28]. However, the use of nanoparticles as contrast agents to improve OCT image in incipient caries lesions and other carious challenges has not yet been fully explored and there is great potential for further uses and improvements. Due to its mature preparation nanotechnology, biocompatibility and colloidal stability, gold nanostructures, in different forms, have not been well investigated for hard tissues. Thus, the aim of this study was to evaluate gold nanoparticles (AuNP) and gold nanorods (AuNR) as contrast agents, comparing with glycerol (a typical OCA material) to enhance the detection of incipient occlusal caries lesions in OCT images.

2 Methods

2.1. Ethics

This experimental laboratory *ex vivo* study was carried out in accordance to the Helsinki Declaration, after approval by the Ethics Committee on Humans Research, under process CAAE 63824216.8.0000.5207.

2.2. Attainment of Gold Nanostructures (spherical and nanorods)

The spherical gold nanoparticles (AuNP) were produced in the Department of Physics and Chemistry of the Universidade Federal de Pernambuco, Brazil by treating hydrogen tetrachloroaurate ($HAuCl_4$) with Polyvinylpyrrolidone (PVP -M_W @ 55.000) in boiling water, where the PVP acts as stabilizing agent. The resulting colloidal gold nanoparticles are spherical and have an 2.0 ± 1.0 nm in size dispersed in aqueous solution, and were characterized by the peak of plasmon resonance is at 550 nm [29]. The nanorods (AuNR), on the other hand, were purchased from Nanopartz^{TM} (Nanopartz Inc., Denver, CO, USA), with 50 nm diameters and 160 nm length, also dispersed in aqueous solution, with two plasmon resonance peaks at 520 nm and 825 nm, corresponding to the transverse and longitudinal plasmon resonances, respectively.

2.3. Teeth preparation

Ten permanent molars teeth with incipient carious lesions were obtained from a teeth bank (Centro Universitário Tabosa de Almeida (ASCES-UNITA), Caruaru, Pernambuco, Brazil). Those teeth contained white or brownish spots accompanying anatomical accidents of the occlusal surfaces, but they did not have evident cavitation when analyzed by visual examination in accordance with the ICDAS code (1) first visual change in dry enamel and (2) distinct visual change in moist enamel. Teeth were excluded when caries cavities were observed by visual examination or restorations.

The teeth selected for this study had their root portions included in colorless chemically activated acrylic resin matrix with the occlusal surface parallel to the ground.

Afterwards they were placed on a PVC platform so they could be repositioned to receive the OCAs for OCT scanning.

2.3.1 Contrast Agents (CA) and Optical Clearing Agents (OCA) adoption

Each sample was analyzed in a total of 6 times, the first one was the negative control (G1), which did not undergo any treatment, and then they were analyzed with five different combinations of Optical Clearing Agents (OCA) and Contrast Agents (CA). The pure glycerol was the positive control (G2). The other OCA/CA combinations were: (G3) gold spherical nanoparticles (AuNP) dispersed in water; (G4) AuNP dispersed in water and diluted to 50% by weight of glycerol; (G5) nanorods (AuNR) dispersed in water; (G6) AuNR dispersed in water and diluted to 50% by weight of glycerol.

After applying the OCA/CA, the specimens were scanned by OCT, and then the samples were washed with neutral detergent (Ypê, Amparo, São Paulo, Brazil) with Robinson's brush, followed by ultrasonic bath in deionized water for 15 minutes between each OCA/CA application. In this way, all samples could be scanned by OCT in the presence of each OCA/CA combination.

2.4. Optical Coherence Tomography System

The OCT system employed in this work was a commercially available model (Callisto, Thorlabs Inc., New Jersey, USA), operating in the spectral domain (SD-OCT), with 930 nm of central wavelength, 100 nm of bandwidth, maximum output power of 5 mW, resolution of 5.3/7 µm in air and water, respectively, lateral resolution of 8 µm and depth of light penetration of 1.7 mm. The analysis was performed along the occlusal surface, capturing two-dimensional images with 8 mm transverse scan of the specimens. To standardize the scanning the samples were positioned on a two-axis linear translation stage with rotating platform and solid top plate, and images were acquired every 250 µm. The two-dimensional images constitute a numerical matrix of 2000 columns at the x-axis, corresponding to maximum 8-mm scanning, and 512 rows at the y-axis, with 1,7 mm maximum depth (in air, refractive index 1).

2.5 Optical Attenuation Coefficient Measurement

The acquired OCT images were analyzed using an in-housed developed software to measure the optical attenuation coefficient (μ). The μ coefficient is a quantitative value that characterizes the decay of OCT signal when light propagates trough the tissue analyzed. Thus, by measuring the μ it is possible to use the OCT signal to quantitatively discriminate between different types of tissues and their state of health [22,30].

For the μ coefficient analysis, the software operator uploaded the images of each studied group. In each image the operator selected the width and position of two windows with the region of interest (ROI). For standardization, the window width was maintained constant (10 A-scan) during all the analyses. As each biological sample presents distinct morphological characteristics, the position of the windows was adjusted for each image, always positioning one window in a region of healthy tissue and the other one in a region of abnormal tissue.

Using the B-scan mode, the software identifies the surface of the tissue (air-tissue interface) and uses it as a reference to perform an average of the normalized A-scan inside each ROI window. The Ascan was normalized by the maximum value to avoid erroneous values due to possible reflection on first surface.

The average A-scan of each ROI window was used to fit an exponential decay, based on BeerLambert law, $I_{(Z)} = I_0 \exp(-\mu z)$, where $I_{(Z)}$ is the intensity as a function of depth z and μ is the optical attenuation coefficient. The obtained μ value was recorded for posterior analysis. This procedure was repeated for each image.

2.6. Statistics

Statistical analysis was performed using GraphPad Prism 7 software (GraphPad Software, Inc). A mean and standard deviation of each group were calculated. Normal distribution was not performed by the Kolmogorov-Smirnov test. To verify if there was difference between groups, the "repeated measures of variance RM-ANOVA" test was used. The statistical significance of all tests should be considered as $p < 0.05$.

3 Results

The OCT images of 10 molars were examined. The top picture in Fig. 1 is the optical polarization microscopy image (1A) of the tooth analyzed by transversal and bidimensional OCT images (OCT Bscans) illustrated in 1B-1G. Also, OCT A-scan mode were obtained of the region of interest (ROI) with and without OCA/CA, across the occlusal surface of a molar that clinically presented a brown stain in the pit and fissures suspecting of incipient caries lesions. Fig. 1B shows the B-scan OCT mode without any OCA/CAs (G1).

The other images where taken after application of the following OCA/CA: fig. 1C, glycerol (G2); fig.1D, gold spherical nanoparticles (AuNP) dispersed in water (G3); fig. 1E, AuNP dispersed in water and diluted to 50% by weight of glycerol (G4); fig. 1F nanorods (AuNR) dispersed in water (G5); fig. 1G, AuNR dispersed in water and diluted to 50% by weight of glycerol (G6). In order to quantify the OCT signal intensity in the DEJ area, the μ coefficient of each group was obtained in sound and affected areas (Tabel 01). Figure 2 shows the B-scan and the A-scan graphic of the window corresponding to the pit area in G1 (control), G3 (AuNP) and G6 (AuNR + glycerol). The last one evidenced the greatest difference of the attenuation coefficient comparing with the control group.

An inspection of table I shows an increase in the light attenuation in all carious tested groups when compared with G1 (0.184). It can be observed that groups 3 and 6 obtained a higher μ (0.224) on carious surface. However, at the sound areas, gold nanorods diluted in glycerol (G6 = 0.168) showed an attenuation coefficient similar to that obtained from the isolated samples in presence of glycerol isolated, G2 (0.169).

4 Discussion

Earlier studies have demonstrated that Optical Coherence tomography OCT has great potential for imaging incipient caries lesions and for monitoring lesion progression in enamel [22,30,31]. By the way, the tactille inspection with exploratory probes can be stimulate tissues in which caries is incipient and cause irreversible damage and accelerate the progression of localized lesions. Conventional radiography is suitable for cavitated lesions but not early incipient lesions, due to low resolution and superimposition of structures that could impede the correct diagnosis of the exact lesion [30]. In effect, the OCT is a noninvasive imaging system that can visualize the internal structures nondestructively.

In addition, OCAs may enhance the OCT depth penetration, whereas a contrast agent that modifies the diffusion properties of a sample may improve the image contrast. Therefore, in the present research, gold nanoparticles were studied to improve the OCT imaging, adding knowledge to the use of this technology in early diagnostic in complex tooth anatomy.

OCT provides cross-sectional images of biological tissues over penetration depths of typically 1-2 mm. In agreement, the OCT device used in this study shows 1.7 mm of light penetration depth within the analyzed samples. The penetration depth of OCT is fundamentally limited by the attenuation of ballistic light propagation via scattering and absorption. As an OCT light beam penetrates deeper into a tissue, the strength signal diminishes. One way of quantifying optical changes is by measuring the optical attenuation coefficient, which has shown promising results in discriminating between healthy and pathological states of various tissues, as well as demineralization and remineralization of enamel [22,30,31]. This study confirmed that the use of contrast agents increased the optical attenuation coefficient of subsurface lesions located under enamel in the occlusal surface. Furthermore, the difference between the optical attenuation coefficients of sound teeth and carious lesion increased, making the gold NP and NR a potential tool to improve the identification of lesions. Similar effect has been reported in ref. 27 for dental tubules.

Glycerol is one of the most used and tested OCA both in soft and hard tissue, as already indicated by several references. It has a high viscosity, 1.42pa at room temperature, and refractive index n = 1.47. This is well suited for use in dental imaging due to its-biocompatibility [23], constituting an important advantage for OCT imaging, therefore justifying the use of glycerol in some groups (G2, G4 and G6) of the present study. Within the spectral range of

interest in this study, the attenuation coefficient remained similar in all groups which had glycerol addition, even with gold nanoparticles.

In contrast with the literature, the glycerol increased the optical attenuation coefficient, which means that the light penetrated less than in the control group, making opposition to the literature findings, as this agent promoted an increase of light penetration [11,34]. One possible explanation is that in the mentioned references the OCA is used in soft tissues, not hard tissue as here. But this needs to be verified. In order to improve the nanoparticles properties, such as viscosity, the dispersion of the nanoparticles in glycerol was tested (to compare with water, which is less viscous). However, the results in this case did not show a significant difference.

Gold nanoparticles play a key role in nanotechnology, with applications in many fields including dentistry [27]. The capacity to control size, shape and the colloid stability of nanoparticle dispersions are important issues related to their practical applications [32]. The advantages of the gold nanoparticles are low toxicity and an ability for maintenance of localized surface plasmon resonances in the NIR region providing enhanced backscattering of laser radiation [33]. Although it is widely used in bioimaging, there are few studies that aim at the use of gold nanoparticles as clearing agents in incipient caries, which justified its application in this experiment. Our results showed a remarkable increase in the attenuation coefficient when using spherical nanoparticles (G3) and gold nanorods diluted in glycerol (G6) in comparison to the control (G1).

5 Conclusion

Monitoring of enamel lesion based on the OCT signal attenuation over time has been shown to be a promising approach for early diagnostic as it reduces the risk of activating and / or increasing carious lesions by using the exploratory probe as a tactile method. Gold nanoparticles are suitable for *in vivo* applications and the safety of the OCA/CA technique should be further pursued, particularly in dentistry. The method should be extended for a larger range of lesions with various shapes, structures, and depths in further studies before clinical procedures.

Acknowledgements

This study was carried out under the INCT-INFO (National Institutes of Science and Technology, Institute of Photonics – 465.763/2014-6), supported by CNPq/MCT (National Council of Technological and Scientific Development and Ministry of Science and Technology and PRONEX program (Center of Excellence on Biophotonics and Nanophotonics – APQ-0504-1.05/14); sponsored by FACEPE/CNPq (Foundation for Science and Technology of Pernambuco State and National Council of Technological and Scientific Development). The authors report no conflict of interest related to this work.

REFERENCES

[1] Fried D, Xie J, Shafi S, Featherstone JDB, Breunig TM, Le C. Imaging caries lesions and lesion progression with polarization sensitive optical coherence tomography. J Biomed Opt. 2002; 7(4):618.

[2] Ito S, Shimada Y, Sadr A, Nakajima Y, Miyashin M, Tagami J. Assessment of occlusal fissure depth and sealant penetration using optical coherence tomography. Dent Mater J. 2016;35(3):432–9.

[3] Frencken JE, Sharma P, Stenhouse L, Green D, Laverty D, Dietrich T. Global epidemiology of dental caries and severe periodontitis – a comprehensive review. J Clin Periodontol 2017; 44 (Suppl. 18): S94–S105.

[4] Melo M, Pascual A, Camps I, del Campo Á, Ata-Ali J. Caries diagnosis using light fluorescence devices in comparison with traditional visual and tactile evaluation: a prospective study in 152 patients. Odontology. 2016;105(3):283–90.

[5] Fejerskov O. Changing Paradigms in Concepts on Dental Caries : Consequences for Oral Health Care. Caries Res. 2004;38:182–91.

[6] Swanson EA and Fujimoto JG. The ecosystem that powered the translation of OCT from fundamental research to clinical and commercial impact [Invited] Biomedical optics express 2017; 8, 1638.

[7] Machoy M, Seeliger J, Szyszka-Sommerfeld L, Koprowski R, Gedrange T, and Woźniak K, (Review Article) The Use of Optical Coherence Tomography in Dental Diagnostics: A State-of-the-Art Review, Journal of Healthcare Engineering 2017, Article ID 7560645, 31 pages.

[8] Jacques SL. Optical properties of biological tissues: a review , Phys. Med. Biol. 2013; 58, R37–R61

[9] Zhu D, Larin KV, Luo Q, Tuchin VV. Recent progress in tissue optical clearing. Laser Photonics. Rev. 2013;757(5):732–57.

[10] Wen X, Jacques SL, Tuchin VV and Zhua D. Enhanced optical clearing of skin in vivo and optical coherence tomography in-depth imaging, Journal of Biomedical Optics, 2012; 17(6), 066022.

[11] Larin KV, Ghosn MG, Bashkatov AN, Genina EA, Trunina NA and Tuchin VV. Optical Clearing for OCT Image Enhancement and In-Depth Monitoring of Molecular Diffusion, IEEE journal of selected topics in quantum electronics, 2012; 18, 1244.

[12] Sudheendran N, Mohamed M, Ghosn MG, Tuchin VV And Larin KV. Assessment of tissue optical clearing as a function of glucose concentration using optical coherence tomography. J Innov Opt Health Sci., 2010; 3(3): 169–176.

[13] Bykov A, Hautala T, Kinnunen M, Popov A, Karhula S, Saarakkala S, Nieminen MT, Tuchin VV and Meglinski I. Imaging of subchondral bone by optical coherence

tomography upon optical clearing of articular cartilage, J. Biophotonics 2016; 9 (3): 270–275.

[14] Xu J, Ma Y, Yu T and Zhu D. Quantitative assessment of optical clearing methods in various intact mouse organs, J. Biophotonics. 2019;12:e201800134.

[15] Hu J, Abujetas DR, Tsoutsi D, Leggio L, Rivero F, Rodríguez EM, Torres RA, Sánchez-Gil JA, Ramírez HL, Gallego D, Rivera HL, Gil PR, Alfonso F, Solé JG and Jaque D. Experimental evaluation of gold nanoparticles as infrared scatterers for advanced cardiovascular optical imaging. APL Photonics 2018; 3, 080803.

[16] Si P, Yuan E, Liba O, Winetraub Y, Yousefi S, SoRelle ED, Yecies DW, Dutta R and Zerda A. Gold Nanoprisms as Optical Coherence Tomography Contrast Agents in the Second Near-Infrared Window for Enhanced Angiography in Live Animals. ACS Nano 2018; 12, 11986-11994.

[17] Oldenburg AL, Hansen MN, Ralston TS, Wei A and Boppart SA. Imaging gold nanorods in excised human breast carcinoma by spectroscopic optical coherence tomography. J. Mater. Chem., 2009, 19, 6407–6411.

[18] Zagaynova EV, Shirmanova MV, Kirillin MY, Khlebtsov BN, Orlova1 AG, Balalaeva IV, Sirotkina MA, Bugrova ML, Agrba PD and Kamensky VA. Contrasting properties of gold nanoparticles for optical coherence tomography: phantom, in vivo studies and Monte Carlo simulation, Phys. Med. Biol. 2008; 53: 4995–5009.

[19] Kirillin M, Shirmanova M, Sirotkina M, Bugrova M and Khlebtsov B. Contrasting properties of gold nanoshells and titanium dioxide nanoparticles for optical coherence tomography imaging of skin: Monte Carlo simulations and in vivo study. Journal of Biomedical Optics, 2009; 142, 021017.

[20] Ratheesh KM, Prabhathan P, Seah LK and Murukeshan VM. Gold nanorods with higher aspect ratio as potential contrast agent in optical coherence tomography and for photothermal applications around 1300nm imaging window. Biomed. Phys. Eng. Express, 2016; 2: 055005.

[21] Shi Y, Fan S, Li L, Li Q, Chai X, Ren Q and Zhou C. PEGylated Aucore–Agshell Nanorods as Optical Coherence Tomography Signal Nanoamplifiers. Plasmonics, 2015; 10(6): 1381-1389.

[22] Maia AMA, de Freitas AZ, de L. Campello S, Gomes ASL, Karlsson L. Evaluation of dental enamel caries assessment using Quantitative Light Induced Fluorescence and Optical Coherence Tomography. J Biophotonics. 2016; 9(6):596–602.

[23] Kang H, Darling CL, Fried D. Use of an optical clearing agent to enhance the visibility of subsurface structures and lesions from tooth occlusal surfaces. J Biomed Opt. 2016; 21(8).

[24] Yang VB, Curtis DA, Fried D. Use of Optical Clearing Agents for Imaging Root Surfaces With Optical Coherence Tomography. IEEE J Sel Top Quantum Electron [Internet]. 2019;25(1):1–7.

[25] Kang H, Darling CL, Fried D. Enhancing the detection of hidden occlusal caries lesions with OCT using high index liquids. Proc SPIE--the Int Soc Opt Eng. 2014;8929:89290.

[26] Jones RS, Fried D. The effect of high index liquids on PS-OCT imaging of dental caries. Lasers Dent XI. 2005; 5687(2): 34–41.

[27] Braz AKS, Araujo RE De, Ohulchanskyy TY, Shukla S, Bergey EJ, Gomes ASL, et al. In situ gold nanoparticles formation: contrast agent for dental optical coherence tomography for dental optical coherence tomography. J Biomed Opt. 2012;17(6):1–5.

[28] Carneiro VSM, Mota CCBO, Souza AF, Silva EJ, Silva AF, Evair J, et al. Silver nanoparticles as optical clearing agent enhancers to improve caries diagnostic by optical coherence tomography. Proc SPIE 2018; 10507: 1050719.

[29] Brito-Silva AM, Sobral-Filho RG, Barbosa-Silva R, de Araújo CB, Galembeck A, Brolo AG. Improved synthesis of gold and silver nanoshells. Langmuir. 2013; 29(13): 4366–72.

[30] Popescu DP, Sowa MG, Hewko MD C-SL. Assessment of early demineralization in teeth using the signal attenuation in optical coherence tomography images. J Biomed Opt. 2009; 13(5):1–17.

[31] Mandurah MM, Sadr A, Shimada Y, Kitasako Y, Nakashima S, Bakhsh TA, et al. Monitoring remineralization of enamel subsurface lesions by optical coherence tomography. J Biomed Opt. 2013;18(4):046006.

[32] Zhou J, Ralston J, Sedev R, Beattie DA. Functionalized gold nanoparticles: Synthesis, structure and colloid stability. J Colloid Interface Sci . 2009;331(2):251–62.

[33] Xia Q, Li H, Liu Y, Zhang S, Feng Q, Xiao K. The effect of particle size on the genotoxicity of gold nanoparticles. J Biomed Mater Res. 2016; 00A(00):1–10.

[34] Liang Y, Yuan W, Mavadia-Shukla J, Li X. Optical clearing for luminal organ imaging with ultrahigh-resolution optical coherence tomography. J Biomed Opt. 2016; 21(8), 081211.

Figures legends and Table Caption

Figure 1: Optical polarization microscopy image (1A) and OCT B-scan images (1B-1G) across the occlusal surface of molars, both evidencing the central pit area (pointed by arrow), according to the distinct optical clearing agents used on surface: (B) G1 – Control, (C) G2 – Glycerol, (D) G3 – AuNPs, (E) G4 – AuNPs in glycerol, (F) G5 – AuNRs, (G) G6 – AuNRs in glycerol. The bright line in figs D to G are reflections at the air-liquid solution interface

Figure 2: OCT B-scan images across occlusal surface of molar, followed at right by the corresponding light intensity decay obtained from an A-scan of the region of interest (ROI) in the central pit area, according to OCAs used on surface: (A) G1 – Control, (B) G3 – AuNPs, (C) G6 – AuNRs in glycerol.

Table 1: Mean ± S.D. of the μ coefficient (mm^{-1}) values, taken from OCT images of sound and carious areas of teeth analyzed with Optical Clearing Agents (OCA/CA). The RM-ANOVA analysis indicates that the values are not statistically different in the groups for sound and caries surfaces (p>0,05).

Surface	Group (G)	N	Mean (mm^{-1})	SD	Minimum	Maximum	p-value[1]
Sound area	Control (G1)	10	0,161	0,04	0,093	0,251	<0,0001
	Glycerol (G2)	10	0,169	0,06	0,087	0,257	<0,0001
	Gold Nanoparticles (G3)	10	0,133	0,06	0,036	0,25	0,0001
	Gold Nanoparticles and glycerol (G4)	10	0,143	0,05	0,063	0,242	<0,0001
	Nanorod (G5)	10	0,135	0,07	0,007	0,233	0,0002
	Nanorod and glycerol (G6)	10	0,168	0,04	0,086	0,248	<0,0001
Carious area	Control (G1)	10	0,184	0,05	0,136	0,292	<0,0001
	Glycerol (G2)	10	0,198	0,07	0,069	0,307	<0,0001
	Gold Nanoparticles (G3)	10	0,224	0,03	0,145	0,276	<0,0001
	Gold Nanoparticles and glycerol (G4)	10	0,191	0,03	0,116	0,259	<0,0001
	Nanorod (G5)	10	0,214	0,04	0,158	0,269	<0,0001
	Nanorod and glycerol (G6)	10	0,224	0,05	0,109	0,291	<0,0001

[1] One sample t test

Figures

Figure 1

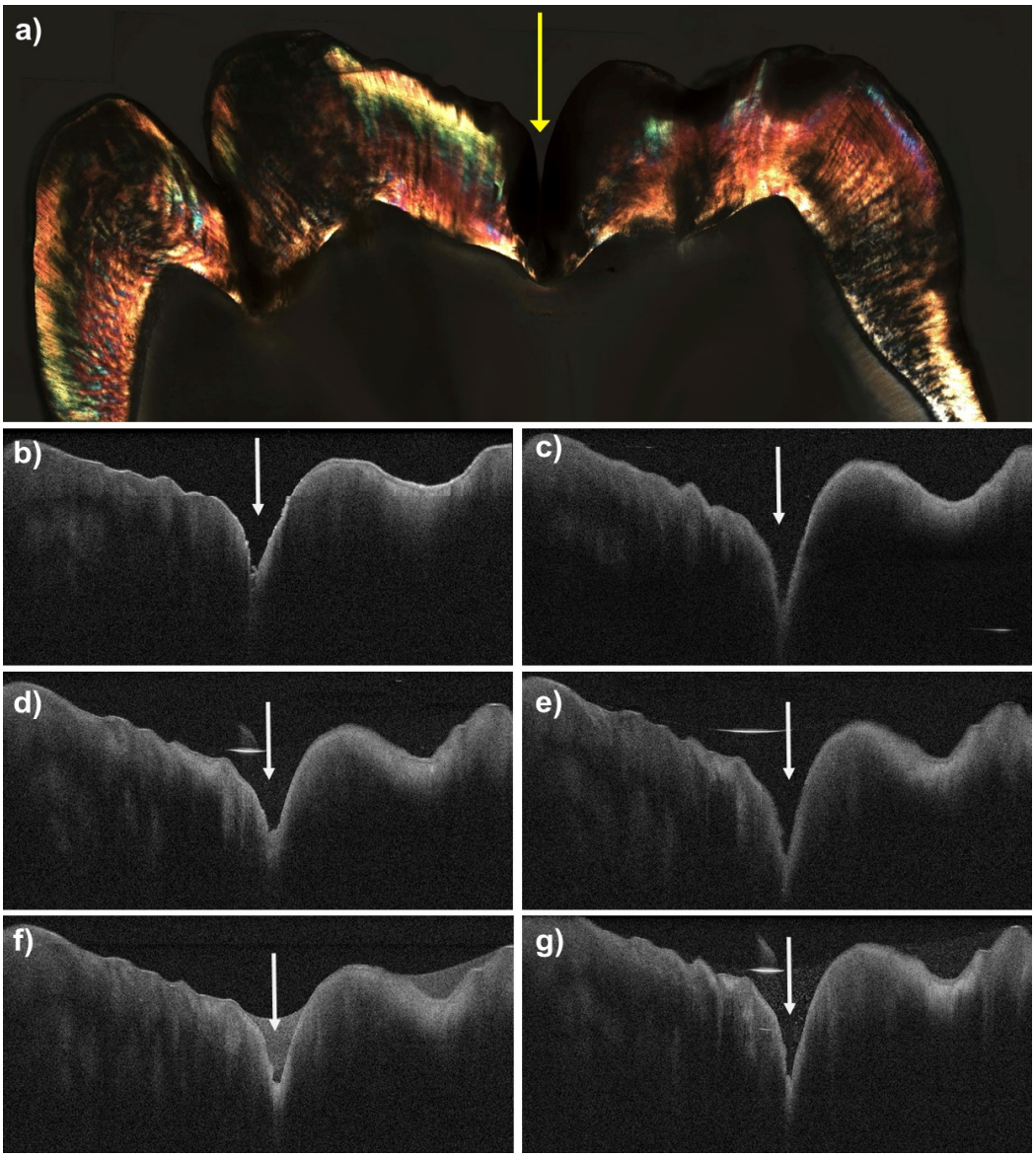

Figure 2

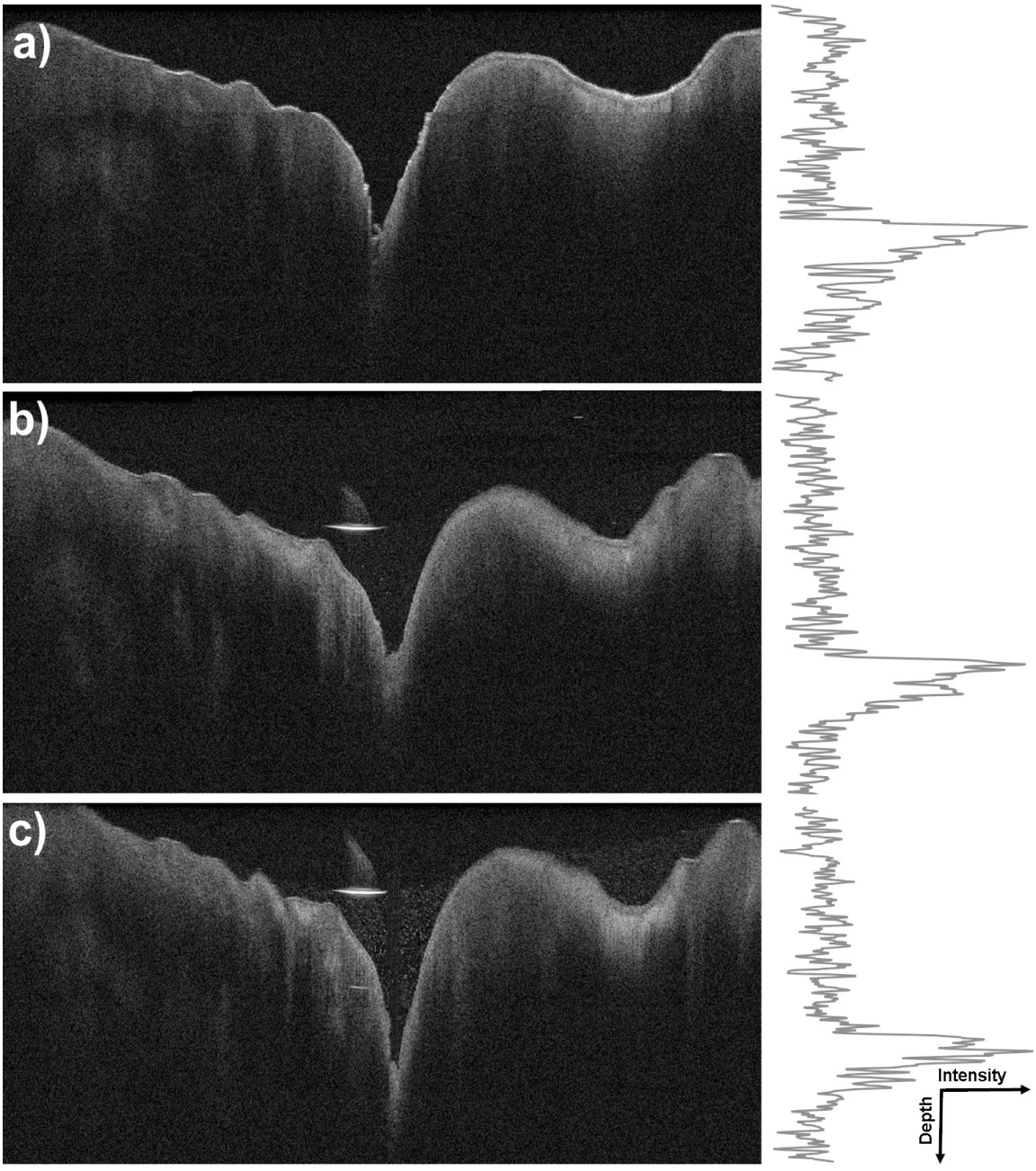

ANEXO A PARECER DO COMITÊ DE ÉTICA EM PESQUISA COM SERES HUMANOS DO CCS/UFPE

ASSOCIAÇÃO CARUARUENSE DE ENSINO SUPERIOR E TÉCNICO - ASCES

PARECER CONSUBSTANCIADO DO CEP

Elaborado pela Instituição Coparticipante

DADOS DO PROJETO DE PESQUISA

Título da Pesquisa: Caracterização dos tecidos biológicos da cavidade bucal através de Espectroscopia TeraHertz e Tomografia Fotoacústica

Pesquisador: Daniela Siqueira Lopes

Área Temática:

Versão: 1

CAAE: 95310418.0.3001.5203

Instituição Proponente: Associação Caruaruense de Ensino Superior

Patrocinador Principal: Financiamento Próprio

DADOS DO PARECER

Número do Parecer: 3.078.881

Apresentação do Projeto:

Será realizado um estudo experimental ex vivo laboratorial utilizando 105 participantes, dividindo-os em 2 grupos: dentes humanos e mandíbulas de

suínos. A pesquisa será desenvolvida no laboratório de Fotônica e Biofotônica do Departamento de Física da Universidade Federal de Pernambuco (UFPE) e no Curso de Odontologia (Laboratório de Biofotônica e Materiais Aplicados à Saúde) do Centro Universitário Tabosa de Almeida (ASCESUNITA).Serão selecionados 100 dentes humanos, obtidos no banco de dentes humanos do centro universitário ASCES-UNITA/PE.Esta pesquisa pretende analisar a tomografia fotoacústica e a espectroscopia TeraHertz na caracterização de estruturas teciduais dentárias e periodontais como recurso diagnóstico. Para tal, será realizado um experimento laboratorial usando os 100 dentes humanos extraídos, hígidos a cariados, além de 5 mandíbulas porcinas para inspeção do periodonto, que serão analisados por THz e TFA, após análise comparativa com OCT e microscopia de luz polarizada. As imagens serão caracterizadas em um software específico de forma a quantificar a intensidade do sinal das amostras analisadas. Serão calculadas as médias e desvio padrão para todos os parâmetros analisados ($p < 0,05$). Espera-se obter duas novas ferramentas de diagnóstico e planejamento não invasivas e não ionizantes, que contribuirão para o sucesso do tratamento periodontal e restaurador, além de aprimorar o ensino e a pesquisa.

Endereço: Avenida Portugal, 584
Bairro: Universitário **CEP:** 55.016-910
UF: PE **Município:** CARUARU
Telefone: (81)2103-2090 **Fax:** (81)2103-2053 **E-mail:** cep@asces.edu.br

ANEXO B PARECER DO COMITÊ DE ÉTICA EM PESQUISA COM SERES HUMANOS DO CCS/UFPE

UNIVERSIDADE FEDERAL DE PERNAMBUCO CENTRO DE CIÊNCIAS DA SAÚDE / UFPE-

PARECER CONSUBSTANCIADO DO CEP

Elaborado pela Instituição Coparticipante

DADOS DO PROJETO DE PESQUISA

Título da Pesquisa: AGENTES DE COMPENSAÇÃO PARA MELHORAR O IMAGEAMENTO DE ESTRUTURAS DENTÁRIAS NA TOMOGRAFIA POR COERÊNCIA ÓPTICA

Pesquisador: Marleny Elizabeth Márquez de Martínez Gerbi

Área Temática: Equipamentos e dispositivos terapêuticos, novos ou não registrados no País;

Versão: 1

CAAE: 63824216.8.3001.5208

Instituição Proponente: FUNDACAO UNIVERSIDADE DE PERNAMBUCO

Patrocinador Principal: Financiamento Próprio

DADOS DO PARECER

Número do Parecer: 2.001.287

Apresentação do Projeto:

Trata-se de projeto de pesquisa de Programa de Doutorado Doutorado em Odontologia da Faculdade de Odontologia de Pernambuco, área de concentração Dentística, apresentado pela dentista Vanda Sanderana Macêdo Carneiro, que busca avaliar o uso de agentes de compensação óptica à base de nanopartículas de titânio e prata para melhorar a profundidade de penetração da luz nos tecidos dentais mineralizados ex vivo, estejam eles hígidos ou com lesões de cárie oculta, utilizando a Tomografia de Coerência Óptica (OCT).

A Tomografia por coerência óptica é uma técnica não invasiva de geração de imagens transversais de estruturas biológicas internas, que já tem sido utilizada para imagens de cáries dentais, superfícies oclusais e tecidos moles. A técnica proporciona imagens em alta resolução de estruturas microanatômicas em tecidos vivos, todavia a profundidade da imagem é limitada devido à elevada dispersão de luz em tecidos biológicos, dificultando as potenciais aplicações, principalmente onde é necessária uma imagem com maior penetração nos tecidos. Na última década as técnicas ópticas de imagem, a exemplo da Tomografia de Coerência Óptica (OCT), tem recebido considerável atenção entre outras modalidades de diagnóstico. A utilização de técnicas ópticas de escaneamento e geração de imagens é bastante limitada em termos de profundidade

Endereço: Av. da Engenharia s/nº - 1º andar, sala 4, Prédio do Centro de Ciências da Saúde
Bairro: Cidade Universitária **CEP:** 50.740-600
UF: PE **Município:** RECIFE
Telefone: (81)2126-8588 **E-mail:** cepccs@ufpe.br

ANEXO C – PARECER DO COMITÊ DE ÉTICA EM USO DE ANIMAIS (CEUA – CCB/UFPE)

Universidade Federal de Pernambuco
Centro de Ciências Biológicas

Av. Prof. Nelson Chaves, s/n
50670-420 / Recife - PE - Brasil
fones: (55 81) 2126 8840 | 2126 8351
fax: (55 81) 2126 8350
www.ccb.ufpe.br

Recife, 25 de agosto de 2015

Ofício nº 80/15

Da Comissão de Ética no Uso de Animais (CEUA) da UFPE
Para: Prof.° Anderson Steves Leonidas Gomes
Departamento de Prótese e Cirurgia Buco Facial
Universidade Federal de Pernambuco
Processo nº 23076.015869/2015-65

Os membros da Comissão de Ética no Uso de Animais do Centro de Ciências Biológicas da Universidade Federal de Pernambuco (CEUA-UFPE) avaliaram seu projeto de pesquisa intitulado "**Avaliação da Força de adesão dos brackets ortodônticos após tratamento da superfície do esmalte por ácido fosfórico e laser Er: YAG".**

Concluímos que os procedimentos descritos para a utilização experimental dos animais encontram-se de acordo com as normas sugeridas pelo Colégio Brasileiro para Experimentação Animal e com as normas internacionais estabelecidas pelo National Institute of Health Guide for Care and Use of Laboratory Animals as quais são adotadas como critérios de avaliação e julgamento pela CEUA-UFPE.

Encontra-se de acordo com as normas vigentes no Brasil, especialmente a Lei 11.794 de 08 de outubro de 2008, que trata da questão do uso de animais para fins científicos e didáticos.

Diante do exposto, emitimos parecer favorável aos protocolos experimentais a serem realizados.

Origem dos animais: Frigorífico Bandeira; Animal; Bovino Nº total de dentes a ser utilizado; 80

Atenciosamente,

Prof. Dr. Pedro V. Carelli
Presidente da CEUA / CCB - UFPE
SIAPE 1801584